Raghunathan, Vanamali

PION PRODUCTION AND ABSORPTION IN HELIUM ISOTOPES

The College of William and Mary in Virginia PH.D. 1983

PLEASE NOTE:

In all cases this material has been filmed in the best possible way from the available copy. Problems encountered with this document have been identified here with a check mark __√__.

1. Glossy photographs or pages _____
2. Colored illustrations, paper or print _____
3. Photographs with dark background _____
4. Illustrations are poor copy __√__
5. Pages with black marks, not original copy _____
6. Print shows through as there is text on both sides of page _____
7. Indistinct, broken or small print on several pages __√__
8. Print exceeds margin requirements _____
9. Tightly bound copy with print lost in spine _____
10. Computer printout pages with indistinct print _____
11. Page(s) _____ lacking when material received, and not available from school or author.
12. Page(s) _____ seem to be missing in numbering only as text follows.
13. Two pages numbered _____. Text follows.
14. Curling and wrinkled pages _____
15. Other _____

PION PRODUCTION AND ABSORPTION IN HELIUM ISOTOPES

A Dissertation

Presented to

The Faculty of the Department of Physics

The College of William and Mary in Virginia

In Partial Fulfillment

Of the Requirements for the Degree of

Doctor of Philosophy

---

by

Vanamali Raghunathan

August 1983

APPROVAL SHEET

This dissertation is submitted in partial fulfillment of

the requirements for the degree of

Doctor of Philosophy

Vanamali Raghunathan

Approved, May 1983

Charles F. Perdrisat

Rolf G. Winter

Franz L. Gross

Herbert O. Funsten

Gary C. DeFotis
Department of Chemistry

Ralph C. Minehart
University of Virginia

DEDICATION

To my parents Ranganayaki and Raghunathan

AND

To my wife Padmini
for the timely and selfless support and encouragement but for which this task would not have been possible

ABSTRACT

Pion production and absorption mechanisms are studied in the exclusive and inclusive reactions $^{3}He(p,t\pi)p$, and $^{3,4}He(\pi^{\pm},p)X$. The data for these two reactions were obtained from the experiments done at TRIUMF and LAMPF laboratories. The behavior of the data obtained in the exclusive reaction suggests deviations from the Impulse Approximation. The data of the inclusive reaction suggests the formation of a Δ in the unobserved system X.

VANAMALI RAGHUNATHAN

THE COLLEGE OF WILLIAM AND MARY IN VIRGINIA

ACKNOWLEDGEMENTS

I am extremely indebted to the following people who have contributed their time in helping me finish this piece of work.

First and foremost I would like to thank my advisor, Dr. Charles F. Perdrisat, who helped me in understanding Nuclear physics since the first day I started working with him. I am extremely grateful to him for his guidance and advice.

I am very thankful to the faculty and staff of the physics department at the college of William and Mary for their instruction, friendliness, and financial aid.

Drs Ralph Minehart and Lew Orphanos for letting me use portions of their data.

The personnel at TRIUMF lab who were very generous with their resources and time during my stay there.

Drs Don Joyce, Kevin Giovanetti, and David Hertzog and to my fellow graduate student Betru Debebe for many useful discussions.

Vina Punjabi for producing some of the plot routines.

My brothers Dr. Krishnaswamy, Kasthuri and their wives for giving me moral support during these past years

Ms. Sylvia Stout for her kind help during my stay at William and Mary.

And I am very much thankful to my wife Padmini who has been a constant source of encouragement and driving force throughout the last

phase of my graduate studies. She was indeed of great help in typing and producing technical drawings for this manuscript.

CONTENTS

Chapter I

INTRODUCTION

Pion production and absorption on nuclei has been an interesting topic since the prediction of the pion in 1935 by Yukawa. Since pions are the dominant exchange particles for the long range part in the strong NN interactions, a detailed knowledge of the reactions of pions with few-nucleon systems is of great interest. Specifically it allows to study the different reaction mechanisms possible for strongly interacting projectiles; the latter are still the most frequently used probes in investigations of the structure of nuclei.

The systematic study of any physical process should be based on a model. The model for the reactions discussed here are based on the Impulse Approximation (I.A.). In the I.A. the projectile interacts only once, either with one nucleon or with a nuclear cluster, while the rest of the nucleus has the status of a spectator in the main interaction. In this picture, the final state products have a kinematics similar to that of a free projectile-nucleon(or quasi-nucleus) interaction and hence are called Quasi-free processes. The most important reactions in π-nucleus interaction are the Quasi-free scattering on a single nucleon (QFS) and Quasi-free absorption (QFA) on a nucleon pair.

In certain reactions, depending on the kinematical conditions, there could be interactions among the products in the final state of the reaction. This Final State Interaction (FSI) between the final reaction

products would distort the partial waves describing these reaction products. The present work involves the study of these three processes, QFS, QFA, and FSI in the interaction of a proton and a pion with ^{3}He and ^{3,4}He, respectively.

For positive pion production on hydrogen by protons, a 290 MeV proton beam is needed. The pion production cross-section rises very quickly and by 900 MeV in proton-proton collisions, the total cross-section equals the reaction cross-section. In the case of nucleon-nucleus collision, pion production is normally the result of a single nucleon-nucleon interaction within the nucleus. In certain situations, the pion might rescatter on another nucleon and this rescattering process might completely shadow the primary process. Due to the fermi motion of the nucleons of a nuclear target, pion production on these systems can occur at a lower proton beam energy than for a free pp collision, contingent that the projectile has a kinetic energy larger than the rest mass of the pion.

Since the pion cannot be absorbed on a free nucleon, due to momentum conservation, absorption must occur only on a pair or a group of correlated nucleons. A typical pion-nucleon absorption process for a π^+ and a π^- is shown in figure 1. Figure 1 (a) is π^- absorption on a pp pair. Figure 1 (b) is π^+ absorption on a pn or nn pair. Figure 1 (c) is π^+ absorption with an intermediate pion-nucleon resonance formation denoted by Δ.

Figure 1: pion nucleon vertex

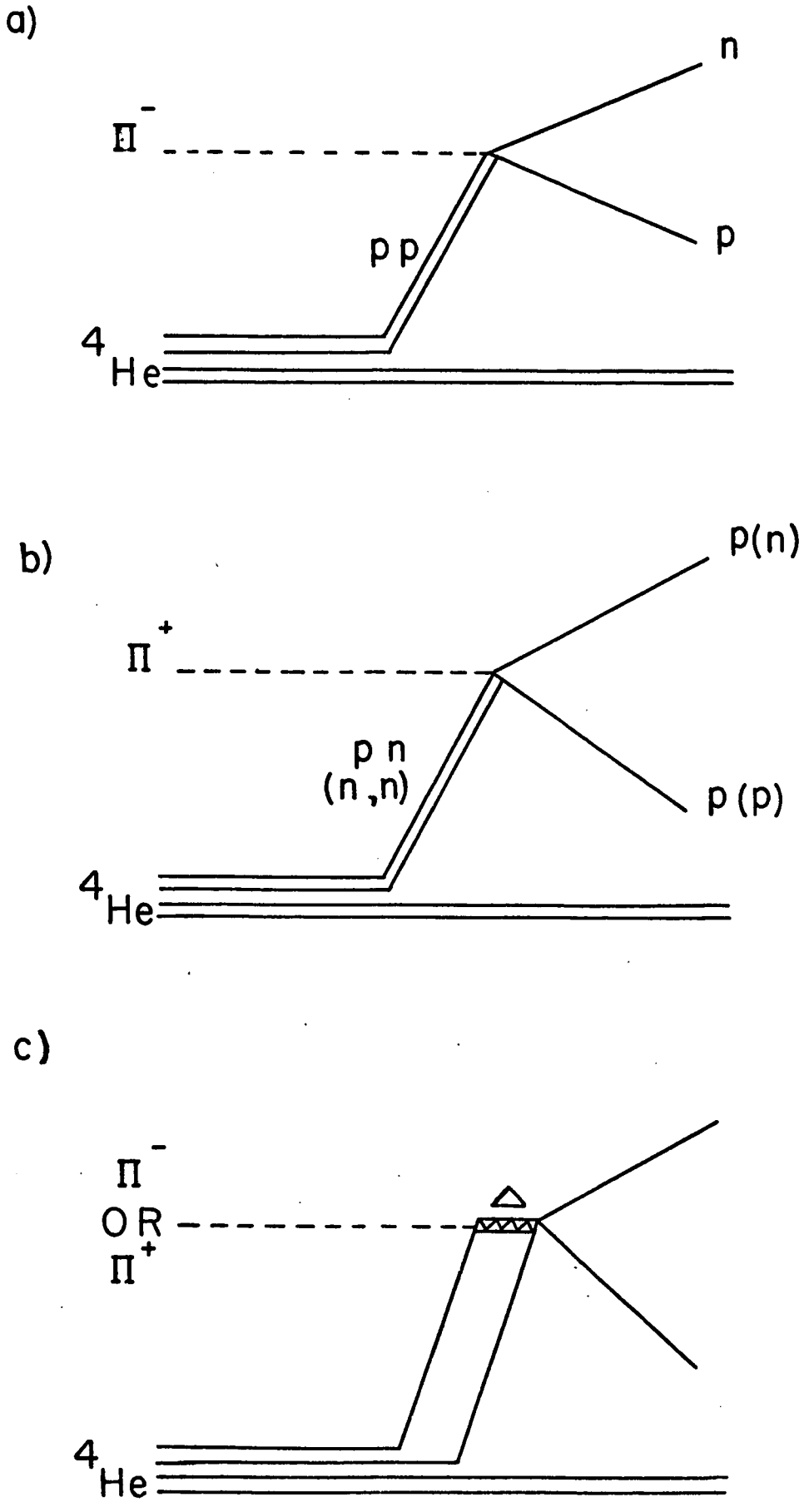

FIGURE 1

1.1 GOAL OF THE EXPERIMENT

We wanted to study final state interaction effects in the exclusive reaction

$^{3}He(p,\pi^{+}t)p$ Reaction (1)

and obtain proton continuum cross sections for the inclusive reaction

$^{3,4}He(\pi^{\pm},p)X$ Reaction (2).

Data were obtained over a large region of the phase space of the final state particles in reaction (1) and in both cases including the (3,3) resonance region, where the pion and a nucleon are resonating in the final state of the reaction at an invariant mass of 1.232 GeV.

1.1.1 Reaction (1)

The interesting feature of reaction (1) is that here the $(\pi^{+}p)$ system, in the final state of this reaction, is in a pure isospin T= 3/2 state as $T_3(\pi^{+}p) = +3/2$. Therefore the interaction is strongly resonating at $m_{\pi p} = m(\Delta)$. In this reaction the triton and the pion were detected in coincidence.

The kinematics of the experiment is completely defined because all the kinematical variables of each one of the particles in the initial and final states have been either measured or can be calculated using energy and momentum conservation. The final state can be entirely determined by measuring the five variables which are the momentum of the triton, its two scattering angles θ and ϕ and the two scattering angles θ and ϕ for the pion. Knowing these five variable, any other unknown variables of interest like the recoil of the proton, and any of the three invariant masses M_{34}, M_{45}, and M_{35} can be calculated.

The fifth order differential cross section

$$\frac{d^5\sigma}{d\Omega_3\ d\Omega_4\ dp_3} \qquad (1.1)$$

was obtained from the data. In the above equation, 3 stands for the triton, 4 for the pion and $d\Omega_3$ and $d\Omega_4$ stands for their respective solid angles. In this reaction validity of the Impulse Approximation(I.A.) will be tested using the factorised form of the cross-section to obtain

$$\phi^2(p_s) = \frac{d^5\sigma/(d\Omega_3\ d\Omega_4\ dp_3)}{k\ (d\sigma/d\omega)_{16\_34}} \qquad (1.2)$$

where the indices are defined in the I.A. graph (Fig2), ϕ^2 is the momentum space density at the vertex $^3He \rightarrow$ 'd' p and $(d\sigma/d\omega)$ at $p'd' \rightarrow t\pi$, is taken to be the free pd cross-section leading to a triton and a pion in the final state and k is a kinematic factor. The 'd' here is a quasi-deuteron as opposed to a free deuteron. The replacing of $p'd' \rightarrow t\pi$ cross-section by the free $pd \rightarrow t\pi$ cross-section is the result of the application of the I.A. In this on-shell approximation and in the exact validity of the I.A., the momentum space density $\phi^2(p_s)$ extracted from eqn 1.2 would be a function of the recoil momentum p_s only. Thus extracting ϕ^2 and investigating its dependance on p_s is the way to check the validity of the I.A. The results are indicative of the validity of the I.A. for restricted kinematical conditions and will be discussed in detail in a later section.

1.1.2 Reaction (2)

For reaction(2) the invariant cross-section

$$\frac{E_p \, d^3\sigma}{d\Omega \; p^2 \; dp} \tag{1.3}$$

was obtained from the data and studied as a function of the missing mass squared M_x^2 of the unobserved system X, where the missing mass squared is given by $M_x^2 = (P_\pi + P_{tgt} - P_p)^2$. In this expression P's stand for the four-momenta of the pion, the target, and the detected proton respectively.

Reaction (2) is an inclusive reaction since only one particle in the final state is observed. The detected proton was going backward in the lab with an energy > 50 MeV. In this reaction, distortions from phase space are expected to occur in the proton continuum spectra, if there exists a final state interaction (FSI) within the components of the unobserved system X. If the final state interaction resulted in a ΔN system with some binding energy, it could manifest itself in the excitation spectrum at a fixed recoil momentum showing an enhancement at the energy for which $M_x = m_\Delta + M_N - B_\Delta$; B_Δ would be the binding energy.

The cross-section does exhibit features of the three processes of quasi-free absorption(QFA), quasi-Free scattering(QFS), and final state interactions(FSI) within the unobserved system X, as will be discussed below.

^{3}He for reaction(1) and ^{3,4}He for reaction(2) were chosen as the target nuclei for this study because, as a few nucleon system, most of the single particle aspects are very well-known from elastic electron scattering electron scattering studies[1,2].

1.2 SUMMARY OF THE FOLLOWING SECTIONS

In chapter II, I discuss the theoretical background for the experiment. Chapter III is a description of the experimental system. In chapter IV the development of the data reduction system along with calculation of the cross-section is discussed. Chapter V contains a discussion of the results and their theoretical implications.

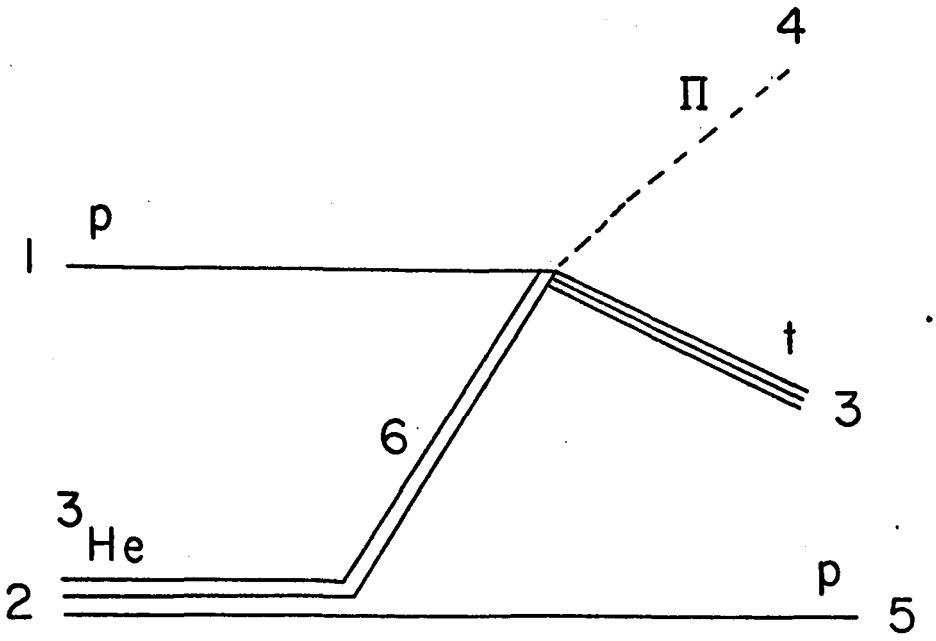

FIGURE 2

Chapter II

THEORY

2.1 PION NUCLEON INTERACTION

The pion has a mass of 139.6 MeV and appears in three different charge states of π^+, π^o and π^-. Its isospin T_π is therefore 1. The interaction of a pion and a nucleon in a state with a given parity and total angular momentum J depends only on their total isotopic spin T which can have the two possible values of T = 3/2 or T = 1/2. The T_3 component can have the values of $T_3 = \pm 1/2, \pm 3/2$ when T = 3/2 and $T_3 = \pm 1/2$, when T = 1/2. The various isotopic spin state vectors for a pion nucleon system can be obtained using the formalism for the addition of angular momentum for ordinary spin. Using linear combinations of these isotopic spin vectors, the different pion nucleon states can be expressed as follows(see reference[3]).

$$|p,\pi^+\rangle = |\tfrac{3}{2},\tfrac{3}{2}\rangle$$

$$|p,\pi^o\rangle = \tfrac{2}{3}^{\frac{1}{2}}|\tfrac{3}{2},\tfrac{1}{2}\rangle - \tfrac{1}{3}^{\frac{1}{2}}|\tfrac{1}{2},\tfrac{1}{2}\rangle$$

$$|p,\pi^-\rangle = \tfrac{1}{3}^{\frac{1}{2}}|\tfrac{3}{2},-\tfrac{1}{2}\rangle - \tfrac{2}{3}^{\frac{1}{2}}|\tfrac{1}{2},-\tfrac{1}{2}\rangle$$

$$|n,\pi^+\rangle = \tfrac{1}{3}^{\frac{1}{2}}|\tfrac{3}{2},\tfrac{1}{2}\rangle + \tfrac{2}{3}^{\frac{1}{2}}|\tfrac{1}{2},\tfrac{1}{2}\rangle$$

$$|n,\pi^o\rangle = \tfrac{2}{3}^{\frac{1}{2}}|\tfrac{3}{2},-\tfrac{1}{2}\rangle + \tfrac{1}{3}^{\frac{1}{2}}|\tfrac{1}{2},-\tfrac{1}{2}\rangle$$

$$|n,\pi^-\rangle = |\tfrac{3}{2},-\tfrac{3}{2}\rangle$$

In the reaction of $^3He(p,\pi^+t)p$, the π^+p system, where the p stands for the recoil proton , is in the pure $|\frac{3}{2},\frac{3}{2}\rangle$ isospin state, which exhibits a number of resonances with different angular momentum and parity, the

lowest one called Δ, occuring at m_{Δ} = 1.232 GeV and having a FWHM of 115 MeV.

2.1.1 Δ resonance

The Δ resonance is the strongest resonance in the pion-nucleon system. The different possible resonances of the pion-nucleon system are shown in table 1. Each one of these resonances corresponds to different angular momentum states. Parity of the Δ is +1 and corresponds to a P wave since it is an L = 1 angular momentum state.

TABLE 1

Lowest energy resonances in the Pion-Nucleon system

$T = \frac{1}{2}$					$T = \frac{3}{2}$				
p_{π} (MeV/c)	Mass (MeV)	L,J	parity	(MeV)	p_{π} (MeV/c)	Mass (MeV)	L,J	parity	(MeV)
					300	Δ(1232)	$1,\frac{3}{2}$	−	115
660	N(1470)	$1,\frac{1}{2}$	+	200	960	Δ(1650)	$0,\frac{3}{2}$	−	140
740	N(1520)	$2,\frac{3}{2}$	−	125	1000	Δ(1670)	$2,\frac{3}{2}$	−	200
760	N(1535)	$0,\frac{1}{2}$	−	100	1030	Δ(1690)	$1,\frac{3}{2}$	+	250
1000	N(1670)	$2,\frac{5}{2}$	−	155					
1030	N(1688)	$3,\frac{5}{2}$	+	140					

This table is taken from ref[8].

The chief interest in the study of reaction (1) and reaction (2) is to look for manifestations of the Δ resonance. A Δ could either have pre-existed inside the nucleus or have been created in the interaction process. In this study, the contribution of a pre-existing Δ is

thought to be very small;such a situation would correspond to a large internal momentum of the Δ inside the nucleus. Such contributions will be very small compared to quasi-free processes like absorption and scattering. Several searches have been made to look for the presence of a Δ component in helium isotopes (Tatischeff et.al. and Jonsson et.al).[10,11] Also investigations of the presence of a two-Δ component in the deuteron have been done by Benz et.al, Beurtey et.al. and Bakken et.al[12-14] and others.

A typical Δ production could proceed as follows

$$\pi + N \Rightarrow \Delta \Rightarrow \pi N \text{ or } NN \Rightarrow N\Delta \Rightarrow NN.$$

The Δ can interact with another nucleon before it decays. In fact reactions like the ones above are the only tools for studying Δ-N interaction since free Δ-N is not possible. One of the ways to look for this Δ-N interaction based on a suggestion by Cartwright[15], later developed by Watson[16] and Migdal[17], is to look for the evidence of a final state interaction (FSI) in a missing mass spectrum, where the missing mass corresponds to the presence of a Δ among the unobserved constituents of the final state. This idea was the motivation for studying (π,p) reaction and the analysis of (p,πt) reaction. The significant feature of these studies would be the width of the Δ and the extraction of the cross-section.

2.1.2 Impulse Approximation

In this work, we first compare the data of reaction (1) with the predictions of the plane wave impulse approximation (PWIA). In the study of reaction (1) the momentum space density of the nucleons within the nucleus is evaluated on the basis of the I.A.

The PWIA is based on a simple picture in which the projectile interacts only with one nucleon(or a nuclear cluster) within the nucleus, the other nucleons remaining spectators. For a brief derivation of the PWIA cross-section see [18].

In the context of the I.A. model, ^{3}He is considered to be consisting of a 'quasi-deuteron' and a proton. The PWIA description of reaction (1) is as follows. The incoming proton interacts with the quasi-deuteron in the target and the other proton remains a spectator, thus not taking part in the interaction either with the incoming proton or with the two outgoing particles. Figure 2 is a Feynmann diagram that describes this reaction according to the PWIA picture. Figure 3 (a), (b), and (c) describe three other graphs based on the I.A. for different kinematical conditions, but including a final state interaction between the pion and the proton(deuteron in (c)). Such graphs must play an important role for large recoil momenta as they do not depend upon large internal momentum in the target nucleus. The recoiling particle obtains its large momentum by undergoing more than one scattering.

Several experiments involving knockout reactions induced by electrons have been performed, which allow a direct determination of the proton momentum distribution in nuclei. Recently the proton momentum distribution in ^{3}He has been determined up to a recoil momentum of 305 MeV/c of the deuteron in the reaction of ^{3}He(e,e'p)^{2}H by Jans et.al.[9] The momentum space density of the nucleons in ^{3}He extracted in this work will be compared with the results in ref 9.

The validity of the PWIA picture in this reaction has not been tested prior to this study. A recent study of d(p,dπ)n has been done to

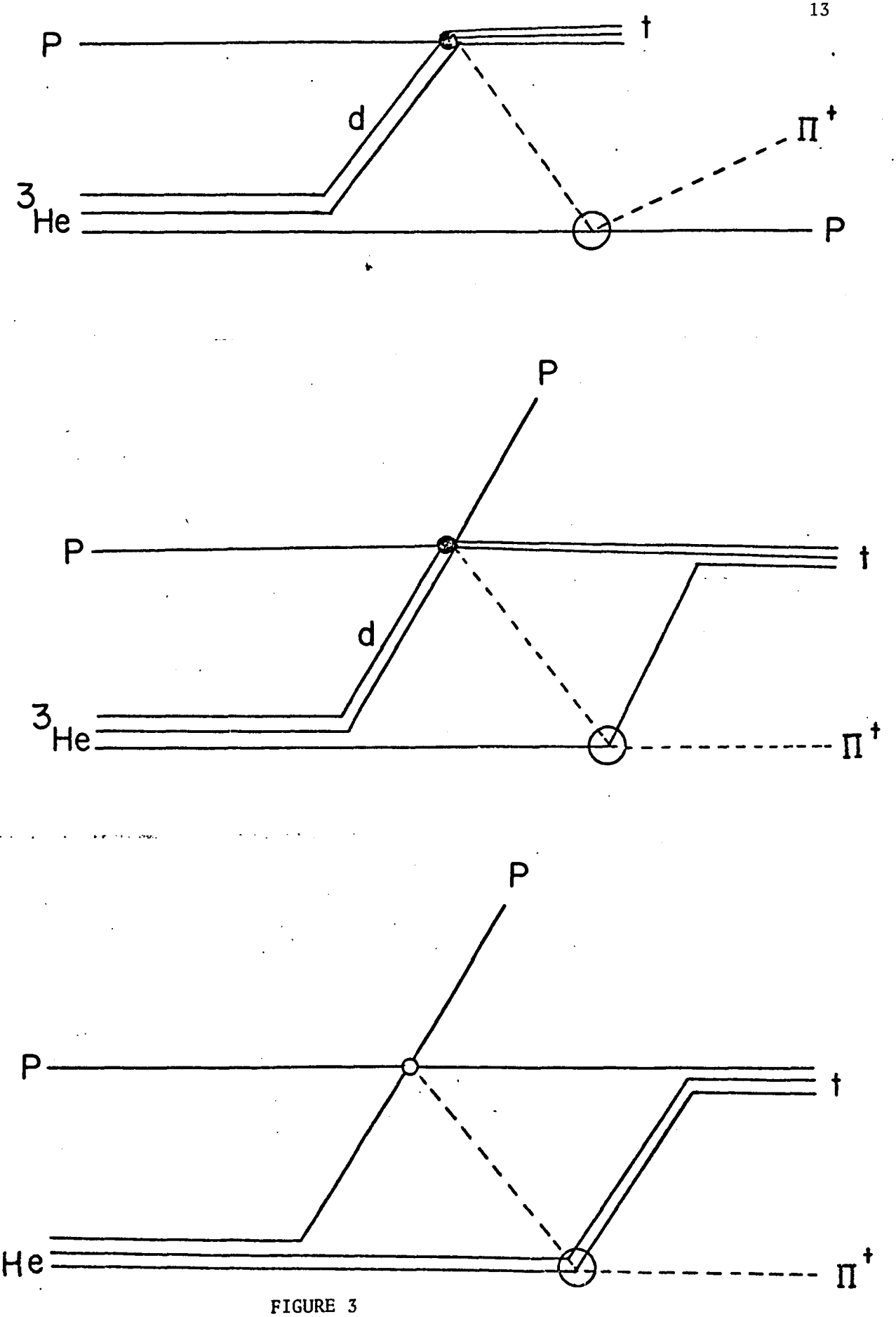

FIGURE 3

check the validity of the Impulse Approximation, at a proton energy of 500 MeV. In this reaction, due to isospin conservation, the π^+n system is in a pure I=1/2 state, which results in a very weak final state interaction in the πN subsystem, at the energy considered. Hence the effects due to rescattering of the pion in the final state should be very small, and this reaction should be described well by the I.A.;indeed, parts of the deuteron data follow the I.A. prescription For a detailed description of this work, see ref [19]. A previous study of the deuteron reaction, with a proton energy of 800 MeV, had revealed significant departure from the I.A.[20]

2.1.2.1 Reaction (2)

Experiments by Jackson et.al[4] for the reactions $^{4}He(\pi^{\pm},p)X$, and Kallne et.al.[5] for the reactions $^{3,4}He(\pi^{+},p)X$, have shown that for forward proton angles and for pion energies between 50 and 250 MeV there are two prominant peaks in the cross-section data. One of this peak appears at an energy corresponding to the kinematics of quasi-free scattering, $\pi N \rightarrow N\pi$ and the other one appearing at a higher proton energy corresponding to the kinematics of quasi-free absorption on a pair of nucleons $\pi NN \rightarrow N P$. These reactions are termed Quasi-free because the final state kinematics correspond approximately to that of a free pion-nucleon, or pion-deuteron interaction, respectively.

In the present study of the inclusive reaction (2) the protons were observed at angles $>90^{o}$ and with energies >50 MeV. From the data of Jackson and Kallne we expect the quasi-free scattering peak to disappear as the detected proton energy gets to be higher than 50 MeV, and quasi-free absorption to dominate the reaction beyond this energy region. Also, protons can be produced backward in single πp collisions (Quasi-free scattering) only if they had a large Fermi momentum prior to collision. Hence, most of the continuum cross section for protons >50 MeV in this study must come from processes like Quasi-free absorption on a pair of nucleons or other multistep processes. FSI is one such process.

Since the absorption of a pion on a single nucleon is forbidden by momentum conservation, the basic pion absorption mechanism is the two nucleon one. The most fundamental process describing this reaction is $\pi d \rightarrow NN$, since the deuteron is the only bound two-nucleon system. In

the case of pion-nucleus interaction, the absorption is usually assumed to take place on a 'quasi-deuteron' in the nucleus as contrasted to a free deuteron. In the I.A. picture, the general form of the cross section can be factorised into

$$\frac{d\sigma}{d\Omega}\Big|_A = C \quad \frac{d\sigma}{d\Omega}_{(\pi d \rightarrow NN)} |F_{d,A}(q^2)|^2$$

where $\frac{d\sigma}{d\Omega}\Big|_A$ is the pion absorption cross-section for a system of A nucleons, C is a kinematic factor and $\frac{d\sigma}{d\Omega}(\pi d \rightarrow NN)$ is the fundamental cross-section for π absorption; $F_{d,A}(q^2)$ is a form factor for a 'quasi-deuteron' inside the nucleus.

Chapter III

EXPERIMENTAL DETAILS

3.1 INTRODUCTION

The experiment designed to study the exclusive reaction

$$^3He(p,\pi^+t)p, \qquad \text{Reaction (1)}$$

was performed on one of the external proton beam lines of the TRIUMF cyclotron. The experiment designed to study the inclusive reaction

$$^{3,4}He(\pi^{\pm},p)X, \qquad \text{Reaction (2)}$$

was performed using the high energy pion channel P^3 at LAMPF.

In the exclusive Reaction (1), a proton beam was impinged on a cryogenic ^3He target and the scattered particles of interest were detected using a two arm detection system. One arm of this detection system consisted of the Medium Resolution Spectrometer (MRS), situated on the left side of beam line 4b of the TRIUMF cyclotron, and on the right side was a pion multicounter hodoscope consisting of 13 pairs of plastic scintillators.

For the inclusive Reaction (2), both $\pi^{\pm}$ beams were impinged on cryogenic $^{3,4}He$ targets and the scattered proton was detected using a telescope consisting of 5 plastic scintillators and two multiwire proportional chambers.

In both experiments information from the chambers and scintillators was processed by a combination of fast 'NIM' and 'CAMAC' electronics and the data were digitised and recorded on magnetic tape.

3.1.1 Reaction (1)

3.1.1.1 Beam Structure

The TRIUMF cyclotron is a six sector isochronous cyclotron accelerating H^- ions. Two simultaneous beams of protons individually variable in energy, from 180 to 520 MeV, are extracted using two stripper foils of carbon or aluminum. Our data was taken at the proton beam energies of 506 and 460 MeV. The beam intensity used was typically 10 - 20 nA and the beam spot was approximately 0.5 cm x 0.5 cm in size at the experimental target postion. The time between each micro-burst of the beam was 43 nsec. A 4-telescope polarimeter viewing a thin CH2-target, located 3.2 m upstream of the target location measured the beam intensity.

3.1.1.2 The Detector System

For Reaction (1) the pion and the triton were detected in coincidence, utilising a two arm detection system. The Medium Resolution Spectrometer, was tuned to detect the triton on the left side and on the right side a telescope consisting of 13 pairs of plastic scintillators detected the pion. Each pair of scintillator on the right side of the detection system consisted of a thin scintillator of size $(12.7)x(12.7)x(.3175)$ cm^3 and behind it a 15 cm thick, circular scintillator of diameter 11.43cm. For a detailed description of the construction of these thick counters see.[22] These counters covered an angular range from 22 degrees to 96 degrees, at an interval of about seven degrees. Each scintillator had a light emitting diode attached to it, which was triggered by a pulser system at a rate proportional to the

beam intensity. The fraction of the pulses accepted by the data acquisition system was used as a measure of the system's dead time. This dead time is defined as the fraction of the time the computer was busy and not able to accept any data

$$\text{Dead Time Fraction} = \frac{\text{Pulses accepted}}{\text{Pulses presented}} \qquad (3.1)$$

Figure 4 is a plot of the live time of the system against the event rate. For the geometrical settings of the pion counters see table 2. For the geometrical layout of each one of the pion counters see figure 5.

3.1.1.3 Medium Resolution Spectrometer

The charged particles were bent vertically by the dipole of the MRS. A thin counter situated at a distance of 80cm from the target was used as an energy loss (ΔE) counter for the tritons. The size of this front counter was 12.9 X 129 X .32 cm^3. The MRS itself consisted of a quadrupole, followed by a dipole, three multiwire proportional chambers(MWPC) and two additional scintillators above the dipole. Figure 6 shows a vertical sectional drawing of the MRS. The quadrupole could be moved so that the system can be set in a large solid angle configuration or small solid angle configuration. For this work, the large solid angle configuration was used.

The three MWPC's defined the three pairs of coordinates (Xo,Yo), (Xt,Yt), and (Xb,Yb). See figure (6). The MWPC'S have 2 mm spacing between wires. The (Xo,Yo) MWPC consisted of 64 wires in each direction. The Xt and Xb consisted of 512 wires each whereas the Yb and

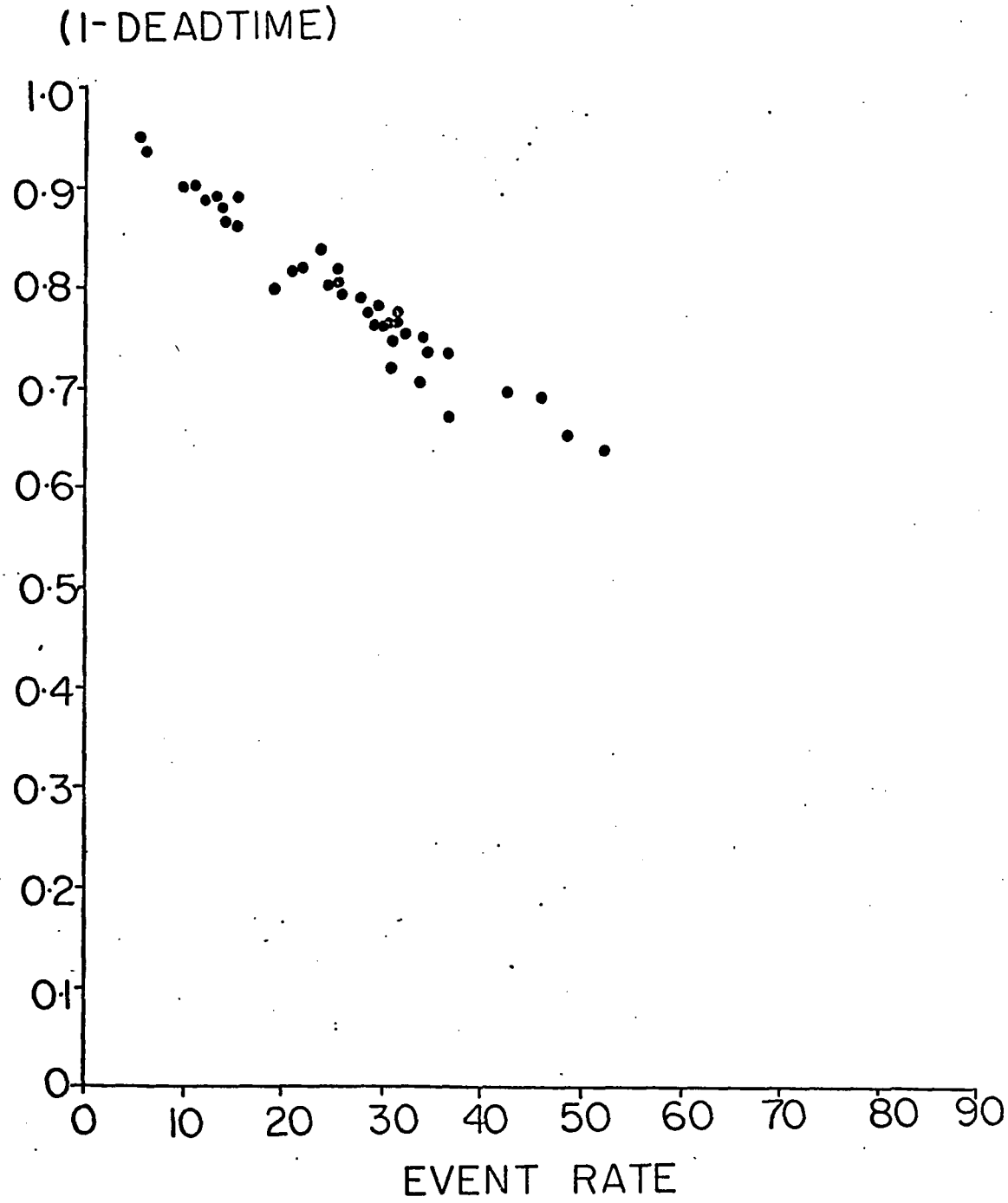
(1-DEADTIME)
1·0
0·9
0·8
0·7
0·6
0·5
0·4
0·3
0·2
0·1
0
0
10
20
30
40
50
60
70
80
90
EVENT RATE

Figure 4.

TABLE 2

Detection System for Reaction (1)

COUNTER	ANGLE(DEGREES)	DISTANCE FROM TARGET(CMS)
1	22.00	205.5
2	28.00	205.5
3	33.70	205.5
4	39.60	176.5
5	46.63	176.5
6	53.66	176.5
7	60.82	176.5
8	67.88	176.5
9	74.76	176.5
10	81.79	176.5
11	87.60	206.5
12	93.60	206.5
13	99.60	206.5

Yt consisted of 64 wires each. The distance from the target to the Xo plane of the first MWPC was 85cm. The MRS can be moved in the horizontal plane to anywhere between 10 and 120 degrees. The central momentum of the MRS was chosen by adjusting the field in the dipole and quadrupole magnets. The momentum acceptance of the MRS was typically $\pm$15%. The total flight path of a particle in the MRS was about 11 meters.

3.1.1.4 The Cryogenic Target System

The liquid ^{3}He target for reaction (1) was built by D.Hassel and R.Abegg at the University of Monitoba.[23] The target was constructed in such a way as to provide either a liquid ^{3}He cell or an identical but empty cell in the beam. This was achieved by the vertical motion of a ladder-like structure. A ZnS film was also put in the target ladder to

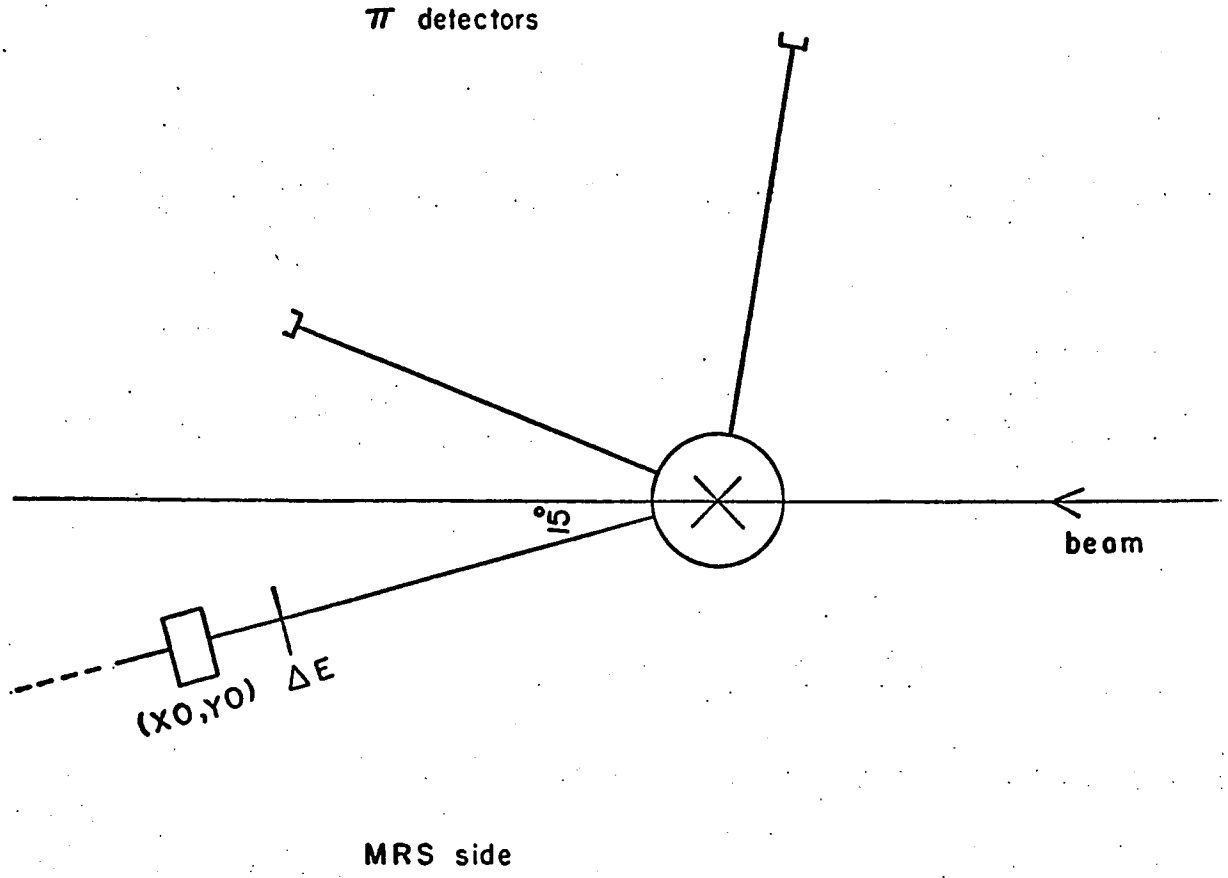

Figure 5.

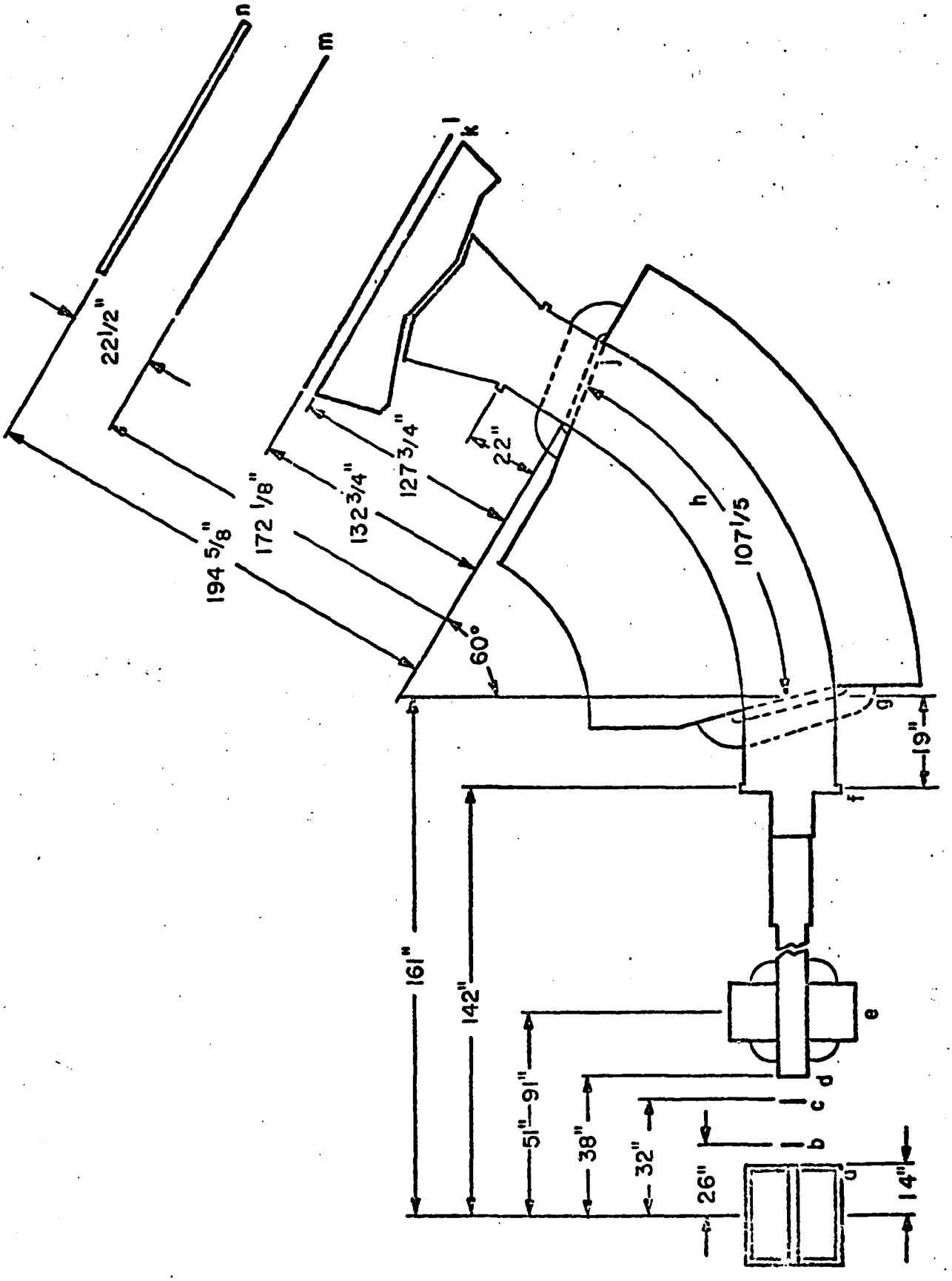

Fig. 6 Vertical section drawing of the MRS.

provide a visual check of the position and shape of the beam spot. The liquid ^{3}He cell was 1.6 $\pm$ cm in thickness. The density was 0.080 $\pm$ gm/cm^3(at a temperature of 1.6^{o}K). The target was positioned at an angle of 44.8 $\pm$ degrees to the beam. The effective density of the target material presented to the beam is given by

$$\rho_{eff} = \frac{\rho\ t}{\cos(\theta)} \qquad (3.2)$$

where θ is the target angle, as defined in figure (5).

Liquid ^{3}He was obtained by liquefying ^{3}He gas in a ^{4}He cryostat. The temperature of liquid ^{3}He was maintained at about 1.6^{o}K during the experiment. The windows of the ^{3}He cell were made of thin nickel foils(0.0025cm). The liquid Nitrogen jacket at 77^{o}K, the liquid ^{4}He reservoir at 4.2^{o}K, the pumped liquid Helium bath at 1.6^{o}K and finally the liquid ^{3}He target cell at 1.6^{o}K are nested one within the other. All four components are housed within the main body of the cryostat and the surrounding volume is evacuated. The empty cell was used to measure the background events arising from the windows of the ^{3}He cell, the windows of the cryostat, and in the air up and down-stream from the target chamber.

About 22 litres of ^{3}He gas at STP is required to fill the target cell and the surrounding coils. Two germanium resistors located at the top and bottom of the ^{3}He target cell were the monitors for the liquid ^{3}He temperature.

3.1.2 Reaction (2)

3.1.2.1 Beam Structure

The LAMPF P^3 channel consists of 3 dipoles and 16 quadrupoles. The pion beam is produced by letting the main proton beam strike a 6 cm graphite target. Protons are removed from the π^+ beam by graphite degraders. The duty factor of the 800 MeV linac is 6%. For more details on the linac and P^3 channel ref.[24]

In the momentum range of our study of reaction (2) (400-700 MeV/C), the electron and muon contamination of the beam was very small (1%), and a pion flux of $10^7 sec^{-1}$ was obtainable within a momentum band of 5%. An ion chamber situated downstream from the target was used as a beam monitor. The beam spot size was 1.5 cm horizontal x 2.5 cm vertical FWHM.

3.1.2.2 The detection System

The detector system for reaction 2, shown in figure (8), consisted of 5 plastic scintillators S1 through S5, and 2 multi-wire proportional chambers MWPC1 and MWPC2. S5 was a veto counter to reject particles that have passed counter S4, which was thick enough to stop 150 MeV protons. The trajectory and angular information was given by determining the two pairs of coordinates (X1,Y1) and (X2,Y2) from the chambers for each event. The geometrical arrangement of the detection system is described in table 3.

3.1.2.3 The Cryogenic Target System

TABLE 3

Detection System for Reaction(2)

DEVICE	HEIGHT(CM)	WIDTH(CM)	THICKNESS(CM)	DISTANCE FROM TARGET(CM)
S1	12.7	30.5	.16	38.1
MWPC1	15.2	48.3	-----	45.1
MWPC2	15.2	48.3	-----	66.0
S2	12.7	48.3	.32	71.9
S3	15.2	48.3	.32	88.3
S4	15.2	50.8	15.24	92.1
S5	20.3	55.9	.64	111.8

The target for reaction (2) was a ^{3}'^{4}He cryostat built by Cryogenic Associates and has been described elsewhere [25]. See figure (7) for a schematic of ^{3}'^{4}He cryostat. The cryostat could hold both liquid ^{3}He and superfluid ^{4}He in separate target cells. The superfluid ^{4}He was maintained at 1.6^{o}K and the non-superfluid ^{4}He was maintained at 4.0^{o}K. The whole target could be raised or lowered using a bellows mechanism, allowing one to switch from the ^{4}He to the ^{3}He. The ^{3}He could be filled and evacuated without affecting the internal operating parameters of the cryostat, thus providing an empty cell in place of ^{3}He whenever a background measurement was necessary. Similar to the target used for reaction(1) this cryostat also had a liquid nitrogen jacket, liquid ^{4}He at 4.2^{o}K, superfluid ^{4}He at 1.5^{o}K and liquid ^{3}He at 1.5^{o}K. Internal temperature of various points inside the target cell were monitored using resistors. Relevant target parameters are summarised in table 4.

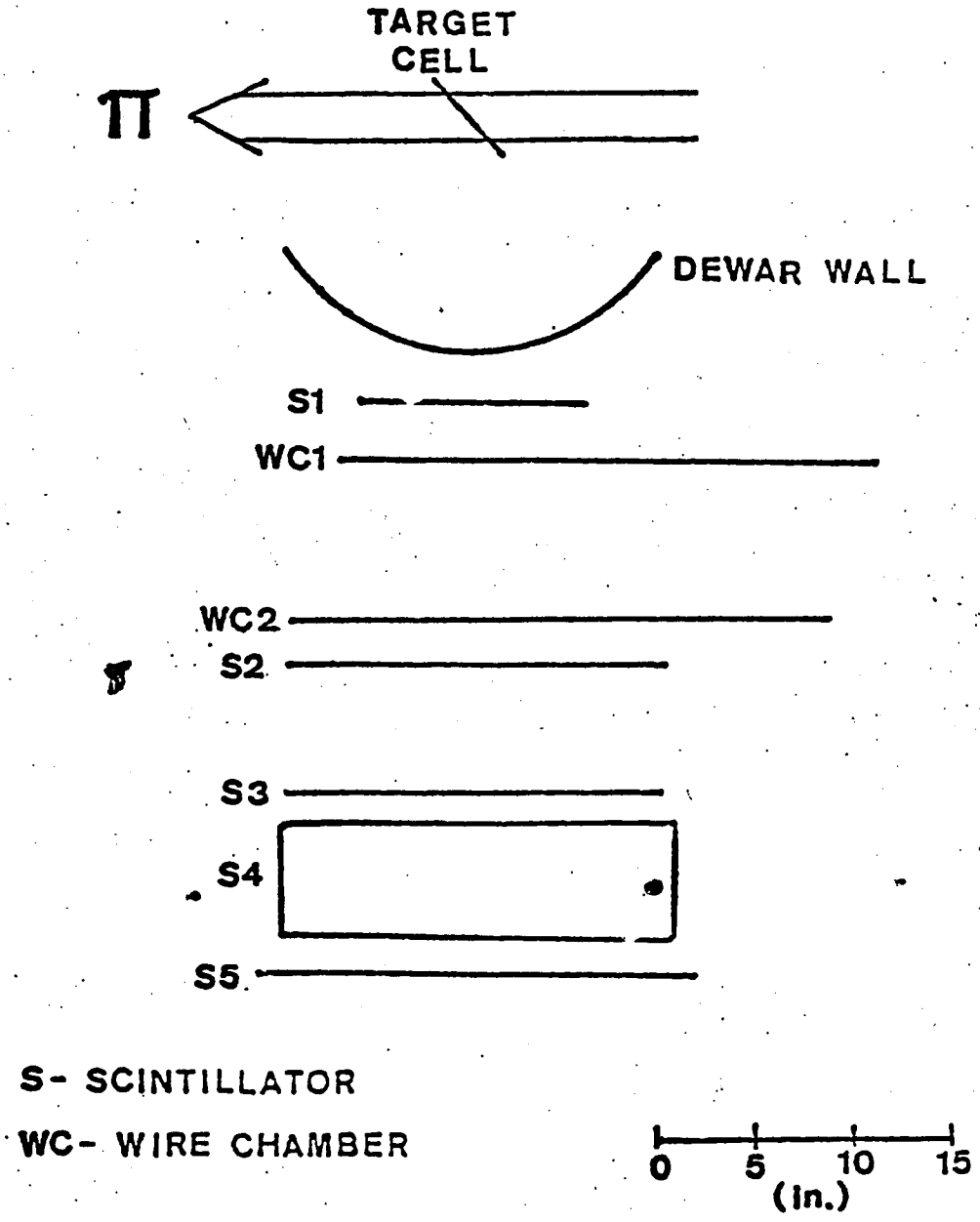
TARGET
CELL
π
DEWAR WALL
S1
WC1
WC2
S2
S3
S4
S5
S- SCINTILLATOR
WC- WIRE CHAMBER
0
5
10
15
(In.)

Figure 7.

TABLE 4

The Cryostat for Reaction (2)

TARGET TYPE	DENSITY (gm/cm^3)	THICKNESS cm	ANGLE (degrees)
3He	.080	0.635	45
4He(*)	.128	0.635	45
4He(**)	.1454	0.635	45

* for non-superfluid Helium ** for superfluid Helium.

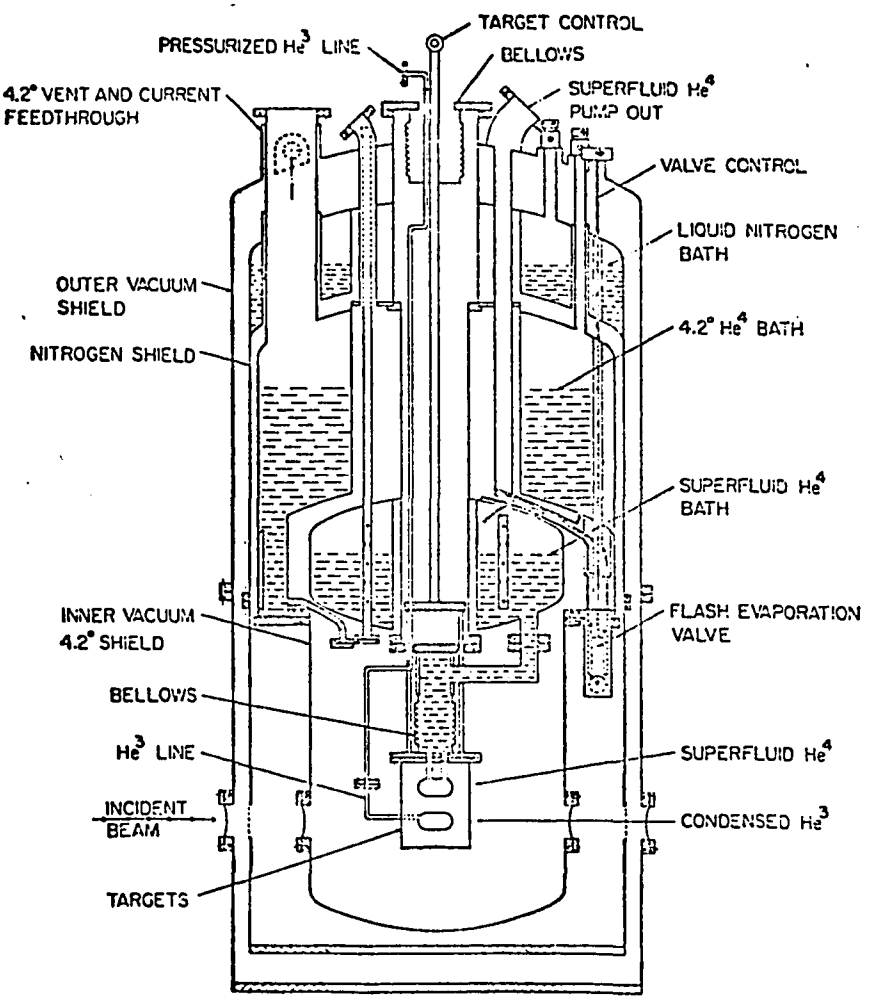
TARGET CONTROL
PRESSURIZED He3 LINE
BELLOWS
4.2° VENT AND CURRENT FEEDTHROUGH
SUPERFLUID He4 PUMP OUT
VALVE CONTROL
LIQUID NITROGEN BATH
OUTER VACUUM SHIELD
4.2° He4 BATH
NITROGEN SHIELD
SUPERFLUID He4 BATH
INNER VACUUM 4.2° SHIELD
FLASH EVAPORATION VALVE
BELLOWS
He3 LINE
SUPERFLUID He4
INCIDENT BEAM
CONDENSED He3
TARGETS

Figure 8.

3.2 ELECTRONICS AND LOGIC

3.2.1 Reaction (1)

3.2.1.1 Logic

The block diagram of the logic for reaction (1) is shown in fig 9.

The criterion for a good event was a coincidence between the signal from the front plastic on the MRS and one of the pion telescopes, which indicated the presence of a charged particle in both arms. The logic requirement for a 'good event' on the pion side was for a real coincidence between the signals from the thin and thick counters, shown as A and B in figure (9), in at least one telescope. This coincidence signal was split into two parts. One was fed to a logical 'AND' circuit containing the signal from the front MRS plastic scintillator. A coincidence between these two was termed a 'real' event, 'real' meaning that these two signals originated from the same beam burst. These events consisted of both (t p) and (t π) events. The other part was fed to another logical 'AND' circuit containing the signal from the front MRS counter, delayed by 172 ns, corresponding to 4 beam bursts, put into it. A coincidence in this channel was termed 'random' events, 'random' meaning that these signals originated from different beam bursts. These events were mostly (t p) events and were used to correct the number of coincidences due to uncorrelated particles occurring in a common beam burst. After the subtraction of the 'random' events from the 'real' events we obtained a sample of (t π) events, with some contamination of (t p) events. A detailed description of these events will be given in section 3.3.1.3. An output signal from each one of these two 'AND' circuits was fed into a

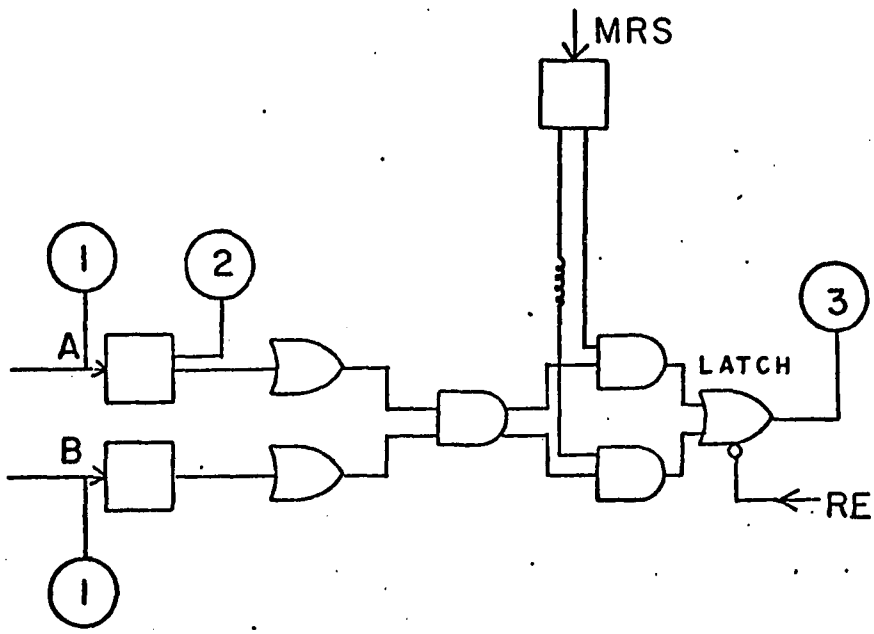

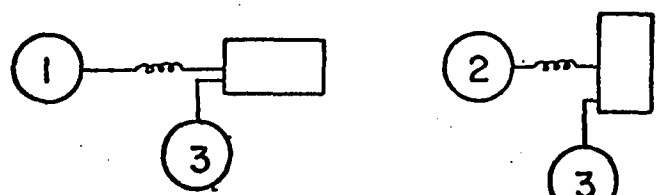

3 = GATE / START

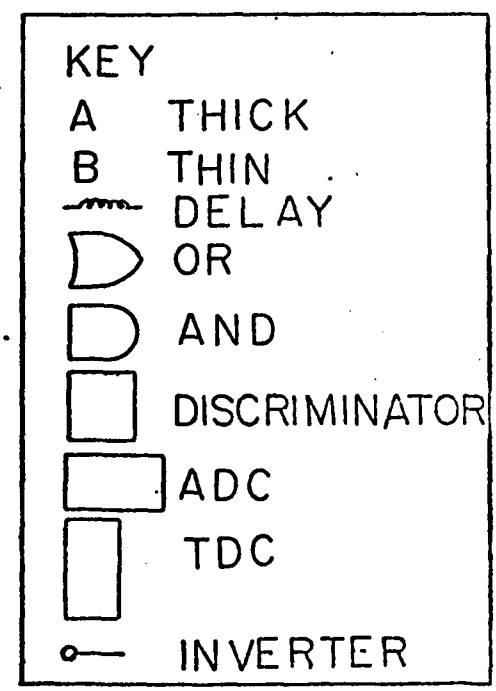

LOGIC FOR REACTION (I)

Figure 9

dual 4-fold logic unit, requiring one-out-of-4 inputs, labelled 'latch' in figure (9). The output of this circuit was fed back into it as its third input, thus functioning in a latching mode. The circuit was kept latched until a veto signal from the MRS side arrived, resetting the entire system.

Output signals from the latch circuit triggered a 'start' pulse for the TDC's(Time to digital converter) and generated a 'gate' pulse for the ADC's(Analog to Digital Converter). The output signals from all the discriminators were counted by scalers along with the output signals from the logic units. This information was used to monitor the system. To determine the delay necessary to insure coincidence between the output pulses from the logic units the initial timing was done using a pulse generator, for 'prompt' (v=c) events. Since all the scintillators had a light emitting diode attached to them it was easy to trigger these with the pulse generator and adjust the timing between different units. The timing for the coincidence between the thick and the thin counter was done with a ^{22}Na source. The timing for the coincidence between the front MRS plastic and the pion side was done utilising a Ruthenium source. Necessary delay cables were added in the timing circuit to account for the time-of-flight correction for the real particles.

3.2.1.2 Computer Interface

The data was written on magnetic tapes using the Honeywell data acquisition program (HONDA), for multi-parameter events with a Honeywell-316 mini computer through CAMAC interface. Events were read into

an input data buffer and when the buffer was full, written to an output data buffer and then stored on magnetic tape. Spectra were formed on-line and displayed on a scope, and a line printer-plotter for a fraction of the data.

3.2.2 Reaction (2)

3.2.2.1 Logic

The block diagram of the logic for reaction (2) is shown in figure (10). Four different kinds of triggers, refered to as H or L in the figure 10, were available, differing by the threshold adjustments on the trigger circuits; one for cutting out low energy particles, one for cutting out high energy particles, one for cutting out both high and low energy particle and the last one used only for detector calibration runs.

3.2.2.2 Computer Interface

The data was written on magnetic tapes using a PDP 11/34 minicomputer utilising an acquisition program written by R.Minehart of UVA.

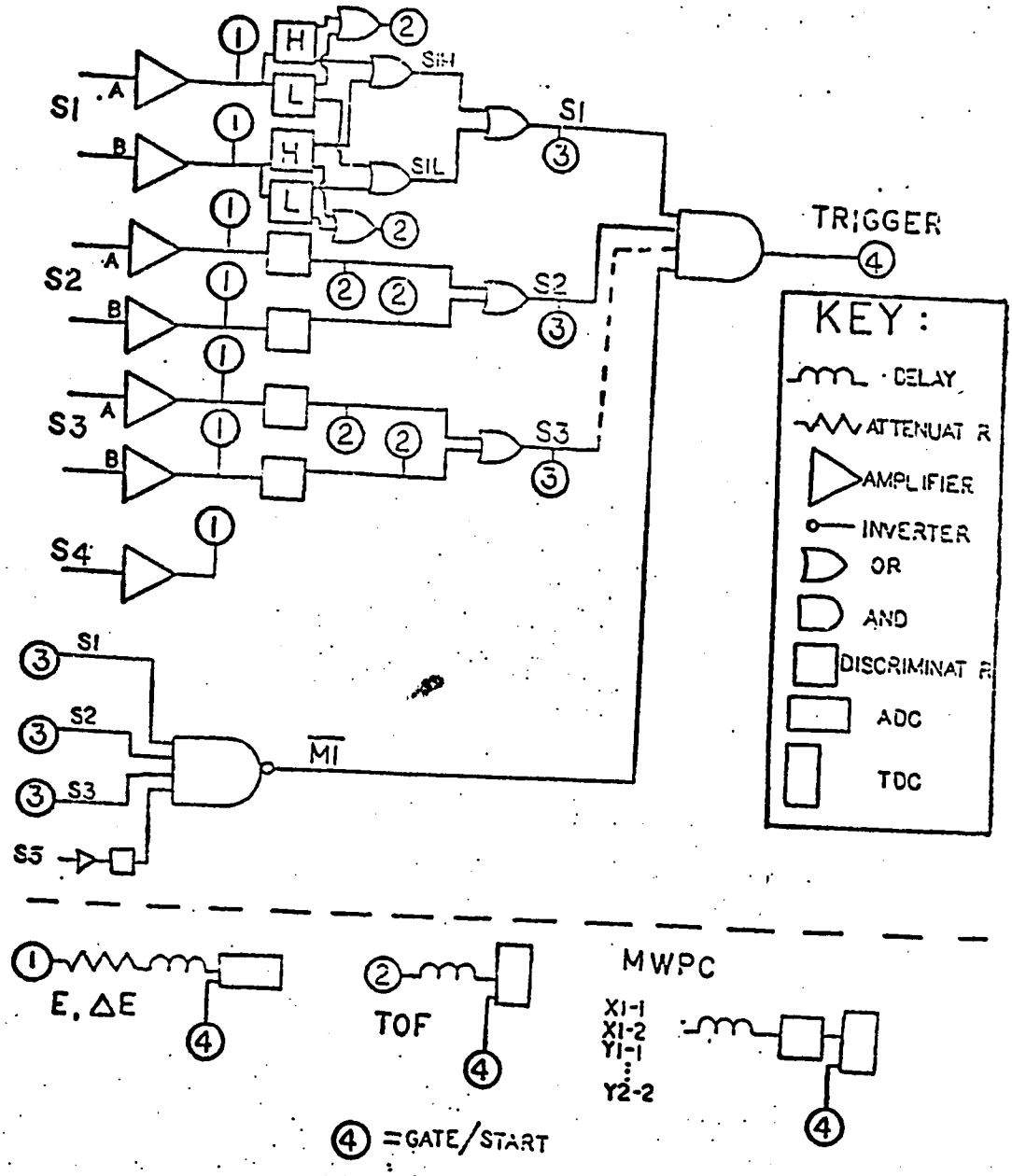

Fig. 10 Trigger Logic and Data Acquisition

3.3 DATA ACQUISITION

3.3.1 Reaction (1)

3.3.1.1 General System

HONDA controls a 3-crate CAMAC branch through a Daresbury DNPL-EC 321A interface. A crate is a structure for mounting the modules, supplying them with power and providing an interconnection 'highway' at the rear for data and control signals; this 'highway' is called the dataway. Typical modules used were 'ADC's, 'TDC's, Scalers etc. Each CAMAC crate has 25 slots numbered (1-25). CAMAC modules can occupy any one or more of the slots(1-23) in a crate. Slot (24-25) is occupied by a special module called a Crate Controller (CC), which has access to all the data and control lines of the dataway and has double the size of a single module. The task of the interface is to make sure that all signal levels and other hardware standards of CAMAC and computer highways are properly converted. Any module may generate a signal on its individual line to indicate that it requires attention. Modules that occupy more than one slot may indicate different demands by signals on the appropriate lines. These signals generated by the modules are called 'look at me' (LAM) signals. The crate number (C) and the slot number (N) of the CAMAC modules that are to be used in the experiment are determined firstp only these modules are initialised and tested whenever the Honeywell-316 computer is enabled to initialise the data acquisition program. Energy and timing information from all the detectors and the positional information from the MWPC'S are collected via the CAMAC system and stored on magnetic tape.

When a charged particle is detected on either one of the two arms of the detection sytem, a LAM signal is produced by one or more of the CAMAC modules. The computer is then set ready to read the data buffers. Since the data taking is of continuous nature, there must be a way to stop collecting further data when an event is being read into the computer. The electronic latch described in section 3.2.1.1 blocks further data from being presented to the ADC's and TDC's while an event is being read into the computer. Each event is uniquely qualified by its LAM pattern. The basic cycle in the processing of an event is as follows:

1) Data are gated into a group of CAMAC modules and the electronic latch is then set.

2) The LAM signal from one or more of the CAMAC modules causes a 'computer interrupt' and the CAMAC service routine is started, which performs operations like reading the modules, reading data into input data buffer etc.

3) The computer is now in a busy mode and not able to process any other routine.

4) The data are read from the CAMAC modules into an event data buffer. When this data buffer has been filled by the CAMAC service routine, it is passed on for further action which typically consists of formation of online spectra and copying this data buffer to an output buffer which may be written on magnetic tape.

5) The electronic latch is reset and the computer returns to its normal program to analyse further data.
For more details on CAMAC see ref[26].

3.3.1.2 Data Collection

A total number of 61 tapes of data were collected, subdivided into 78 runs. Runs were classified according to the momentum in the MRS, the angle of the MRS and the beam energy. All scaler values were displayed, as well as 15 different spectra, including the raw wire cham-

ber positions, TOF versus E display on the MRS side, TOF in each detector on the pion side etc. See table 5 for a summary of the data groups. The condition of the counters were checked easily by periodically looking at the scalers, since these scalers indicate the singles rate in the counters; any faulty one could be identified by its abnormal singles count. The scaler information was also used to check the maximum singles rate in these counters. All the scalers were initialized to zero at the beginning of each run.

TABLE 5

Run summary for Reaction (1)

BEAM ENERGY	MRS MOMENTUM	MRS ANGLE	RUN NUMBER
506 MeV	0.950	14.63	16-21
	1.050	14.63	23-26
	0.820	14.63	29-37
	1.020	18.00	38-46
	0.850	18.00	47-51
	1.110	14.77	52-60
	0.760	14.77	61-64
480 MeV	1.080	14.77	65-68
	0.900	14.77	69-72
	0.760	14.77	73-78

3.3.1.3 Event Types

An event is defined by the electronic logic and corresponds to the detection of a charged particle in the MRS and another charged particle detected in one of the pion telescopes within the time resolution of the circuitry (20ns). Each event consists of several charecteristic parameters such as the time of flight of the particle detected, its pulse height, the addresses of the wires hit in the MWPCs etc.

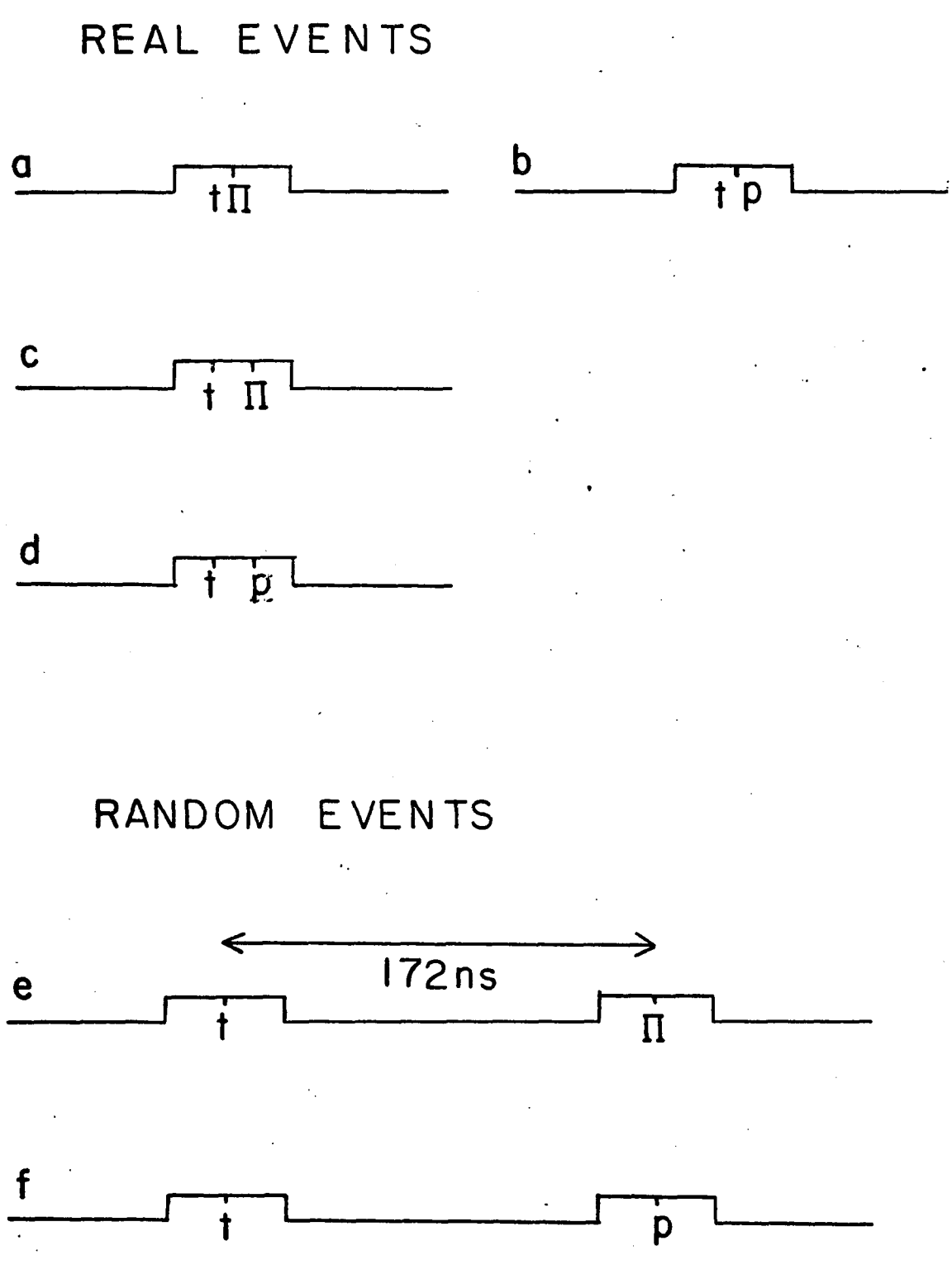

Figure 11.

Events were classified into three main categories. 1) 'Real events', 2) 'Random events', and 3) 'Pulser events'.

Real Events: These are the events with a particle on the MRS side and a particle on the right hand side in one or more of the pion telescopes. The real events would consist of four different sub-group configurations denoted by (a) through (d) in figure (11). The first group (a) consists of a pion-triton coincidence, each particle originating from the same beam burst. The second group (b) consists of a proton-triton coincidence, both of which having originated from the same beam burst. The third group (c) consists of a pion-triton coincidence, in this case they both originated from the same beam burst, but they correspond to different reactions,i.e. they were created by the reactions of different protons in the same burst. The fourth group (d) consists of a proton-triton coincidence, both of which having originated from the same beam burst but again by different reactions induced by different protons in the same burst.

Random Events: These are the events for which there was a particle on the MRS side and a particle on the right hand side in one or more of the pion telescopes but the latter originated from another beam burst 172 ns later. A delay of 172 ns inserted in the timing circuit generated this kind of events and the electronic gates defining a coincidence was wide enough to accept them. The random events consists of two different sub-groups. The first group, shown as (e) in figure 11, consists of a pion-triton coincidence where one of the particles had originated from a beam burst 172 ns later. The second group, shown as (f) in figure 11, consists of a proton-coincidence where again one of

the charged particles had originated from a beam burst 172 ns later. These artificially delayed events, consisting of (t p) and (t π) were subtracted from the 'real' events thus eliminating any 'random' coincidences occuring during a common beam burst. That is, events shown as (e) anf (f) under 'randoms' were subtracted from the 'reals' thus eliminating types (c) and (d).

Pulser Events: These were triggered by a pulser system operated at a rate proportional to the beam intensity. These events were used during off-line analysis to account for dead time of the system as defined in eqn (3.1).

3.3.1.4 Tape Format

The Honeywell magnetic tape drives wrote on tapes in IBM standard 9-track format at 800 BPI(bytes per inch). Each block of data consisted of 516 words, the first four words being fixed-format I/O control words. These control words allow the tapes to be read by any IBM standard Fortran program using the unformatted read statement. When these blocks were processed by the Fortran read subroutine in Variable Block Span (VBS) format the four control words were deleted and the remaining 512 words were passed to the program.

A file consists of a header block, any number of data blocks and a trailer block and an end-of-file (tape) mark. More than one file can be written on a tape, depending on the length of files written, tape density and the length of the tape itself. After the last file on the tape, a double tape mark is written. The header block contains user supplied run identification parameters and scaler values at the begin-

ning of each run. The scaler information was used as a tool to check the proper initialisation of each run.

The trailer block contains scaler values at the end of the run and some other additional run information such as the scaler overflow information etc. 66 scalers were used during data taking. These 66 scalers occupied words 77 through 143 of the trailer block. Each scaler consists of two words. The first word contained the high order 8 CAMAC bits as its least significant 8 bits. The second word is the low order 8 bits of the CAMAC scaler. If there is a software overflow associatd with the scaler then the most significant bit of the first word is set. After word 276 of the trailer block there is one word for each scaler that had a software overflow . To decipher the scaler words, the following formula should be used: (overflow word)X2^{24}+(1st word, low-byte)X2^{16}+(2nd word).

Each data block had more than one event in it. If the data block reached its full quota of 512 words during the middle of an event, then the rest of the words of this event were written on to the next block. Thus we had in general events crossing the block boundaries. If the data taking is stopped during the middle of a block, the rest of the data blocks were filled with -1's.

3.3.1.5 Event Structure

The event structure is shown in table 6. Each event consisted of a total of 96 words plus the addresses of the wires of the MWPC's which were hit. If there were no multiple hits on these MWPCS, then the total event length would be 96 + (3x2) = 102 words. Any event that has

TABLE 7

Thick counter Bit pattern Unit.

bit	counter
0	1
1	2
2	3
3	4
4	5
5	6
6	7
7	8
8	9
9	10
10	11
11	12
12	blank
13	14
14	blank
15	blank

Word 33 in the event structure corresponds to the event type. i.e.a real, random or pulser event. These were labelled in an event by setting a bit in the bit pattern unit. If more than one pion counter fired, then more than 1 bit of the thick counter 'bit pattern unit' was set. Decoding word 34 specifies whether it was a single event or a multiple event on the pion telescope side meaning that more than one telescope had a particle going through it at the same time.

3.3.2 Reaction (2)

3.3.2.1 General System

For reaction (2), a PDP 11/34 minicomputer was available to collect[1] data utilising the data acquisition system at LAMPF. The data were recorded on magnetic tape. Two kinds of data buffers were used, one for writing data on to a tape and the other one for on-line analysis. When the tape-write data buffer was full, data was copied on to a tape. The on-line analysis program processed the data of the analysis buffer to produce scatter plots of raw data like TOF, ΔE etc.

3.3.2.2 Data Collection

The run summary for this reaction is shown in table 8. The set of data analysed here was part of a large volume of data collected during experiment 248 at LAMPF to study the reaction $^{3,4}He(\pi^-,n)^{2,3}H$.

TABLE 8

Run summary for Reaction (2)

BEAM ENERGY (MeV)	TARGET	PROTON ANGLE (Degrees)	PROJECTILE
284	^3He	142.5	π^-
284	^4He	125.0	π^-
284	^4He	120.0	π^+
428	^3He	140.0	π^-
428	^3He	115.0	π^-
525	^4He	110.0	π^-
574	^4He	117.5	π^-

TABLE 6

Event Data Structure

Word	Source
1	-Length(of total words in the event)
2	Flag(-1 or -2)
3	Lam signal
4	Bit pattern unit
5-12	TDC
13-20	ADC
21-32	Scalers
33-34	Bit pattern unit
35	Bit pattern unit
36-47	ADC
48-59	ADC
60-71	ADC
72-79	TDC
80-87	TDC
88-95	Scaler
96	Nhits+1
97-onwards	Addresses of wires hit

a total length exceeding 102 words must have been a multiple wire event. Word 96 equals the number of wires hit +1.

The first word of each event gives the total number of words in that event(this had a negative sign). The second word was a flag word which has the value of either -1 or -2 (-2 if this was the last event of an input buffer). Word 3 characterises the LAM pattern word. 2 bit pattern units were used, one for the MRS side and the other one for the pion telescope side. The 'bit pattern unit' bit assignments for the pion telescope side is shown in table 7. Table 7 shows the 16 bits of the unit which was read as one word(word 34 in the Event Structure). The next 8 bits of this unit were read as another 8 bit word(word 33 in the Event Structure).

3.3.2.3 Tape Format

The data tapes for reaction (2) had to be copied under a different format on to other storage mediums due to the non-compatibily of these tape formats for the IBM system at William and Mary. A detailed description of the method involved in changing the tape format will be given in the section of data analysis.

For reaction (2), each block of data consisted of 520 words. The first 20 words were header words consisting of necessary run information and the rest of the 500 data words consisted of 5 events of 100 words each. Each event consisted of the following information: 8 TDC words, 16 ADC words, 8 TDC words, 48 scaler words (2 words per each scaler), 2 switch register words; the last 18 words were not used.

Chapter IV

DATA ANALYSIS

4.1 INTRODUCTION

In any detailed analysis of large volumes of data, it is essential that the format of storage of on-line data collection be the same as that of the off-line computer. Otherwise the task of handling the data off-line is very time consuming, as happened in this work. The data tapes for this work were written on two different computer systems and analysed on a third system different from the first two.

A Honeywell-316 minicomputer was used to acquire data for reaction (1) at TRIUMF and a PDP 11/34 minicomputer was utilised for reaction (2) at LAMPF. All the data tapes were read and analysed on the IBM/370 computer at the College of William and Mary. For both sets of data, the tape format had to be changed for compatibility with the IBM system. A detailed description of the procedures involved in the transformation of the data will be given in chapters 4.2.1.1 and 4.2.2.1.

4.2 TAPE REPLAY AND DATA REDUCTION

4.2.1 Reaction (1)

4.2.1.1 Data Transfer

The tapes written at TRIUMF had a density of 800 bytes per inch (BPI). The tape drives at William and Mary read tapes of 1600 BPI onwards. Hence it was necessary to change the tape density for these

data tapes. Changing the tape density also reduced the total number of data tapes (by a factor of two in our case). One of the IBM-Utility program was used to achieve this goal.

Each data file on a tape contained one or several data blocks and a data block consisted of 516 words. The first 4 words were the control words necessary for the data to be read on the IBM computer. Hence the actual data words in a block were only 512. As described in chapter 3.2.2, an event characterising a particular signature of the reaction of interest, has a variable number of data words. As a consequence, the number of event data words per block was not a constant. Parts of the event data words were written at the end of one block and the rest of it were written at the beginning of the next block resulting in event data words crossing block boundaries.

4.2.1.2 Event Analysis

The analysis was broken down into two major parts. In the first part, the data was reduced by excluding all the events that did not satisfy specific criteria which are described in detail below. The result of this analysis was the creation of a group of 12 variables characterising each event. Each event, defined by these 12 variables was stored on a magnetic tape. The scheme used to obtain these 12 variables for each event is described in detail in the following sections. Initially the chamber information on the the MRS side was extracted, the solid angle was defined for the selected tritons, and the scattering angle of the particles on the pion side established.

In the second part, the pion signature was established, by its TOF . and energy loss, dE/dx, and the kinematic calculations were done, using the information contained in the 12 variables, and the cross-section defined in equation 1.1 was calculated. The single nucleon momentum density $\emptyset^2$ was then extracted, following the procedure explained in section 4.3.1.

The reasons for dividing the analysis into two parts were: 1) The procedure for each part was quite different, and involved extensive computations. Dividing the analysis into two parts simplified the procedure, allowing to complete the first section before working on the second. 2) Much of computing time was saved by taking the information of the data in part 1 and doing the subsequent calculations in part 2, so that dealing with raw data each time was avoided.

4.2.1.3 Dead-Time correction

An efficient on line data acquisition program requires very minimal time for the computer to process the data, so that the system is almost always available for taking more data and processing them. The 'dead-time' of the system is an indication of the fraction of the total time the system was unable to process any further data. This dead-time correction must be kept as small as possible to ensure best efficiency of the data acquisition system. The typical dead-time correction for this work is 20% or less. The dead-time correction was estimated as follows. Word 4 in the event structure corresponded to the bit pattern unit for the MRS side. The pulser trigger signal was connected to bit 7 of this bit pattern unit. If this bit was set, it identified a pulser

event rather than a real one. The whole data in each run was analysed to count for these pulser events. This pulser event count, when compared to the scaler which counted the number of times the pulser was effectively triggered, gave a measure of the effective dead-time of the data acquisition system(see equation 1.1).

4.2.1.4 Part 1- Initial Analysis

The data were analysed on an event by event basis. Each event was analysed by interrogating the words of the event structure shown in table 6 in chapter 3.3.1.5. A few events were found to be non-analysable since they did not satisfy certain criteria. These events were :

1) Any event that had total data words less than 96;these were dropped because they did not contain any chamber information. The trajectories of particles for these events could not be determined. Less than 1% of the total number of events were of this kind.

2) Word 33 in the event structure was read as an eight bit word. The 3rd and 4th bit of this 8 bit word corresponded to 'random', and 'real' events respectively(see table 6). Decoding this word determined the nature of the event. There were some events for which both the 'random' and the 'real' bits were set. The data contained about 2% of these kind.

3) Due to the intermittent malfunction of the 'bit pattern unit(see table 7), for some events none of the bits in the bit pattern unit were set. Hence these events could not be classified as belonging to any specific pion channel. About 3% of the total data consisted of these events and were discarded.

4.2.1.5 Particle Identification

To identify the reaction of interest one needs to identify the proper reaction particles. For reaction (1), a pion signature in one of the pion telescopes and a triton signature on the MRS side, in coincidence, were the identification requirements.

4.2.1.6 Chamber Information

In the initial processing of the data all the wire hits in each chambers were considered for a given event, which was classified according to certain criteria. The information from the chambers (Xt,Yt) and (Xb,Yb) were used to determine the single track and multi-track events and the (Xo,Yo) chamber defined the solid angle for the particle on the MRS side.

The (Xt,Yt) and (Xb,Yb) chamber informations were decoded first to obtain the position of the particle in the focal plane. Of these 4 coordinates, only the Xt and Xb coordinates, given by the hit wire number, was decoded to calculate the position of the particle in the focal plane, given by the intersection of the straight line passing through Xt-Xb with the focal plane. All the events with single hits in both Xt and Xb were considered good. For the others, which consisted of multi-hits in Xt or Xb, the following procedure was carried out to save some of them. The reason for saving these events was that some of these multi-track hits would have been caused by the 'soft electrons' ejected from the chamber material by the reaction particles, instead of the reaction particles themselves. Criteria for saving an event were established based on the number of wire misses within the group of hit wires.

For each event the number of wires hit in Xt and Xb was calculated(Xt and Xb consisted of 512 wires each, with a wire gap of 2 mm). If the number of wires hit in either Xt or Xb was more than 5, the event was discarded. For events consisting of multiple wire hits of 5 or less, the number of misses in the wire number configuration given by the total number of wires in that configuration minus the number of wires hit, was decoded. Events with a multiple hit of 2, 3, or 4 wires, were saved, provided, the total number of wires in that configuration was less than or equal to the number of wires hit +2. Events with a multiple hit of 5 wires were saved if the total number of wires in the wire hit configuration was less than 6. This procedure was adopted for all the multi-wire hit events, regardless of the nature of the particle. For all the multi-wire hit events that were saved by the above criteria, the central value of the wires hit in Xt and Xb was obtained and was assigned as the Xt Xb coordinates for these events. We assumed the number of wires hit to be independant of the nature of reaction and particle identity.

To keep an account of the distribution of single and multiple hits in Xt and Xb, for a given run a (3X3) matrix M_{ij} where i = 0,1,and 2 and j = 0, 1, and 2 was formed. The rows of this matrix defined the hits along Xt and the columns of this matrix defined the hits along Xb. The last row and the last column contained the events that had hits of 2 or more in Xt and Xb respectively. All the multi-track events that were saved due to gap criteria were included in the (1,1) element of the matrix M_{ij}. The efficiency ε for this work was based on the efficiency of both (Xt,Yt) and (Xb,Yb) chambers combined. This efficiency was given

by the ratio of the total number of events considered good(consisting of single hits and multiple hits that were saved) to the total number of events in the whole run.

$$\varepsilon = \frac{M_{11}}{\Sigma M_{i,j}} \qquad (4.1)$$

The (Xo,Yo) chamber information was used to define the solid angle. Only those events that were saved from the Xt,Xb wire hits, were subjected to the solid angle cut. Two dimensional display of Xo,Yo was created and events with uniform distribution in this display were selected by software cuts.

The momentum of the particle on the MRS side was calculated as follows. First the x-coordinate in the focal plane, XFC, was calculated using the following equations.

$XFC = X1 + 0.01\ X2^2$, where

$X1 = (220\ Xb - 440\ Xt)/(Xb - Xt - 220)$

$X2 = (Xt - Xb + 56) - (1/4)\ X1)$

From XFC, the momentum p_s of the particle was evaluated by the relation

$$p(XFC) = p_{s0}(1 - \alpha X - \beta X^2)$$

where p_{s0} is the central momentum chosen for the particle, α = 5.485 E-14, β = 2.0 E-7, and X = (XFC-256). After defining the solid angle and the calculation of the momentum it was necessary to separate tritons from the rest of the reaction particles.

Words 9 and 18 in the event structure corresponded to the time of flight (TOF) and energy loss dE/dX of the particle in the MRS, respectively. Figure 12 is a typical two dimensional plot of TOF vs dE/

dX. Different kinds of particles are seen here clearly. The triton island is very well seperated from the rest of the reaction particles. Tritons were selected by applying software cuts on both the TOF and dE/dX. These cuts have to be changed for each different configurations of the MRS setting, since the triton island shifted on this TOF-dE/dX plot for different MRS setting.

4.2.1.7 Pions

Interrogating word 34 in the event structure(see table 6) gave the information as to which one of the pion telescopes generated a signal, indicating the presence of a charged particle. Bits from 0 to 13 excluding bit 12 was used for counters starting from 1 through 14(slot 12 was left blank since counter 13 did not exist). Once this information was decoded, the other quantities like the TOF and the pulse height of this particle were obtained by interrogating the corresponding TDC and ADC channels(words 36 to 87 in the event structure shown in table 6). In the off-line analysis only the thick pion counter pulse height information was taken into account, since the pulse height resolution was better for the thick counter than for the thin counter.

Displays were created for the time-of-flight for each one of the pion channels. A typical time-of-flight spectrum is shown in figure 13. Though pions and protons seem to be well separated in this spectrum, the left tail of the proton spectrum extends well into the pion region. This indicated that the pions have to be seperated by two software cuts. The selection of a pion was hence done with a correlated cut, the first cut was imposed in part 1, and the final cut in part 2 of

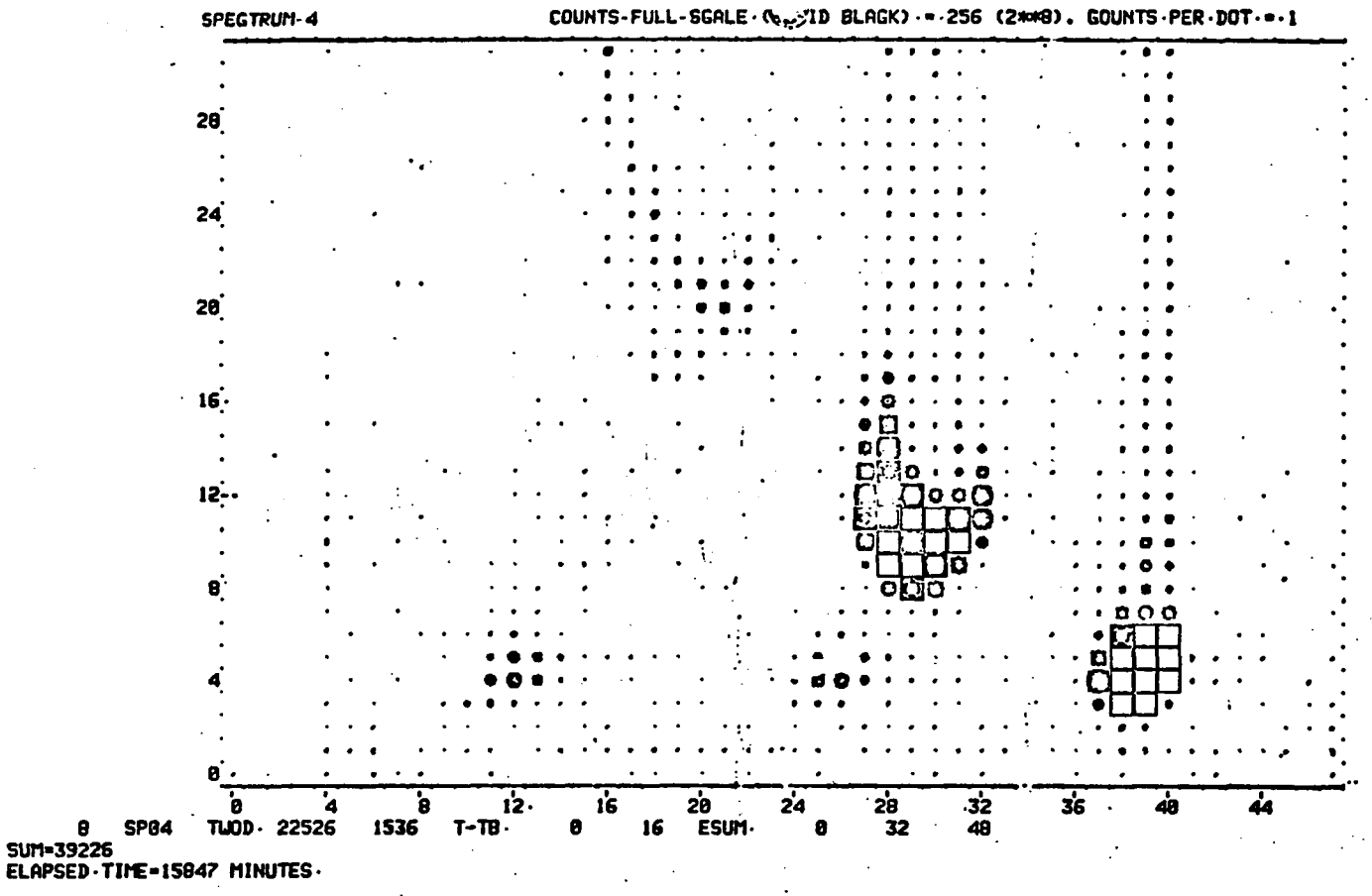
SPECTRUM-4
COUNTS-FULL-SCALE-(MID BLACK)-=-256 (2**8). COUNTS-PER-DOT-=-1
28
24
20
16
12
8
4
0
0 4 8 12 16 20 24 28 32 36 40 44
0 SP04 TWOD- 22526 1536 T-TB- 0 16 ESUM- 0 32 48
SUM=39226
ELAPSED-TIME=15847 MINUTES-

Figure 12.

the analysis. Non-pions were eliminated in part 1, by putting software cuts in the TOF spectrum. To make sure we eliminated non-pions, for those events that did not survive the TOF cut, their corresponding pulse height was displayed and compared with the raw pulse height spectrum and indeed the eliminated events had TOF different from that for pions. Events that survived the TOF cut consisted of both pions and protons. Elimination of the protons from this group will be discussed in part 2.

Each event consisting of a triton with a given momentum on the MRS side, and a mixture of protons and pions on the pion side, was characterised by 12 variables: the pion channel, the energy deposited by the particle in the pion channel, its pulse height, its TOF, the TOF of the triton, its pulse height, the 'real'-'random' signature, the momentum of the triton, its position in the focal plane, the Xo and the Yo wire hit information, and lastly a tag for those multiple wire hit events that were saved and given the central value in the X0,Y0 wire hits.

4.2.1.8 Part 2 - Final Analysis

The second part, involving also event by event analysis, used the results of the first part. Since the momentum of the triton has been calculated for each event, momentum acceptance cuts were applied to eliminate the tritons on the MRS side that had momentum larger than the acceptance cuts, which were taken to be $\pm$ 12%. For the events that survived the momentum acceptance cut, the signature of a pion was then analysed. The particles chosen on the pion side from the TOF cuts made in part 1, still contained some protons. A display of pulse height

Figure 13.

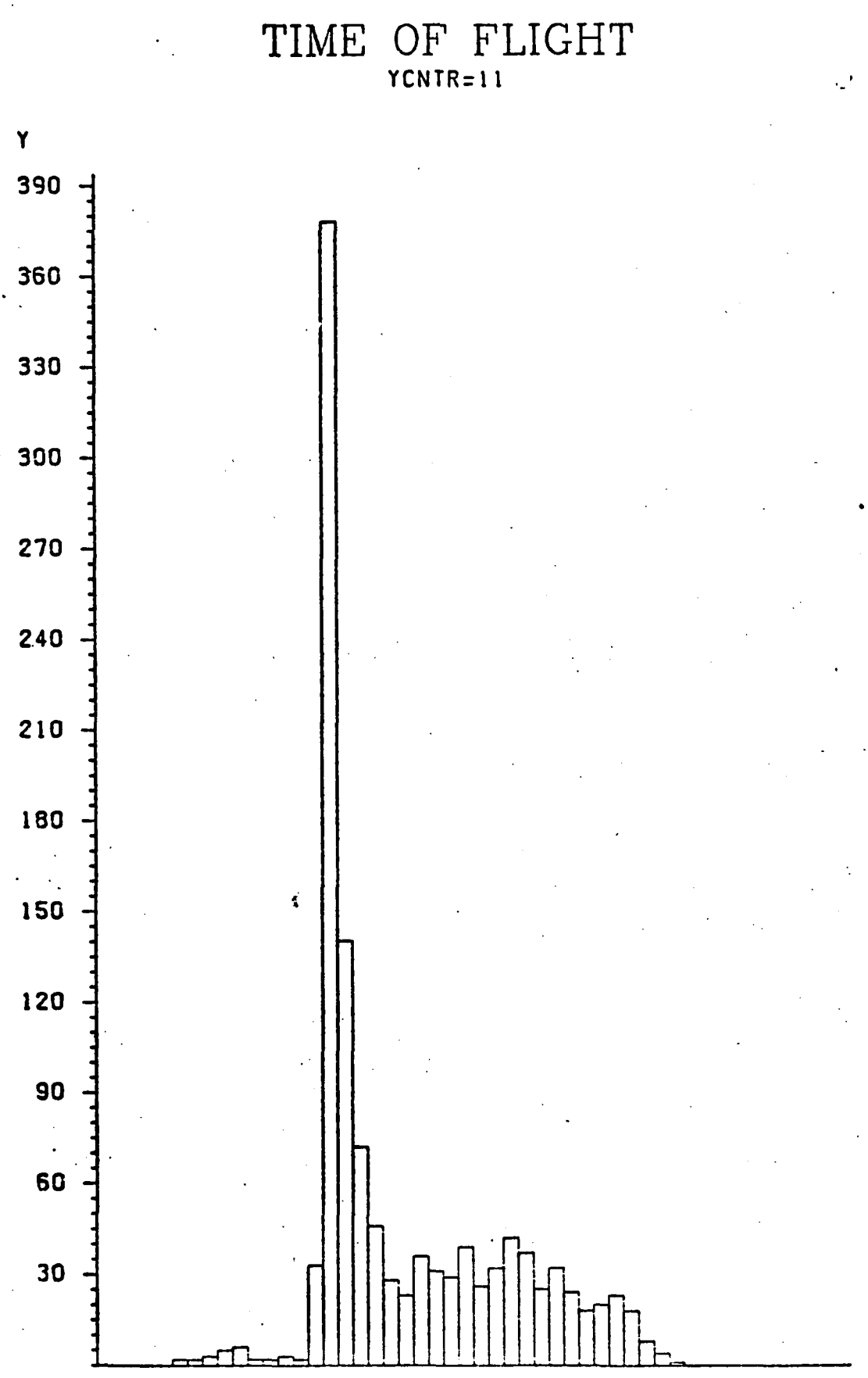
TIME OF FLIGHT
YCNTR=11
Y
390
360
330
300
270
240
210
180
150
120
90
60
30

spectrum for these particles is shown in figure 14. Protons and pions are seen well separated in this spectrum. Software cuts were applied to eliminate the protons thus leaving a sample of $t\pi$ events consisting of 'reals' and 'randoms'.

A kinematic program was then used to calculate the following kinematic variables; the momentun of the pion, p_4, the momentum of the recoil proton, p_5, its two direction angles, θ_5 and ϕ_5, and the three invariant masses M_{34}, M_{45}, and M_{35}, defined in equation 5.2. A 3 dimensional binning was created to classify the events according to three of the measured variables, the momentum of the triton, p_3, the triton scattering angle θ_3, and the scattering angle of the pion, θ_4.

This binning was done seperately for 'reals' and 'randoms'. As discussed in section 3.3.1.3, 'reals' contained some 'random' events corresponding to reaction particles created by different beam protons of the same beam burst. To eliminate these 'randoms', we removed for every event in the sample of artificially created 'random' events in a given bin of p_3, θ_3, and θ_4 an event in the corresponding bin for 'real'. This method guaranteed that for an event that was counted as 'randoms', an event of similar signature was eliminated from the sample of 'reals'. This resulted in the final sample of $t\pi$ events.

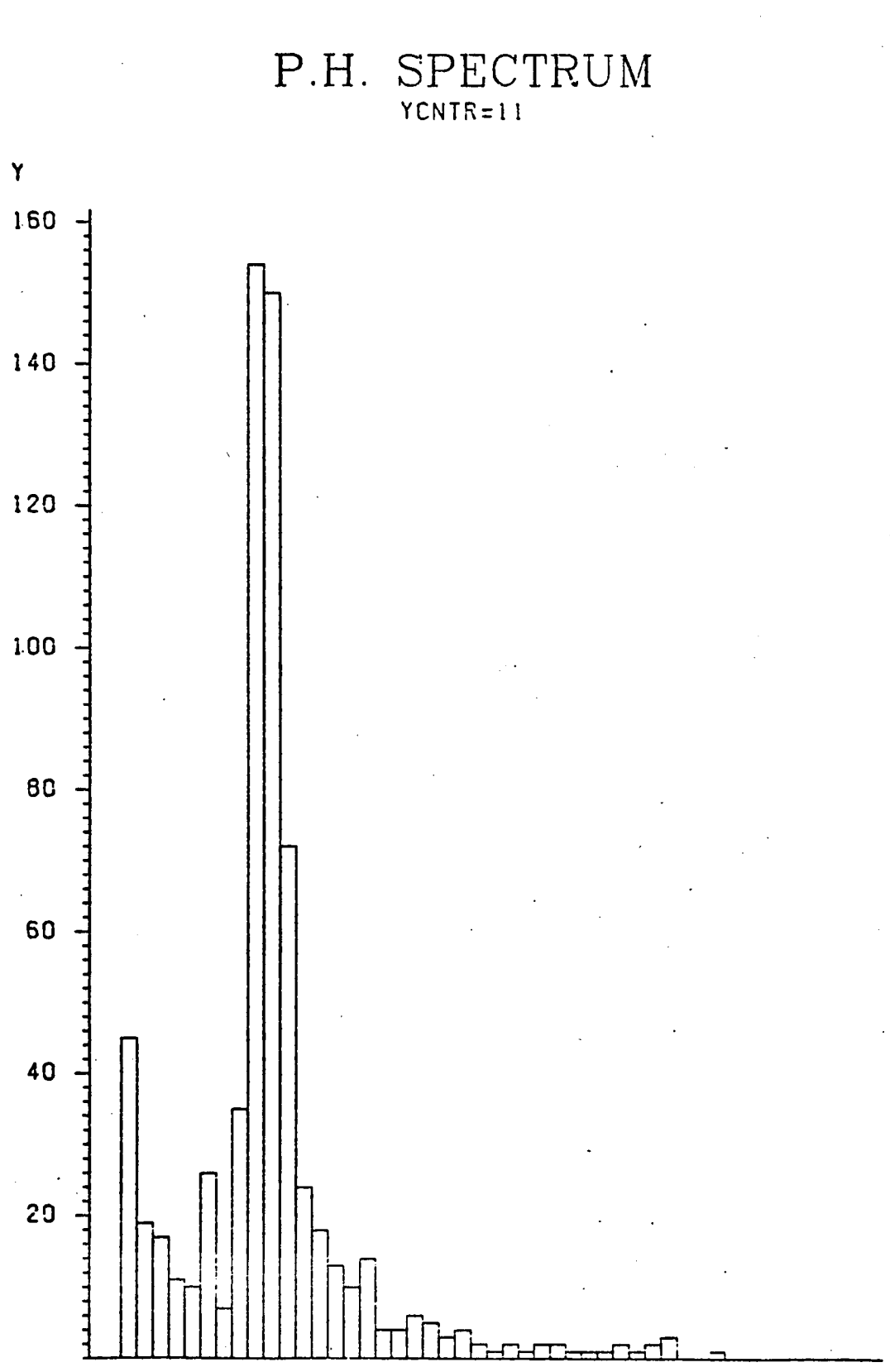

Figure 14.

4.2.2 Reaction (2)

4.2.2.1 Data Transfer

The data tapes for reaction (2) were written with a PDP 11/34 computer. Each data word written by this computer consisted of 2 bytes of 8 bits each. The order of bytes had to be reversed when this data was read on an IBM computer, because the low order byte on the PDP corresponds to the high order byte on the IBM. To achieve this task the program 'Flipbyte.PL1' was written in Programming Language 1(PL1). This PL1 program reversed the byte order in about 20 seconds for a whole tape, reducing the computer CPU time by a factor of 10 if the same had been attempted by a FORTRAN program.

4.2.2.2 Event Analysis

Each of the three counters S1, S2, and S3 was viewed by two P.M. tubes which gave two different measurements of ΔE. The net signal from each one of these counters was defined as the geometric average i.e. S1= S1A.S1B etc, where A and B stand for the pulse height of the two P.M. tube signals. Gathering signal from both sides of these counters minimized the position dependence and improved the time resolution for the time-of-flight measurements. The pulses from each one of the scintillators had to be corrected with respect to each other, so that the same pulse height corresponded to a given DE in each one of them. The scintillator normalisations required the empirical determination of the 4 constants $\Delta 1$, $\Delta 2$, $\Delta 3$, $\Delta 4$, defined by $\Delta 1\ L1 = \Delta 2\ L2 = \Delta 3\ L3 = \Delta 4\ L4$, where in each case L_i is the pulse height from the i^{th} scintillator for a given energy deposition DE. For a detailed description of the

evaluation of these constants refer to[27]. The total energy E was defined as E = DE1 + DE2 + DE3 + DE4, where DE1, DE2, DE3, and DE4, were the energy deposited in each one of the four counters. The calibration for the pulse height versus energy will be given in section 4.2.2.4.

Counter S4 was viewed by only one PM tube. Since S4 was quite long (508 mm), a position response correction had to be applied for the signals collected from S4. The measured signal from S4 was multiplied by the factor $f(x) = 0.00047x + 1.0333$, obtained by calibration, where $-254 \text{ mm} < x < 254 \text{ mm}$, and is the position of the particle in S4, measured in mm from the center.

Event by event analysis of the data was done as follows:

1) DE1, DE2, DE3, and DE4 were determined by reading the corresponding ADC words.

2) A subroutine was incorporated in the main program, which tested the data from a MWPC. These MWPCs were external delay-line chambers(2.5 nsec/cm). A sum time calculation was performed for each one of the planes of each MWPC. The sum of the time signals t_1 and t_2, given by the propagation signal from opposite sides of the planes was calculated. If this summed time did not fall within the prescribed limits, the chamber was deemed to have misfired.

3) For events with good sum times, the position (x1,y1) and (x2,y2) were calculated from MWPC1 and MWPC2 respectively. From these two pairs of coordinates, direction tangents were drawn and the scattering angle θ was computed. The trajectory of the particle was calculated from this information.

4) From (x,y) coordinates in each chamber, the intercept of the trajectory at the target location was extracted. If the trajectories did not originate from the target cell, the event was rejected.

5) The times of flight T21 = S2-S1 and T31 = S3-S1 were calculated(see figure 8), but only the T31 information was used in the analysis. From the TOF, ΔE, and E two-dimensional plots of TOF - E and E- ΔE were created to identify the reaction particles of interest. Some typical scatter plots of ΔE vs E and TOF vs E are shown in figure 15. The mass separation for different reaction particles is well seen in this plot. Protons were selected by the appropriate software cuts in the TOF spectrum. The data was then binned in angles of 28^{o}(the angular acceptance of the detector was 30.8^{o}).

4.2.2.3 Dead-Time correction

A scintillator telescope, used as beam monitor, monitored the forward muon halo from the decay $\pi^{-} \rightarrow \mu^{-} + \nu_{\mu}$. Two scalers were connected with this beam monitor. One of the scalers was computer-gated and the other one not computer gated. The ratio of the computer gated to the non-computer gated was scalers was used to apply a dead-time correction.

4.2.2.4 Calibration

Several calibration runs were taken with the detector placed in the beam, $\theta_{D} = 0^{o}$. Tuning the P^{3} channel to a given momentum for π^{+}, fluxes of protons, deuterons, and tritons of the same momentum were present as beam contaminants. The mean ADC channel(pulse height) for each of these

particles were obtained for beam momentums of 450, 550, and 650 MeV/c. A calibration curve was drawn with the kinetic energy of the detected particles versus the ADC channels. ADC channel - energy relation was obtained by a linear fit, as shown in figure 16.

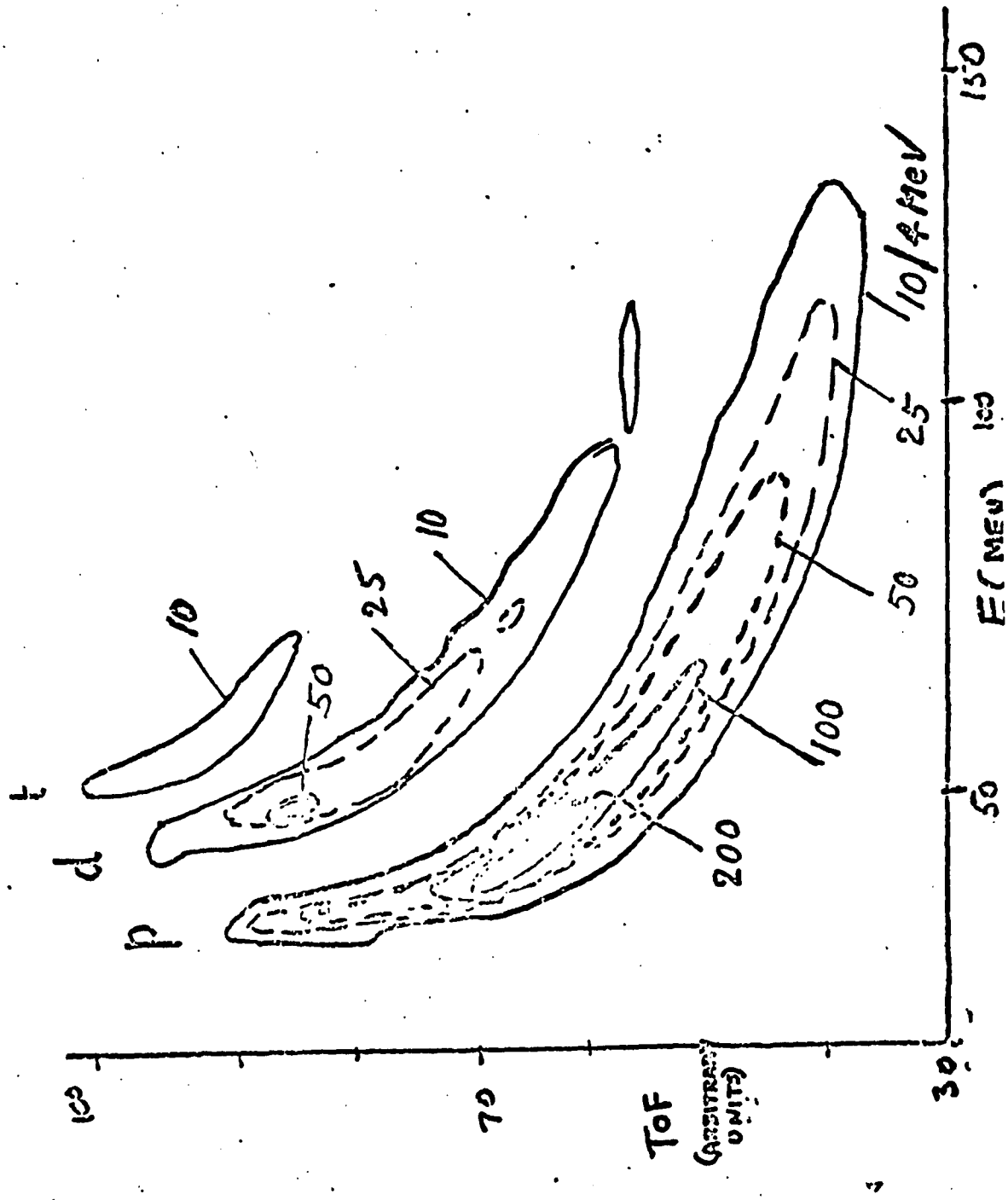
10
25
50
10
25
50
100
200
1/10/4 MeV
E (MeV)
TOF
(ARBITRARY UNITS)
d
p
150
100
50
70
30

Figure 15.

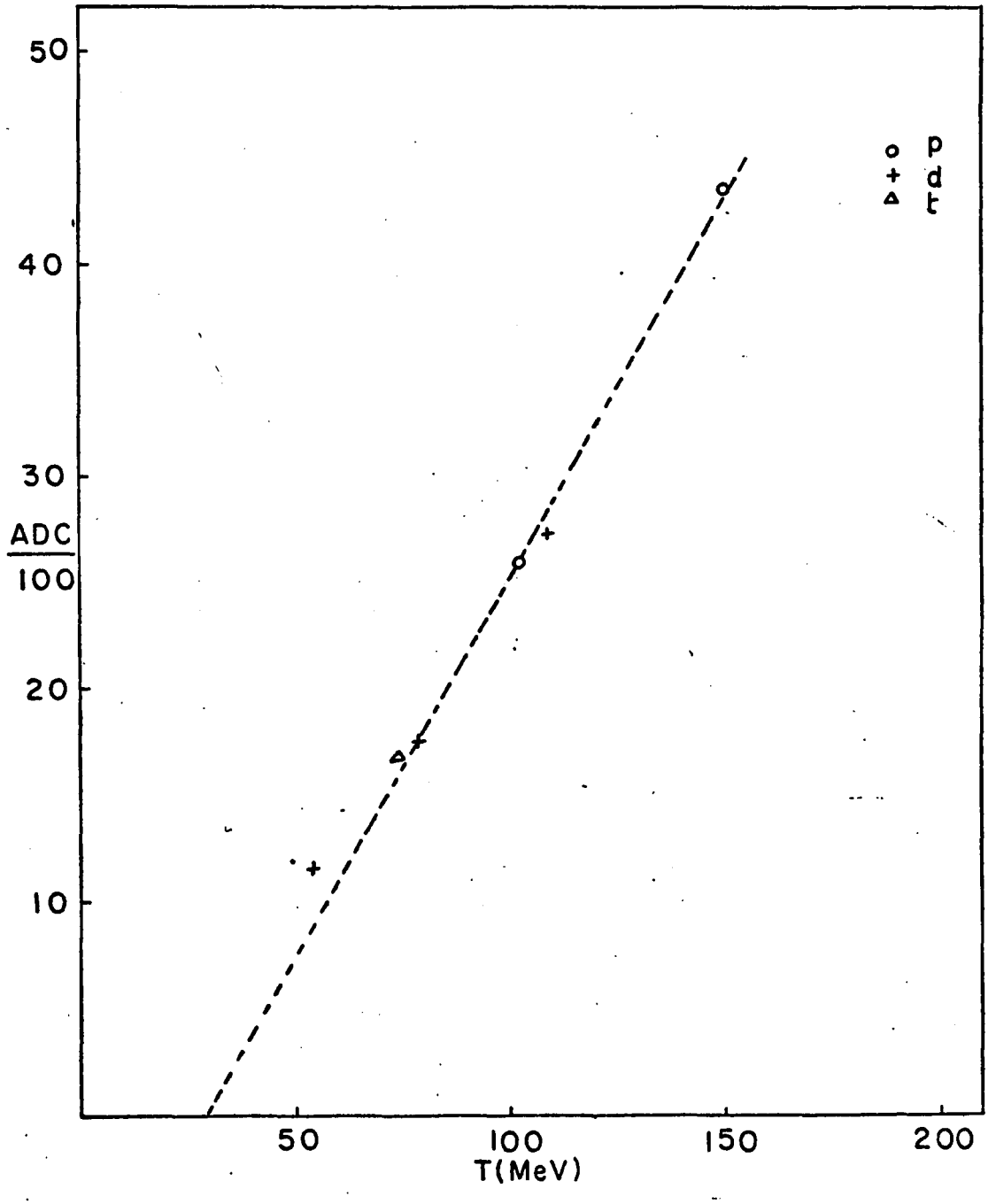

Figure 16.

4.3 CALCULATION OF THE CROSS-SECTIONS

4.3.1 Reaction (1)

The fifth order differential cross-section to be extracted from the data is given by

$$d^5\sigma/d\Omega_3 d\Omega_4 dp_3 = \frac{N(\Delta p_3)}{I\ N_{tgt}\ \varepsilon\ DT\ \Delta\Omega_3\ \Delta\Omega_4\ \Delta p_3} \qquad (4.2)$$

where $N(\Delta p_3)$ is the number of events in a given triton momentum bin, I is the number of beam protons incident on the target, N_{tgt} is the number of target nuclei per cm^2, ε is the efficiency of the system, $\Delta\Omega_3$ and $\Delta\Omega_4$ are the solid angles for the triton and the pion respectively and Δp_3 is the size of the momentum interval used for binning the data, DT is the correction factor for the dead-time of the data-acquisition system.

The number of beam protons incident on the target I, is determined by the monitor count;it is obtained from the sum of proton-proton events due to the scattering of the protons by the CH_2 target of the polarimeter. Two pairs of telescopes placed symmetrically on either side of the beam line measured these events. i.e.the number of monitor counts is given by the sum of the coincidence events in these two telescopes. The polarimeter has been calibrated previously against a Faraday cup installed in the beam line. The actual number of protons in the beam is given by

$$\frac{\text{Number of monitor counts}}{(C\ e)}$$

where e is the electronic charge, and C is the calibration factor and is given by C = 400 counts per nano-coulomb.

The efficiency of the system in this work is defined by the efficiency of the (Xt,Xb) wire hits, given in equation 4.1. The solid

angle for the triton $\Delta\Omega_3$ is defined by the cuts on the trajectories in the (Xo,Yo) chamber, the cut on Xo defining the vertical acceptance and the cut on Yo the horizontal acceptance. For the pions, the solid angle $\Delta\Omega_4$ is a product of the acceptance in the scattering angle θ_4 and the acceptance in the azimuthal angle ϕ_4 of each pion counter. In this work all the pion counters were positioned in the plane of the beam axis. $\Delta\Omega_4$ is given by the ratio of the area of the counters to the distance of the counters from the target to the square. The pion counters were not all positioned at the same distances from the target since the angular separation between the neighboring counters were not equal for all the counters(see table 2). The typical value of $\Delta\Omega_4$ is 3 msr.

To compare the results with the IA, a momentum density distribution was extracted from the cross-section in the following way:

$$\phi^2(p_s) = \frac{d^5\sigma/d\Omega_3\ d\Omega_4\ dp_3}{K\ (\frac{d\sigma}{d\Omega})^{cm}_{pd->t\pi}} \qquad (4.3)$$

where the pd->tπ cross section is to be taken at the collision energy squared $s = M_{34}^2$ and the momentum transfer t_{14}(see figure 2). The kinematic factor K is

$$K = \frac{M_{34}^2\ p_3^2\ p_4^2\ E_s}{E_3\ E_4\ p_1\ (p_4\ E_s - p_s\ E_4\ \cos\theta_{45})} \qquad (4.4)$$

where θ_{45} is the angle between the pion and the recoil proton.

4.3.1.1 pd->tπ data

In the extraction of the single nucleon momentum density ϕ^2 defined in equation 4.3, the kinematic factor k and the fifth differen-

tial cross-section $d^5\sigma$ were calculated. The pd -> tπ differential cross-section was obtained from the data in the literature, in the neighborhood of the five proton energies 350, 465, 500, 600, and 800 MeV. These data have been taken from the work of [28-35].

The collision energy T_{16} between the incoming proton and the quasi-deuteron, defined as

$$T_{16} = \frac{M_{34}^2 - (M_1 + M_6)^2}{2M_6} \qquad (4.5)$$

where $M_6 = M_d$(on-shell approximation), and the pion scattering angle $\theta_{\pi cm}$, defined as

$$\theta_{\pi cm} = \frac{t_{14} - M_1^2 - M_4^2 + 2\,E_1E_{4cm}}{2\,p_{1cm}\,p_{4cm}} \qquad (4.6)$$

corresponding to the momentum transfer squared t_{14}, where $t_{14} = M_1^2 + M_4^2 - 2(E_1E_4 - p_1p_4\cos\theta_4)$, were calculated for each event. The value of T_{16} varied between 250 MeV and 800 MeV for the different kinematical conditions. The following procedure was carried out to get an estimate of the pd -> tπ cross-section at the different values of T_{16}. In the first step, the pd -> tπ cross-section data at each of the energies available were fitted using a 7^{th} order polynomial. From the eight coefficients obtained, the pd -> tπ cross-section for a given $\theta_{\pi cm}$ was evaluated for each one of the five energies. In the second step, the value of the cross-section at the specific value of the collisison energy T_{16} was calculated using Legendre interpolation formula(taken from [36]):

$$Y(x) = |(x-x1)(x-x2)\ldots(x-xn)/(x0-x1)(x0-x2)\ldots(x0-xn)|y_0$$
$$+ |(x-x0)(x-x2)\ldots(x-xn)/(x1-x0)(x1-x2)\ldots(x1-xn)|y_1$$

$$+ \ldots\ldots\ldots\ldots$$

$$+ \left|(x-x0)(x-x1)\ldots(x-xn-1)/(xn-x0)(xn-x1)\ldots(xn-xn-1)\right| y_n$$

given $y_0=y(x0)$, $y_1=y(x1)$, $y_2=y(x2)$,.....$y_n=y(xn)$. The pd -> tπ data used here along with the polynomial fit are shown in figures 17-21, and also tabulated in tables A-E in the appendix.

4.3.1.2 Reaction (2)

The invariant cross-section E $d\sigma/d\Omega$ p^2 dp as a function of the missing mass $M_X^2 = (P_\pi + P_{tgt} - P_p)^2$ where P_π, P_{tgt}, and P_p are the four vectors of the incident pion, the target, and the detected proton, was calculated. The invariant cross-section is given by

$$E \quad d\sigma/d\Omega \quad p^2 \quad dp = \frac{\text{Number of protons}}{\Delta\Omega \; N_\pi \; N_{tgt} \; p^2 \; \Delta p} \qquad (4.7)$$

where $\Delta\Omega = \Delta\phi\Delta\theta$

N_π = Number of pions incident on the target

N_t = Number of target particles, given by,

$$N_t = \frac{\text{Avogadro's Number X Effective target density}}{\text{Mass of target in g per mole}} \qquad (4.8)$$

N_π is given by the normalised ion chamber count. The solid angle for this work is 73 msr. Δp is the momentum acceptance of the event bin in MeV/c.

Chapter V

RESULTS

5.1 REACTION (1)

5.1.1 Introduction

For this reaction the data were taken at the two different proton beam energies of 506 MeV and 460 Mev. The data at 506 MeV consists of 6 groups, each one characterised by the average triton angle and the average triton momentum, determined by the MRS position and tuning respectively. The data at 460 MeV consists of three groups.

5.1.2 Kinematics

Before discussing the results of this work, a brief description of the calculation of various kinematical quantities will be given here. The recoil proton momentum was reconstructed event-by-event from the triton momentum, p_3, its two scattering angles, ϕ_3 and θ_3, and the pion scattering angle, $\theta_4(\phi_4=0)$. For any given event, the total momentum of particles 4 and 5,

$$P_{45} = p_1 - p_3 = p_4 + p_5, \text{ and energy}$$

$$E_{45} = E_1 + M_2 - E_3 = E_4 + E_5$$

where the indices 1, 2, 3, 4, and 5 represent the incident proton, the target, the triton, the pion, and the recoil proton respectively, were calculated. The invariant mass squared of the particle pair 45 is given by

$M_{4s}^2 = E_{4s}^2 - P_{4s}^2$. The momentum of the pion p_4 was then obtained from

$$p_4 = \frac{P_{4s}\cos\alpha\ \varepsilon^2 + E_{4s}\ A}{2\ B} \qquad (5.1)$$

where $\varepsilon^2 = M_{4s}^2 - M_s^2 + M_4^2$, α is the steric angle between P_{4s} and p_4, $A = \varepsilon_{4s}^2 - 4M_4^2\ B$, and $B = (E_{4s}^2 - P_{4s}^2\cos^2\alpha)$.

The recoil momentum of the proton, p_s, was then calculated from

$$|p_s| = |P_{4s} - p_4|.$$

The invariant mass squared of the pair 35 is given by

$$M_{3s}^2 = E_{3s}^2 - P_{3s}^2 \qquad (5.2)$$

where $E_{3s} = E_1 - M_2 - E_4$ and

$$P_{3s} = p_1 - p_4.$$

Knowing M_{4s}^2 and M_{3s}^2, the other invariant mass squared M_{34}^2 can be obtained from the relation

$M_{34}^2 = (M_1^2 + M_2^2 + M_3^2 + M_4^2 + M_s^2 + 2\ E_1M_2 - M_{4s}^2 - M_{3s}^2)$.

For a given pion counter the cross-section $d^5\sigma$, and the recoil proton distribution density $\emptyset^2$, were displayed as a function of p_s.

5.1.3 General Discussion

The fifth order differential cross-section

$$d^5\sigma/d\Omega_3\ d\Omega_4\ dp_3$$

was calculated using equation 4.2 for central values of the triton momentum, p_3 = 1.11, 1.02, .95, .85, .82, and .76 GeV/c at the beam energy of 506 MeV, and at p_3 = 1.08, .90, and .76 GeV/c at the beam energy of 460 MeV. Background subtraction was done as explained in section 4.2.1.8. These cross-sections are shown as a function of the proton re-

coil momentum p_s in figures 22-30. Plots of the proton momentum density ϕ^2 defined in equation 1.2, and extracted from these cross-section data for the different values of p_s using 4.3 and 4.4 are shown in figures 31-39. These figures display only the statistically significant data obtained in this experiment. The error bars shown represent the statistical errors only.

The discussion of the data will be done in sections 5.1.4. and 5.1.5. In part 1, the general behavior of the data that follows the I.A. graph shown in figure (2) will be discussed, whereas the portion of the data that does not follow the I.A. graph will be considered in part 2.

To aid in identifying the I.A. region in these data, we will compare the proton momentum density distribution, ϕ^2 extracted from this work with the ϕ^2 extracted from the most recent (e,e'p) data of Jans et.al.[9] The momentum distribution ϕ^2 versus the recoil proton momentum p_s, of the electron data is shown in figure 44. The value of the normalised integral $4\pi\ \phi^2 p^2 dp$, evaluated up to the maximum recoil momentum of 305 MeV/c, obtained from the electron data is 1.62 ± 0.14. This number, also called the spectroscopic factor, should be equal to the number of protons in ^{3}He, i.e. 2 in the limit of exact validity of the impulse approximation. The lower value for the spectroscopic factor obtained in the electron data is an indication of the presence of final state interactions or of more complicated processes.

A kinematical plot of the proton recoil momentum versus the triton momentum for a beam energy of 506 MeV and triton angle of 14.8o is shown in figure 45 as an illustration of the complexity of the kine-

matics in this experiment. Each one of the curves labelled 1 through 13 corresponds to one of the pion telescopes used(see table 2), covering the range from 22° to 99.6°. The momentum acceptance of the MRS was taken to be ± 12%. It can be seen from this plot that for many central values of p_3 some of the pion channels have the same value of p_5 for two different values of p_3 that are well within the momentum acceptance of the MRS. Also zero recoil momentum occurs in two pion channels, and therefore at two values of p_3. These two values of p_3 for which there is zero recoil wil be referred to as the high and low p_3 solutions in the text. The features of this plot will be used in explaining the behaviour of the data in the following sections.

The range of values of the three invariant masses, M_{34}, M_{45}, and M_{35}, of the three pairs of particles, tπ, πp, tp, covered in this data are between 2.96-3.17, 1.11-1.28, and 3.78-3.93 GeV, respectively. The range of invariant masses of the $M_{\pi p}$ sytem spans the (3,3) resonance region. The data of this work cover a proton recoil momentum range from 0 to 350 MeV/c.

5.1.4 Part 1

First consider the 506 MeV data for the highest p_3 central value of 1.11 GeV/c shown in figure 22. The angular range of the pion telescopes covered in these data is from 46.7° to 99.6°. The corresponding recoil momentum of the proton goes from 0 to 270 MeV/c. The plot of $\emptyset^2$ for the same data is shown in figure 31. The single nucleon momentum density is maximum when the recoil momentum is 0, as expected from the momentum distribution of an S state. To guide the eye, the

electron data is shown as dotted lines in the same figure. The value of the momentum density corresponding to zero recoil is 9.3 ± 0.6 GeV/c^{-3} to be compared with the value of 6.8 ± 0.4 obtained by Jans et.al. Both the $d^5\sigma$ and the $\emptyset^2$ data show two different branches. The lower branch falls off smoothly and compares well with the shape of $\emptyset^2$ from the electron data upto a recoil momentum of 120 MeV/c. The data points in the lower branch of the $\emptyset^2$ curve correspond to pion angles smaller than 68^o. The other branch has a slower fall off in $\emptyset^2$;it comes from the backward pion counters. Thus the $\emptyset^2$ data has a strong pion angle dependance, whereas the I.A. predicts no such θ_4 dependance, as $\emptyset^2$ is a property of the target and not the reaction. The separation into two branches, might be due to the on-shell prescription and the free pd -> tπ cross-section data used in the calculation of $\emptyset^2$ or to the combination of non I.A. processes. A further discussion of the portion of the data that does not follow the I.A. graph can be found in part 2.

The cross-sections and $\emptyset^2$ for all the other data at this beam energy are shown in figures 23-27 and 32-36. Except for the data at p_3 central = 0.950 and 0.760 GeV/c all the other data have two branches in the $\emptyset^2$ plots. The lower branch in all these data have a uniform fall off in $\emptyset^2$ with small differences in slopes and absolute values. The data at p_3 central = 1.02, and 0.850 GeV/c and for triton angle of 18^o does not reach down to zero recoil momentum for kinematic reasons. In free pd -> tπ, the maximum possible triton angle is 16^o. A larger triton angle can only occur for a non-zero recoil. The cross-section and $\emptyset^2$ for the data at a beam energy of 460 MeV are shown in figures 28-30 and figures 37-39, respectively. The data at p_3 central = 0.760 GeV/c

have two branches in the $\emptyset^2$ plot whereas such a feature is absent in the other two data corresponding to p_s = 1.08 and .900 GeV/c respectively.

TABLE 9

$d^5\sigma$ and $\emptyset^2$ values for zero recoil

Beam energy	MRS momentum (MeV/c)	MRS angle degrees	$d^5\sigma$ E-29 cm^2/ster GeV/c	$\emptyset^2$E2 GeV/c^{-3}
506 MeV	1.110(a)	14.63	26.4 ± 1.8	9.34 ± 0.6
	0.950(b)	14.7	13.44± 1.9	1.86 ± 0.3
	0.820(b)	14.8	25.17± 1.7	2.2 ± 0.2
	0.820(b)	14.8	13.78± 1.1	1.9 ± 0.2
	0.760(b)	14.8	19.44± 1.2	1.7 ± 0.2
	0.760(b)	14.8	10.0 ± 1.2	1.4 ± 0.2
	1.020(c)	14.8	25.0 ± 2.0	8.0 ± 0.6
	0.850(c)	14.8	20.0 ± 2.0	6.0 ± 0.5
460 MeV	1.080(a)	14.8	15.51± 2.3	6.69 ± 1.0
	0.900(b)	14.8	19.48± 3.0	5.44 ± 0.8
	0.900(a)	14.8	14.47± 2.7	6.32 ± 1.2
	0.700(b)	14.8	11.77± 1.5	3.28 ± 0.4

(a) These correspond to zero recoil solution close to high p_s.
(b) These correspond to zero recoil solution close to low p_s.
(c) These $\emptyset^2$ are extrapolated values at zero recoil.

The zero recoil momentum densities for the 506 MeV and 460 Mev data are shown in table 9. The zero recoil momentum densities cover a wide range of $\emptyset^2$ values. The values of $\emptyset^2$ near zero recoil corresponding to the low p_s solution(denoted by (b) in table 9) for 506 MeV data are all compatible. The average value of $\emptyset^2$ for these 5 data points is 1.81 ±0.3. The single nucleon momentum density for the data at p_s central of 1.11 GeV/c does not seem to be compatible with the values obtained at the other data points. The average value of $\emptyset^2$ at the beam

energy of 460 Mev corresponding to the low p_s solution is 4.36 $\pm$1.5. For the high p_s solution the average values of $\emptyset^2$ is 6.50$\pm$1.1. The average values of $\emptyset^2$ corresponding to the two solutions for p_s at the two energies considered here are shown in table 10 along with the value obtained from the electron data. It is obvious that there is a disagreement between this data and the electron data especially for the data of this work taken at the higher beam energy.

TABLE 10

Average values of $\emptyset^2$ in GeV/c^{-3}

	506 MeV	460 MeV	electron data
High p_s	9.34 $\pm$ 0.6	6.50 $\pm$ 1.1	6.75 $\pm$.3
Low p_s	1.81 $\pm$ 0.3	4.36 $\pm$ 0.6	

The value of the momentum distribution $\emptyset^2$ at zero recoil for the different beam energies are not compatible. The reason for the non compatibility of the $\emptyset^2$ values at zero recoil momentum could have stemmed from the values for the pd -> tπ cross-section data used in evaluating $\emptyset^2$.

5.1.5 Part 2

The data for the p_s central values of .850 at 18^o and .820, and .760 GeV/c at 14.8^o at the beam energy of 506 MeV, and for a central value of p_s = .760 GeV/c at 14.8^o at the beam energy of 460 MeV, are shown in figures 40-43 for a few selected pion channels. The selection

of a certain portion of the data is done to emphasize the absence of the I.A. behavior in the data and the existance of another feature at large recoil where the I.A. process does not contribute appreciably. A wide enhancement is seen at a recoil momenta from about 200 to 300 MeV/c. At the peak of this bump the invariant mass $M_{3,5}$ is equal to the sum of the physical masses of a triton and a proton indicating that these two particles are moving with the same relative velocity in their rest frame. Indeed the value of the triton momentum is about three times the recoil proton. The invariant mass of the proton-pion pair $M_{4,5}$ at this bump is about 40 MeV above the Δ mass of 1236 MeV. Considering the large width of a free Δ, it is possible that this enhancement is due to final state interaction within either the tp pair or the $p\pi$ pair. The original motivation of this experiment was in fact to study an expected resonance behavior in the πp system. But we see an enhancement in a kinematic region where both the tp system and the πp system are likely to contribute strongly at the peak of this enhancement. It should be emphasised that the enhancement is not created in the process of dividing the measured $d^5\sigma$ by the pd -> tπ cross-section, since it is already visible in the $d^5\sigma$ data. The enhancement seen is not due to double pion production since at 506 MeV we are just at the threshold for single pion production.

5.1.5.1 Conclusions

We have found that a portion of the data follows the prediction of the I.A. of figure (2) rather well in shape, upto a recoil momentum of 120 MeV/c. Beyond this momentum range, the data is sugges-

tive of final state interaction in the tp and πp system. The value of $\emptyset^2$ at zero recoil obtained in this work are scattered around the value obtained by Jans et.al.[9] More data would be needed near the proton recoil momentum of 300 MeV/c, or above to establish the origin of the enhancement seen in the data. Also the values of $\emptyset^2$ extracted from the data and seen in table 10 suggest that they are not converging towards a unique value, contrary to the expectation based on the I.A. There are other non-I.A. graphs, which might explain the behavior of the portions of the data in this work where the I.A. model seems to be non-applicable. Two such graphs are shown in figure 46.

5.2 REACTION (2)

The invariant cross-sections $E\, d\sigma/p^2\, d\Omega\, dp$ for the reaction $^{3,4}He(\pi^{\pm},p)X$ and the missing mass squared $M_x^2 = (P_\pi + P_{tgt} - P_p)^2$, where P_π, P_{tgt} and P_p are the four vector momenta of the incident pion, the target and the detected proton respectively, were calculated from the data according to the method described in section 4.2. Preliminary results in terms of the inclusive cross-section $d\sigma/d\Omega\, dT_p$, for a pion energy of 284 MeV, have been reported earlier.[38]

There are several possible Feynmann graphs one can think of which contribute to the reaction $^{3,4}He(\pi^{\pm},p)X$. Three graphs are most relevant to this work and will be discussed here; they are shown in figure 47 for the case of π^- and ^3He, namely quasi-free scattering (QFS), quasi-free absorption (QFA), and final state interactions (FSI) among the unobserved constituents of X. Figure 47 (a) represents the absorption of a pion on a pp pair. Figure 47 (b) shows scattering of a pion on a single nucleon. Figure 47 (c) is a possible graph showing FSI between the π^- and two nucleons.

Consider first the data for the reaction $\pi^- + {}^3He$. The proton was detected backward in the lab and had a kinetic energy between 50 and 150 MeV. The probability that the detected proton is a spectator is small because the energy of this proton corresponds to a very large internal momentum in the nucleus(the ratio of the single nucleon momentum density in ^3He for a proton at rest to that of a proton of 50 MeV energy is of the order of 10^4). The detected proton may not have been a spectator, but the result of either πN single scattering or π absorption on a nucleon pair. In free πp scattering, the maximum proton angle is 90^o.

However, on a nuclear target protons can be emitted backwards in single πp collisions if the target nucleon had a large Fermi momentum prior to the interaction;this situation also has a small probability because the nucleons in ^{3}He seldom have such a large momentum. A simple I.A. calculation described below indicates that an important process producing the backward protons detected in this experiment, is pion absorption on a nucleon pair at rest in ^{3}He.

The invariant cross-sections for the reaction $^3He(\pi^-,p)X$ at an incident pion energy of 428 MeV and mean lab proton angles of 115^o and 140^o, respectively, are shown in figure 48 against the missing mass squared of the unobserved system X. The intrepretation of the data will be presented in three parts corresponding to the three processes of QFA, QFS and FSI.

It is important to consider the isospin aspects of ^{3}He and ^{4}He before discussing the present results for this reaction in the context of quasi-free absorption. Since the absorption of a pion occurs predominantly on a nucleon pair, we need to know the number of NN pairs and their isospin values in these nuclei. In considering NN pair it should be noted that the basic pion-two nucleon absorption reaction that can be observed is $\pi^+ + d \rightarrow pp$, although $\pi^- d \rightarrow nn$ can also be studied.

Consider first a system of three nucleons. This system can have the four possible combinations of neutrons and protons as follows: nnn,nnp,npp,ppp. Of these four, the trineutron (nnn) and the triproton (ppp) are unbound. Hence the only two possible bound systems are nnp and npp, corresponding to ^{3}H and ^{3}He respectively, which in their ground state form an isospin doublet. ^{3}He has one pp pair and between the 2

protons and a neutron it can have two pn pairs which can be considered as two quasi-deuterons. The pp pair is in an isospin I=1 state whereas the two np pairs are in isospin I=1 and I=0 state. On the other hand ^{4}He has I=0 in its ground state; it consists of one nn, one pp pair and four quasi-deuteron pairs. The pp and nn pair are in isospin I=1 state and of the four np pairs three are in an isospin I=0 and one is in an I=1 state.

Considering the quasi-free absorption process first, an enhancement in the cross-section can be expected at a missing mass corresponding to the absorption of a pion on a nucleon pair at rest in ^{3}He. Since the basic pion absorption process on two nucleons is pion absorption on a deuteron, π+d -> pp, calculations were done to estimate the pion absorption cross-section on a quasi-deuteron in ^{3}He using the plane wave impulse approximation (PWIA). The momentum distribution of this quasi-deuteron is assumed to be the same as that of a single nucleon in ^{3}He, as the nuclear vertex in figure 47 (a) corresponds to ^{3}He -> (pp)n. The needed momentum distribution of a nucleon in ^{3}He can be taken from the ^{3}He(e,e'p)d data of Jans e.a[9], which extends up to a deuteron recoil momentum of 305 MeV/c. Since no information on the absorption cross-section of a π^- on two protons in ^{3}He is available, the result is normalised to the data in figure 47, after a background subtracction as explained below was done. The resulting curves are A and A' respectively for the two sets of data. These curves are peaked at a missing mass squared M_x^2 corresponding to zero recoil for the QFA process. The values of these missing masses squared are 4.335 GeV^2 for 140^o and 4.272 GeV^2 for 115^o. The width of the peak is determined by the single-nucleon momentum distribution and is approximately ΔM_x^2 = .2 GeV^2.

Looking at the 140^{o} data in figure 48, we see an enhancement near the expected values of M_x^2 for π^-absorption on a nucleon pair at rest, whereas at 115^{o} the data stops just short of the region of interest. For this set of data, the maximum proton energy which could be detected corresponds to $M_x^2 = 4.40\ GeV^2$.

Turning our attention to the right of the QFA peak, we see a continuum increasing towards increasing M_x^2 values. To understand this continuum, a PWIA calculation was done for π^-- N quasi-free scattering in ^3He. Since our data covers a region of momentum outside of Jans data, first an exponential extrapolation of Jans data was used, as suggested by the observed shape of it below 305 MeV/c. The resulting curve B' is obtained; obviously it decays too rapidly. However the momentum region of curve B' lies entirely outside that of the work of Jans et.al; indeed, the recoil momentum is 350 MeV/c at $M_x^2 = 5.0\ GeV^2$ and 630 MeV/c at $M_x^2 = 4.3\ Gev^2$. Bosted et.al[40] have done a recent study of inclusive (e,e') on $^{3,4}He$. Sick et.al.[41] have done a similar study on ^3He. They have obtained an inclusive cross-section that flattens out rapidly for recoil momenta beyond 200 MeV/c. Within the I.A. model, both the (e,e') and the (π,p) cross-sections are proportional to an integral over the recoil momentum density. The limits of this integral are determined by the kinematics; the lower limit is the minimum possible recoil, or the variable 'y' in the data of Sick et.al. and Bosted et.al.

The portion of the data to the right of the QFA peak in figure 48, suggests that the physical background that must be subtracted in both cases is exponential in nature. The last few data points in both these spectra that lie near the highest M_x^2 were used to estimate such an

exponential, denoted by C and C' in figure 48. It turns out that the two exponentials which fit the data in this way have the same slope. The unique slope obtained for C and C' is also the same as the slope of the scaling function F(y) obtained in ref[40]. The normalisation of C and C' was obtained by fitting the data in the high region of M_X^2 ($4.8 < M_X^2 < 5.0$ Gev^2).

There is one other feature of the data that still needs explanation. This is the bump near 4.7 GeV^2 seen at both angles. To further study this bump, the following procedure was carried out. For both data, subtraction of the exponentials C and C' was done. The resulting spectrum is shown in figure 49, as open circles for the 140^o data and open triangles for the 115^o data, along with the quasi-free absorption peak A for 140^o data. Notice that after this subtraction is done the data at 115^o lie entirely outside the region of the QFA peak denoted by A' in figure 49. For the 140^o data, the QFA peak A was subtracted and is shown as shaded circles in figure 49. For the 115^o data, there was no such subtraction since we did not have data covering the QFA region. Curves D and D' are drawn to emphasize the presence of a residual feature. In each of these two sets of data there is an obvious bump near M_X^2 = 4.67 GeV^2;the shape and width of the bump is the same at both angles. It remains to be proved that these two peaks are not a feature of the ^{3}He single nucleon momentum distribution. This enhancement feature was compared with that of (e,e') data. The minimum recoils corresponding to these two peaks are 560 MeV/c and 500 MeV/c. There is no noticeable feature seen in (e,e') data in this momentum range.

A possible explanation for the residual peak appearing in both data is as follows. The sum of the physical masses squared of a non-interacting Δ-N pair is 4.710 GeV². Comparing this value with the data, it is seen that the invariant mass squared corresponding to the bump in the data is about 10 MeV less than that of a physical Δ-N pair(with an uncertainty of 10 MeV). This may suggest formation of a Δ-N state bound by approximately 10 MeV due to final state interaction among the constituents of the unobserved system. The widths of these two peaks are not only the same, 50 MeV (FWHM), but they are much narrower than that of a free Δ. This narrowing could be the result of the Δ-N interaction. This would suggest that the corresponding life-time for a ΔN state is considerably longer than that of a free Δ. Some of the previous results in the literature are compared to supplement this narrowing effect. Argan et.al.[42] have measured the photoproduction cross-section in the reaction $^4He(\gamma,p\pi^-)X$, and found an anomaly in the value of the cross-section for recoils above 300 MeV/c, which they attribute to a resonant process due to πNN. The width of the resonance is 35 MeV;much smaller than that of a free Δ. In a study of $^3He(p,t)X$ at T_p = 850 MeV and for tritons at 6°, Tatisheff et.al.[10] have observed a peak in the missing mass spectrum corresponding to the mass of a Δ. In this case, the Δ is interpreted as a spectator Δ in the nucleus. The width of this Δ peak is 60 ± 20 MeV, the reason for the narrowing having possibly the same origin as of our data. But in the study of $^6Li(p,p\pi^+)^6He$, Hennino et.al.[43] have observed a width for the Δ peak of 90 MeV FWHM, very close to that of a free Δ. This agreement may be due to their kinematical conditions, which favours forward Δ production.

The data for $^4He(\pi^+,p)X$ and $^4He(\pi^-,p)X$ are shown in figure 50. Figure 50 (a) shows the missing mass spectrum for π^+ on ^4He at a pion energy of 284 MeV and protons at 120^o. The π^- data at the same energy and for protons at 125^o are shown in figure 50 (b). The data of figure 50 (a) exhibit a strong QFA peak at the invariant mass around M_X^2 = 9.0 GeV^2, whereas the same evidence is very weak in figure 50 (b). The kinematics for the absorption of a pion on a nucleon pair at rest in ^4He corresponds to M_X^2 = 8.96 GeV^2. Again here a PWIA for quasi-free absorption was made. For the momentum density of nucleons in ^4He the (p,2p) data of van Oers[44] is used. The physical background that has to be subtracted is obtained from the continuum of π^- data. This continuum is presumably due to Quasi-Free scattering and it is assumed to be the same in shape in both π^+ and π^- data, the only difference being due to the difference in π^+N and π^-N interaction. After subtracting this background, we obtained the data shown by open circles in figure 50 (a). The result of a quasi-free absorption calculation is shown as curve A, normalised to the data after the subtraction of the background.

The ΔN- enhancement cannot be seen in ^4He for experimental reasons. For ^4He, assuming one spectator nucleon, a ΔN enhancement would be at M_X^2 = 9.805 GeV^2;a ΔNN enhancement would be at M_X^2 = 9.67 GeV^2. In both cases the missing mass squared values lie outside the region covered in the present data, determined by the range of the proton energies accepted by the detector.

5.2.1 π^+/π^- ratio

The QFA peak is visible both in the π^+ and π^- data. The ratio of π^+/π^- was calculated at the QFA peak. For this work, the ratio is 22 $\pm$ 5 after taking into consideration the subtraction of the exponential C. McKeown et.al.[45] have obtained a value of 15 for this ratio for forward going protons. Jackson et.al.[6] have obtained a value of 22 for π^+/π^- ratio at the QFA peak in the case of ^{4}He and for forward protons. If one were to assume a simple isobar model, in which the absorption went through a two step process,

$\pi + N \rightarrow \Delta \rightarrow \Delta + N \rightarrow 2N$

a calculation of the proton yields with π^+ and π^- could be obtained in ^{4}He by taking into consideration of the different possible isospin values of the pp, nn, and pn pairs. The ratio of π^+/π^- so obtained is 27(for a detailed description of the calculation see[45])however at 284 MeV the isobar model need not be correct.

5.2.2 Conclusion

In conclusion the QFA peaks observed in ^{3}He for π^- and ^{4}He for both π^+ and π^- are compatible in position, and shape. Furthermore, the π^+/π^- ratio obtained at the position of the QFA peak is compatible with the data of McKeown et.al., Jackson et.al., and the calculation using isospin considerations. The intrepretation for the second enhancement observed in ^{3}He data is based entirely on the value of M_x^2 being nearly equal to $(m_\Delta + m_N - B)^2$, where B is the binding energy. THe value of B is about 10 MeV. A very interesting feature of the data is the width of this enhancement;which is the same at both angles. The value of B is

also interesting. However, it should be mentioned that the experimental uncertainty in calculating the M_x^2 values is of the order of B. More data is needed at other energies and angles to confirm the value of M_x^2 and to establish a definite signature for this resonance peak.

TABLE 11

Cross-section and phi squared data

triton central momentum = 760 MeV/c

22.0	28.0	33.7	39.6	46.6	53.7	60.8	67.9	74.8
3.60	6.54	9.41	9.99	4.90	1.33	1.17	1.28	0.64
25.61	33.44	29.66	10.24	4.35	1.85	2.46	2.18	7.76
19.44	11.17	4.05	1.48	1.34	1.51	0.74	7.28	17.34
9.46	2.86	1.37	1.20	0.91	0.90	13.24	21.58	20.85
3.13	0.88	0.85	0.71	0.73	25.08	35.29	23.31	7.90
1.40	0.91	2.40	1.86	44.71	53.64	26.31	8.23	3.64
0.87	3.73	1.43	43.44	41.67	15.97	5.78	2.99	2.24
1.62	2.24	37.54	32.78	14.50	4.07	3.13	3.60	1.52
0.84	18.24	15.65	6.95	1.18	2.46	1.83	0.95	0.88

following are the corresponding statistical errors

1.03	1.13	1.34	1.16	0.93	0.67	0.61	0.62	0.57
2.35	2.46	2.13	1.56	1.29	1.18	1.20	1.17	1.33
1.87	1.35	1.04	0.80	0.86	0.80	0.80	1.33	1.75
1.27	0.84	0.81	0.76	0.72	0.73	1.50	1.92	1.83
0.97	0.81	0.75	0.76	0.76	2.06	2.34	2.13	1.32
0.96	0.82	0.90	0.90	2.70	2.92	2.41	1.63	1.39
1.14	1.29	1.15	2.80	2.82	2.23	1.49	1.47	1.43
1.36	1.34	2.59	2.58	2.13	1.57	1.38	1.35	1.19
1.17	1.86	1.77	1.47	1.01	1.02	0.86	0.85	0.87

following are the phi-squared values

3.595	6.536	9.410	9.987	4.896	1.329	1.166	1.278	0.640
25.611	33.438	29.663	10.241	4.352	1.853	2.455	2.178	7.764
19.435	11.165	4.049	1.481	1.341	1.506	0.736	7.282	17.343
9.456	2.860	1.373	1.200	0.910	0.903	13.244	21.580	20.850
3.129	0.884	0.854	0.709	0.727	25.082	35.292	23.313	7.895
1.404	0.908	2.402	1.863	44.712	53.640	26.311	8.233	3.637
0.866	3.725	1.434	43.441	41.668	15.970	5.777	2.994	2.242
1.619	2.240	37.536	32.775	14.503	4.071	3.129	3.599	1.519
0.843	18.238	15.651	6.946	1.182	2.460	1.825	0.947	0.876

TABLE 12

cross-section and phi squared data

triton central momentum = 820 MeV/c

22.0	28.0	33.7	39.6	46.6	53.7	60.8	67.9	74.8
2.03	4.05	3.44	4.04	3.18	1.36	1.34	0.68	-0.06
7.98	12.50	10.44	6.75	2.44	1.65	1.63	0.79	4.67
11.80	8.79	3.37	1.71	1.15	0.70	0.11	4.21	14.63
6.46	2.46	1.64	1.48	0.37	-0.16	8.52	19.60	17.44
3.09	1.98	1.36	0.23	1.05	15.48	25.17	17.21	5.10
1.58	-0.06	1.08	1.39	21.22	31.83	15.99	4.44	0.33
2.03	1.45	1.73	20.21	20.73	9.54	0.50	2.47	0.61
1.01	1.76	6.60	7.35	3.91	0.92	0.62	0.71	0.46
0.83	1.21	1.45	0.80	0.35	0.05	0.03	-0.01	0.02

following are the corresponding statistical errors

0.59	0.75	0.63	0.59	0.55	0.37	0.39	0.25	0.26
1.16	1.11	0.93	0.76	0.46	0.48	0.50	0.40	0.95
1.15	0.95	0.69	0.51	0.54	0.46	0.26	0.92	1.28
0.82	0.66	0.48	0.52	0.46	0.35	1.24	1.53	1.18
0.69	0.47	0.59	0.49	0.39	1.43	1.74	1.31	0.89
0.51	0.50	0.48	0.43	1.58	1.95	1.26	0.83	0.62
0.63	0.54	0.47	1.46	1.51	1.00	0.72	0.66	0.49
0.49	0.41	0.98	0.88	0.68	0.47	0.40	0.33	0.33
0.34	0.38	0.41	0.33	0.31	0.15	0.15	0.22	0.19

Following are the corresponding phi-squared values in GeV/c e-3

0.110	0.352	0.488	0.955	1.059	0.524	0.558	0.303	-0.029
0.692	1.746	2.440	2.222	0.945	0.695	0.741	0.403	0.256
1.647	2.041	1.102	0.672	0.497	0.319	0.057	0.234	1.270
1.495	0.812	0.655	0.641	0.175	-0.086	0.476	1.705	2.424
1.031	0.805	0.617	0.111	0.605	0.875	2.206	2.407	1.190
0.664	-0.025	0.576	0.824	1.218	2.830	2.266	1.056	0.111
0.973	0.787	1.071	1.180	1.878	1.377	0.123	0.875	0.270
0.578	1.139	0.391	0.680	0.577	0.228	0.230	0.318	0.249
0.562	0.073	0.137	0.124	0.093	0.019	0.010	-0.006	0.009

TABLE 13

cross-section and phi squared data

triton cebntral momentum =850 MeV/c

0.90	1.93	0.92	1.72	2.35	2.90	2.85	1.10	1.12
4.53	4.01	4.46	5.26	6.42	6.12	2.36	2.11	2.81
5.28	6.89	6.97	6.06	3.08	1.82	0.59	3.28	4.57
6.02	5.09	3.35	1.46	0.58	0.96	6.01	6.56	10.97
5.34	2.61	1.36	0.58	1.31	5.24	8.56	10.50	7.54
1.58	1.10	0.94	1.02	7.92	13.53	14.12	6.57	4.04
0.89	1.92	1.37	15.75	25.16	16.58	7.80	2.83	1.48
4.21	3.33	19.51	23.60	11.14	5.79	2.53	1.25	1.64
2.38	3.84	5.92	2.15	1.55	-0.11	0.10	0.93	0.62

following are the corresponding statistical errors

0.96	1.05	0.97	0.97	0.95	1.00	0.99	0.93	0.91
1.24	1.17	1.11	1.14	1.13	1.10	0.99	0.93	0.96
1.00	0.99	0.99	0.92	0.79	0.73	0.61	0.82	0.92
0.83	0.79	0.60	0.53	0.42	0.41	1.00	1.17	1.13
0.86	0.66	0.60	0.54	0.54	1.19	1.29	1.23	1.03
0.68	0.67	0.67	0.61	1.31	1.48	1.35	1.02	0.89
0.76	0.76	0.73	2.14	2.32	2.03	1.70	1.59	1.51
1.56	1.51	2.81	2.79	2.55	2.32	2.23	2.18	2.23
2.18	1.02	1.10	0.84	0.78	0.68	0.70	0.75	0.71

following are the phi-squared values in GeV/c e -3

0.04	0.15	0.12	0.37	0.69	0.99	1.04	0.42	0.47
0.35	0.50	0.92	1.54	2.20	2.25	0.92	0.91	0.14
0.65	1.39	2.01	2.09	1.15	0.74	0.27	0.16	0.35
1.21	1.47	1.17	0.56	0.25	0.45	0.30	0.51	1.35
1.56	0.93	0.53	0.26	0.66	0.27	0.67	1.31	1.55
0.58	0.44	0.42	0.55	0.41	1.08	1.78	1.39	1.23
0.37	0.93	0.79	0.84	2.05	2.16	1.71	0.90	0.58
2.15	2.04	1.07	1.99	1.50	1.33	0.85	0.50	0.75
1.55	0.22	0.52	0.30	0.37	-0.04	0.04	0.46	0.36

TABLE 14

cross-section and phi squared data

triton central momentum =950 MeV/c								
2.46	2.21	2.79	1.77	5.27	7.69	10.43	6.23	5.63
-1.09	2.45	2.70	6.36	11.69	10.61	6.95	4.42	1.57
2.02	3.49	5.92	2.25	1.95	1.84	2.21	2.50	1.53
5.76	7.52	5.22	1.81	2.24	1.67	2.74	3.42	3.75
4.62	1.63	1.98	0.82	1.95	5.26	9.53	6.28	5.31
2.51	0.51	1.10	0.57	12.59	15.54	18.64	7.44	7.06
4.40	1.42	0.70	21.47	22.04	15.89	11.39	5.38	4.50
3.03	0.03	22.95	20.14	11.05	6.51	4.95	2.09	1.98
2.02	13.44	9.49	3.88	1.12	0.99	2.72	0.76	0.94
following are the corresponding statistical errors								
1.53	1.46	1.37	1.34	1.59	1.66	1.79	1.65	1.60
2.20	2.25	2.20	2.36	2.45	2.42	2.29	2.30	1.77
1.80	1.83	1.92	1.84	1.80	1.76	1.81	0.71	0.50
0.98	1.13	0.92	0.55	0.56	0.70	1.50	1.53	1.43
1.55	1.29	1.28	1.23	1.38	2.96	3.00	2.93	2.89
2.72	2.71	2.69	2.73	3.16	3.14	3.31	2.84	2.92
2.77	2.69	2.73	3.31	3.35	3.24	2.97	2.89	2.77
2.75	2.72	3.23	3.12	2.85	2.60	2.59	2.45	2.43
2.50	1.88	1.71	1.56	1.26	1.37	1.39	1.25	1.23
following are the corresponding phi-squared values in GeV/c e-3								
0.32	0.57	1.04	0.69	1.92	2.71	3.79	2.39	2.33
-0.28	0.91	1.06	2.37	4.25	4.00	2.80	1.93	0.22
0.73	1.36	2.25	0.85	0.79	0.78	1.03	0.36	0.38
2.20	2.89	2.05	0.76	1.02	0.81	0.39	0.84	1.26
1.81	0.66	0.87	0.39	1.00	0.75	2.27	2.07	2.03
1.05	0.22	0.55	0.31	1.78	3.65	6.13	2.85	2.90
2.17	0.76	0.41	2.99	5.08	5.20	4.41	2.26	2.06
1.68	-0.00	3.18	4.62	3.63	2.57	2.15	1.00	1.07
1.28	1.86	2.17	1.29	0.45	0.43	1.34	0.43	0.57

TABLE 15

cross-section and phi squared data

triton central momentum =1020 MeV/c

0.17	0.54	1.27	1.44	2.46	2.38	3.59	2.73	0.0
1.01	0.79	1.08	3.52	3.38	3.58	3.80	0.0	0.36
0.64	1.27	3.75	3.66	3.77	2.59	0.0	0.83	0.47
2.45	4.20	4.23	3.08	0.85	0.0	1.54	2.37	3.90
9.68	6.14	4.41	2.16	0.0	4.48	3.92	8.90	14.13
7.70	5.40	2.83	0.0	6.18	8.66	14.06	18.96	15.65
4.28	2.46	0.0	8.78	9.03	13.48	15.28	8.94	5.55
2.88	0.0	9.78	11.42	19.78	14.27	6.39	3.04	3.37
0.0	13.06	13.80	14.12	7.20	3.76	0.80	1.00	1.33

following values are the corresponding statistical errors

0.85	0.85	0.80	0.87	0.85	0.85	0.92	0.94	0.0
0.90	0.86	0.92	1.03	0.96	1.00	1.08	0.0	0.71
0.67	0.78	0.80	0.83	0.81	0.90	0.0	0.86	0.87
0.88	0.88	0.91	0.84	0.89	0.0	1.06	1.02	1.01
1.24	1.05	0.97	1.05	0.0	1.49	1.42	1.47	1.69
1.48	1.36	1.32	0.0	1.61	1.63	1.66	1.80	1.73
1.42	1.40	0.0	1.74	1.74	1.77	1.91	1.69	1.53
1.55	0.0	1.75	1.70	1.81	1.73	1.52	1.41	1.38
0.0	1.60	1.60	1.50	1.40	1.30	1.14	1.15	1.29

following are the corresponding phi-squared values in GeV/ c e-3

0.03	0.16	0.46	0.48	0.73	0.68	1.05	0.84	0.0
0.33	0.29	0.36	1.10	1.03	1.14	1.28	0.0	0.08
0.24	0.43	1.22	1.18	1.30	0.95	0.0	0.18	0.16
0.85	1.42	1.45	1.12	0.33	0.0	0.34	0.78	1.40
3.38	2.21	1.72	0.88	0.0	1.01	1.25	3.15	5.03
2.92	2.20	1.22	0.0	1.34	2.65	4.92	6.81	5.77
1.83	1.14	0.0	1.86	2.70	4.65	5.54	3.39	2.28
1.41	0.0	2.02	3.34	6.79	5.23	2.47	1.31	1.59

TABLE 16

cross-section and phi squared data

triton central momentum = 1110 MeV/c

9.05	12.80	18.63	28.04	23.49	12.74	7.08	6.59	0.0
6.96	11.17	19.66	22.79	14.49	10.14	8.17	0.0	5.28
5.57	15.31	26.39	22.34	13.49	11.66	0.0	4.18	6.24
10.20	18.09	27.03	20.62	14.92	0.0	3.47	2.67	2.73
11.15	20.74	19.69	18.72	0.0	0.32	0.57	1.67	1.20
11.59	16.33	15.40	0.0	1.24	1.23	0.86	1.53	2.05
6.61	8.35	0.0	0.05	0.33	0.96	1.19	1.14	2.69
4.56	0.0	1.28	-0.17	0.56	0.73	1.58	1.81	2.16
0.0	0.0	1.34	0.61	-0.21	0.93	1.41	1.13	1.28

following are the corresponding statistical errors

1.89	1.84	1.78	1.94	1.83	1.55	1.46	1.60	0.0
1.65	1.55	1.75	1.78	1.54	1.49	1.60	0.0	1.70
1.39	1.62	1.78	1.65	1.50	1.61	0.0	1.71	1.62
1.53	1.66	1.74	1.62	1.77	0.0	1.41	1.37	1.19
1.42	1.57	1.57	1.75	0.0	1.17	1.19	0.98	1.02
1.20	1.31	1.51	0.0	0.72	0.76	0.71	0.74	0.76
0.88	1.07	0.0	0.77	0.72	0.65	0.66	0.69	0.67
0.82	0.0	0.86	0.82	0.78	0.79	0.80	0.74	0.84
0.0	0.49	0.66	0.58	0.56	0.62	0.61	0.58	0.68

following are the phi-squared values in Gev/c e-3

2.33	4.64	7.20	10.66	8.94	5.16	3.11	3.09	0.0
2.58	4.36	7.31	8.35	5.58	4.14	3.63	0.0	1.34
2.19	5.60	9.34	8.13	5.20	4.85	0.0	1.02	2.33
3.66	6.13	9.23	7.46	5.78	0.0	0.76	0.95	1.06
3.62	6.67	6.61	6.71	0.0	0.08	0.20	0.64	0.41
3.51	5.07	5.12	0.0	0.23	0.39	0.33	0.52	0.61
1.92	2.51	0.0	0.01	0.09	0.36	0.40	0.33	0.73
1.26	0.0	0.20	-0.05	0.22	0.25	0.47	0.48	0.55
0.0	0.0	0.42	0.25	-0.08	0.29	0.38	0.28	0.31

TABLE 17

cross-section and phi squared data

triton central momentum = 760 MeV/c and beam energy = 460 MeV

3.16	4.27	9.81	15.49	11.77	5.29	2.07	2.07	0.68
11.24	21.84	22.19	15.65	4.06	3.00	3.24	1.89	6.65
19.53	18.48	9.88	2.66	1.79	1.51	1.60	5.18	11.53
18.00	6.00	0.97	0.78	0.21	0.91	13.29	22.61	36.44
8.07	3.02	0.51	2.44	2.20	20.20	32.18	38.50	20.31
2.53	1.15	2.38	3.15	20.35	34.13	30.87	12.06	3.59
0.33	2.14	4.64	21.85	28.99	24.76	10.19	3.87	1.48
3.13	6.68	24.09	28.36	19.51	6.52	2.87	3.02	1.47
3.74	9.71	8.36	6.73	1.21	1.92	0.84	-0.33	2.17

following are the corresponding statistical errors

1.07	1.12	1.50	1.61	1.45	1.06	0.88	0.81	0.76
1.68	2.15	1.89	1.72	1.18	1.07	1.06	0.98	1.46
2.07	1.84	1.56	1.12	1.11	1.05	1.05	1.29	1.67
1.67	1.13	0.81	0.81	0.74	0.77	2.06	2.35	2.86
1.62	1.44	1.31	1.35	1.33	2.33	2.63	2.90	2.05
1.29	1.24	1.24	1.40	2.38	2.66	2.69	1.85	1.45
1.26	1.31	1.39	2.22	2.54	2.30	1.61	1.28	1.08
1.16	1.30	2.44	2.52	2.23	1.55	1.41	1.43	1.31
1.36	1.57	1.53	1.40	1.12	1.03	1.00	0.93	1.02

following are the phi-squared values in GeV/c e-3

0.11	0.25	0.91	2.42	3.28	2.20	1.02	1.04	0.34
0.66	2.07	3.51	4.34	1.71	1.49	1.67	0.99	0.25
1.88	2.92	2.73	1.11	0.90	0.80	0.88	0.20	0.71
2.85	1.66	0.41	0.41	0.11	0.51	0.54	1.42	3.58
2.23	1.28	0.27	1.40	1.30	0.84	2.06	3.84	3.27
1.10	0.64	1.42	1.94	0.87	2.22	3.11	1.96	1.00
0.19	1.33	2.97	0.96	1.93	2.53	1.67	1.11	0.69
2.05	4.51	1.08	1.92	2.04	1.09	0.85	1.41	0.91
2.66	0.44	0.58	0.71	0.21	0.58	0.40	-0.21	1.55

REFERENCES

1. J. S. McCarthy, I. Sick, R. R. Whitney, Phys.Rev., C15, 1396 (1977).

2. J. M. Cavedon, L. S. Cardman, B. Frois, D. Goutte, M. Huet, Ph. Leconte, J. Martino, X. H. Phan, S. K. Platchkov, S. E. Williamson, W. Boeglin, I. Sick, and P. deWitt Huberts, Proceedings of the Ninth international conference on High Energy Physics and Nuclear Structure, Versailles, France, 1981.

3. W. O. Lock and D. F. Measday, Intermediate Energy Nuclear Physics, Methuen and Co Ltd.

4. H. E. Jackson, S. Kaufman, L. Meyer-Schutzmeister, J. P. Schiffer, S. L. Tabor, S. E. Vigdor, J. N. Worthington, L. L. Rutlege Jr., R. E. Segel, R. L. Burman, P. A. M. Gram, R. P. Redwine and M. A. Yates, Phys.Rev., C16, 730 (1977).

5. J. Kallne, J. Davis, R. C. Minehart, R. R. Whitney, R. L. Boudrie, J. McClelland, and A. W. Stetz, Physics letters., 97B, 205 (1980).

6. H. E. Jackson, R. E. Segel, L. L. Rutledge, S. L. Tabor, K. E. Rehm, J. P. Schiffer, and M.A.Yates, Phys.Rev., 39, 1601 (1977).

7. G. Jacob and Th. A. J. Maris, Rev.Mod.Phys., 38, 121 (1966).

8. D. KOLTUN, Theory of meson interactions with nucleii, John Wiley and sons, (1980).

9. E. Jans, P. Barreau, M. Bernheim, J. M. Finn, J. Morgenstern, J. Mougey, D. Tarnowski, S. Turck-Chieze,S. Frullani, F. Garibaldi, G. P. Capitani, E. de Sanctis, M. K. Brussel, and I. Sick, Phys.Rev.Let., 49, 974 (1982).

10. B. Tatischeff, I. Brissaud, R. Frascaria, M. Morlet, F. Reide, R. Beurtey, A. Boudard, J. L. Escudie, M. Garcon, L. Schecter, J. P. Tabet, and ,Y. Terrien, Phys.Lett., 77B, 254 (1978).

11. S. Jonsson, S. Dahlgren, T. Ekelof, P. Grafstrom, E. Hagberg, A. Hallgren, S. Kullander, B. Badelek, J. Nassalski, J. Berthot, P. Cotte, C. Dore, L. Meritet, M. Querrou, F. Vazeille, J. P. Burq, M. Chemarin, M. Chevallier, B. Iile, M. Lambert, G. Faldt, and P. C. Gugelot, Phys.Rev., C21, 306 (1980).

12. P. Benz and P. Soding, Phys.Lett., 52, 367 (1974).

13. R. Beurtey, J. C. Duchazeaubeneix, H. H. Duhm, J. C. Faivre, J. C.Lugol, J. Saudinos, I. Goldzahl, G. Cvijanovich, L. Dubal and C. F. Perdrisat, Phys.Lett., 61B, 409 (1976).

14. B. Bakken, H. Gennow, P. Lundborg, J. Makela, M. Pimia, B. Sellden and E. Sundell, Physica Scripta., 19, (1968).

15. W. F. Cartwright, Phys.Rev., 82, 460 (1951).

16. K. M. Watson, Phys.Rev., 88, 1163 (1952).

17. A. B. Migdal, JETP., 1, 2 (1955).

18. M. Jain, P. G. Roos, H. G. Pugh, and H. D. Holmgren, Nucl. Phys, A 153, 49 (1970).

19. B. Debebe, Ph.D thesis, College of William Mary, (1983).

20. J. W. Lo, E. V. Hungerford, J. C. Allred, B. W. Mayes, L. S. Pinsky, M. L. Warneke, T. M. Williams, J. M. Clement, W. H.Dragoset, R. D. Felder, J. H. Hoftiezer, J. Hudomalj-Gabitzsch, G. S. Mutchler, and G. C. Phillips, Phys.Rev., C20, 1479 (1979).

21. R. Abegg, Private Communication.

22. D. Axen, G. Duesdieker, L. Felawka, C. H. Q. Ingram, G. Jones, M. Salomon, and W. Westlund, Nuclear Instruments and Methods, 118 435 (1974).

23. D. K. Hassel, R. Abegg, B. T. Murdoch, W. T. H.van oers, H. Postma, and J. Soukup, Nuclear Instruments and Methods, 189, 341.

24. R. D. Werbeck and R. J. Macek, IEEE transactions in Nuclear Science, NS-22, 3, June (1975).

25. R. R. Whitney, Ph.D.thesis (unpublished), Stanford University, (1978); J. S. McCarthy et al., Phys.Rev., C15, 1396 (1977).

26. B. Zacharov, 'CAMAC System: A pedestrian's Guide, Daresbury Nuclear Physics Laboratory, Warrington WA4-4AD, England, (1972).

27. L. Orphanos, PhD Thesis, University of Virginia, 1980.

28. E. Aslanides, R. Bertini, O. Bing, F. Brochard, Ph.Gorodetzky, F. Hibon, T. S. Bauer, R .Beurtey, A .Boudard, G. Bruge, H. Catz, A. Chaumeaux, P. Couvert, H. H.Duhm, D. Garreta, G. Igo, J. C. Lugol, M. Matoba, Y. Terrien, L. Bimbot, Y. Le Bornec and B. Tatischeff, phys.Rev.Lett, 39, 1654, (1977).

29. J. Carroll, D. H. Fredrickson, M. Goitein, B. Macdonald, V. Perez - Mendez, A. Stetz, C. A. Heusch, R. V. Kline and K.T.McDonald, Nuclear Physics, A305, 502, (1978).

30. K. K. Seth, Private Communication.

31. J. M. Cameron, L. G. Greeniaus, D. A. Hutcheon, C. A. Miller, G.A.Moss, R. P. Liljestrand, H. Wilson, R. Abegg, W. T. H. van Oers, A. W. Stetz, M.B.Epstein, and D.J.Margaziotis, Phys.Let., 103B, 317, (1981).

32. W. Dollhopf, C. Lunke, C. F. Perdrisat, W. K. Roberts, P. Kitching, W. C. Olsen and J. R. Priest, Nuclear Physics., A217 (1973). 381-399.

33. W. J. Frank, K. C. Bandtel, R. Madey and B. J. Moyer, Phys. Rev., 94, 1716, (1954).

34. D.Harting, J.C.Kluyver, A.Kusumegi, R.Rigopoulos, A.M.Sachs, G.Tibell, G. Vanderhaeghe, and G. Weber Phys.Rev., 119, 1716 (1960).

35. A. V. Crewe, B. Ledley, E. Lillethun, S. M. Marcowitz, and C. Rey, Phys.Rev., 118, 1091 (1960).

36. G. A. Korn and T. M. Korn, Mathematical Handbook for Scientists and Engineers, McGraw Hill, p-746, (1968).

37. L. Orphanos, J. Kallne, R. Altemus, P. C. Gugelot, J. S. McCarthy, R. C. Minehart, P. A. M.Gram, B.Hoistad, C.L.Morris, E.A.Wadlinger, and C. F. Perdrisat. Phys.Rev.Let., 46, 1562 (1981).

38. C. F. Perdrisat et.al., ICOHEPANS, Versailles, p.188 (1981).

39. A. W. Stetz, Phys.Rev., C21, 1979 (1980).

40. P.Bosted, R.G.Arnold, S.Rock, and Z.Szalata, Phys.Rev.Let., 49, 1380 (1982).

41. I.Sick, D.Day, and J.S.McCarthy, Phys.Rev.Lett., 45, 871 (1980).

42. P. E. Argan, G. Audit, N. De. Botton, J. M. Laget, J.Martini, C.Schuhl, and G. Thomas, Phys.Rev.Lett, 29, 1191, (1972).

43. T. Hennino, D. Bachelier, O. M. Bilaniuk, J. L. Jourdain, M.Roy-Stephan, P. Radvanyi, M. Bedjidian, E. Descroix, P. Foessel, S. Gardien, J. Y. Grossiord, A. Guichard, M. Gusakow, R. Haroutunian, M. Jacquin, J. R. Pizzi, and A. Garin, Phys.Rev.Let., 48, 997 (1982).

44. W. T. H. van Oers, B. T. Murdoch, B. K. S. Koene, D. K. Hasell, R.Abegg, D. J. Margaziotis, M. B. Epstein, G. A. Moss, L. G.Greeniaus,J.M.Greben, J. M. Cameron, J. G. Rogers, A. W. Stetz, Phys.Rev., C25, 390 (1982).

45. R. D. McKeown, S. J. Sanders, J. P. Schiffer, H. E. Jackson, M. Paul, J. R. Specht, E. J. Stephenson, R. P. Redwine, R. E. Segel, Phys.Rev., C24, 211 (1981).

Chapter VI

FIGURE CAPTIONS

1) (a) A Feynmann diagram describing the π^- absorption on a pp pair.

(b) A Feynmann diagram describing the π^+ absorption on a nn pair.

(c) A Feynmann diagram describing π^+ absorption with an intermediate Δ formation.

2) Impulse Approximation picture of the reaction ^3He $(P,t\pi^+)P$.

3) Three Feynmann graphs based on the I.A. for diffrent kinematical conditions.

4) Plot of the dead-time vs the event rate for reaction (1).

5) The configuration of the experimental system for reaction (1).

6) Vertical sectional drawing of the Medium Resolution Spectrometer.

7) The Cryostat used for reaction (2).

8) The Configuration of the experimental system for reaction (2).

9) The logic diagram for reaction (1).

10) The logic diagram for reaction (2).

11) Diagram explaining the classification scheme for 'reals' and 'randoms' for reaction (1).

12) The time-of-flight vs dE/dX distribution from the MRS side for reaction (1).

13) The time-of-flight distribution from the pion telescope side for reaction (1).

14) The pulse height distribution from the pion telescope side for reaction (1).

15) The time-of-flight vs dE/dX distribution for the protons in reaction (2).

16) Calibration curve for ADC-channel vs energy for reaction (2).

17) Pd -> tπ data with the polynomial fit at 350 MeV.

18) pd -> tπ data with the polynomial fit at 465 MeV.

19) pd -> tπ data with the polynomial fit at 500 MeV.

20) pd -> tπ data with the polynomial fit at 600 MeV.

21) pd -> tπ data with the polynomial fit at 800 MeV.

22 - 27) The fifth differential cross-section data at the 6 p_s . central values of 1.11, 1.02, .900, .850, .820 and .760 MeV/c at a beam energy of 500 MeV.

28 - 30) The fifth differential cross-section values at the 3 p_s central values of 1.08, .900, and .760 MeV/c at a beam energy of 460 MeV.

31 - 39) The proton momentum density $\emptyset^2$ values for the p_s central values of 1.11, 1.02, .950, .850, .820, and .760 MeV/c at a beam energy of 506 MeV and for p_s central values of 1.08, .900, and .760 GeV/c at a beam energy of 460 MeV.

40 - 43) The $\emptyset^2$ values for a selected pion channels for p_s at .850, .820, .760 GeV/c for 506 MeV beam and at p_s centarl value of .760 GeV/c for 460 MeV beam.

44) Plot of $\emptyset^2$ versus the recoil momentum for the (e,e'p) data.

45) A plot of the proton recoil momentum versus the triton momentum explaining the complexity of the kinematics for reaction (1).

46) Two possible non-I.A. graphs which might explain the behavior of part of the data in reaction (1).

47) Feynamnn graphs explaining the three processes of quasi free scattering, quasi free absorption and final state interaction of π^- on ^{3}He.

48) π^- data at 140^o and $\beta 115^o$.

48) π^- data at 140^o and 115^o with the calculated quasi free scattering subtracted is shown here.

50) π^+ data for ^{4}He at 120^o is shown here.

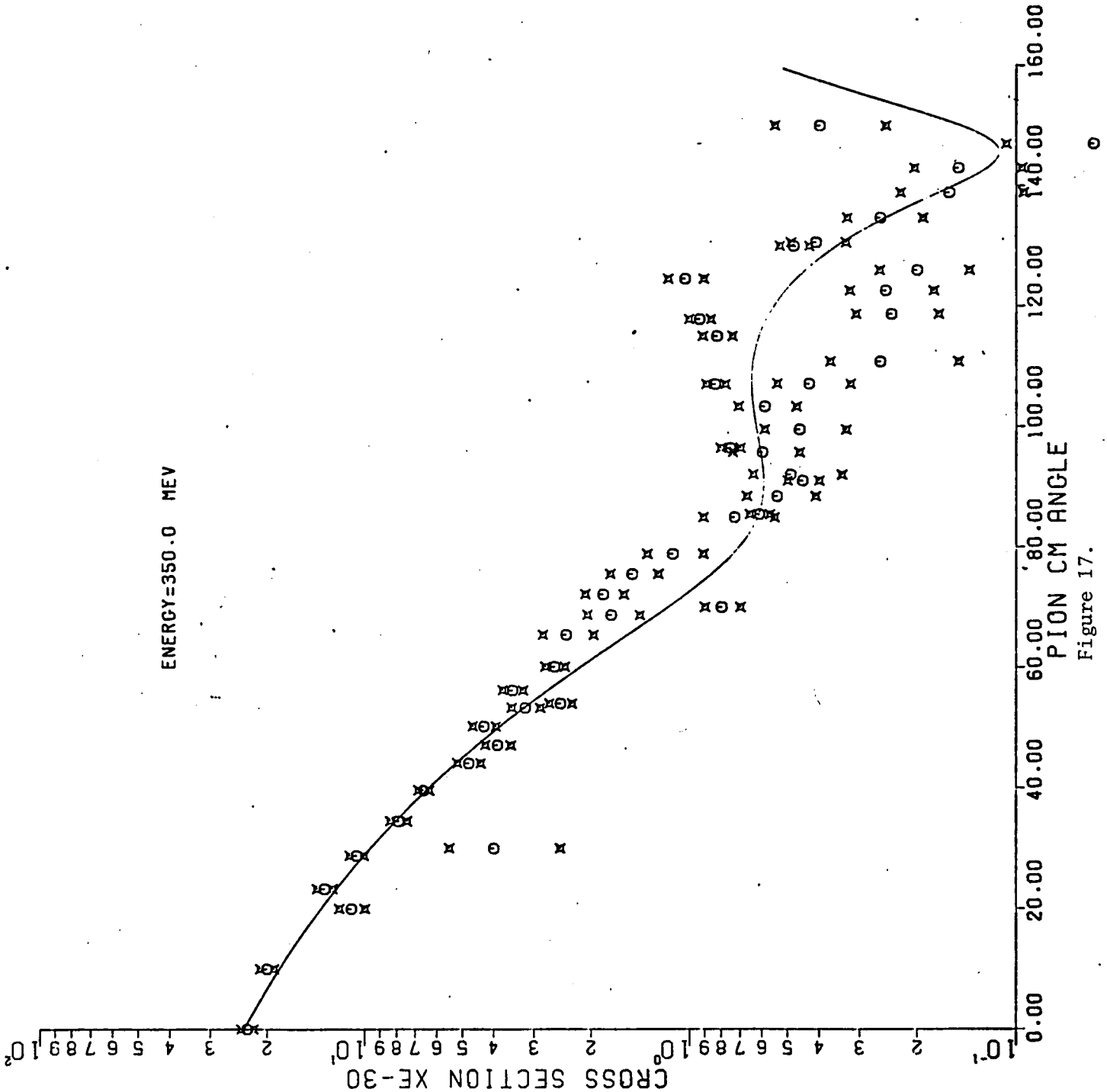
ENERGY=350.0 MEV
CROSS SECTION XE-30
PION CM ANGLE
0.00
20.00
40.00
60.00
80.00
100.00
120.00
140.00
160.00

Figure 17.

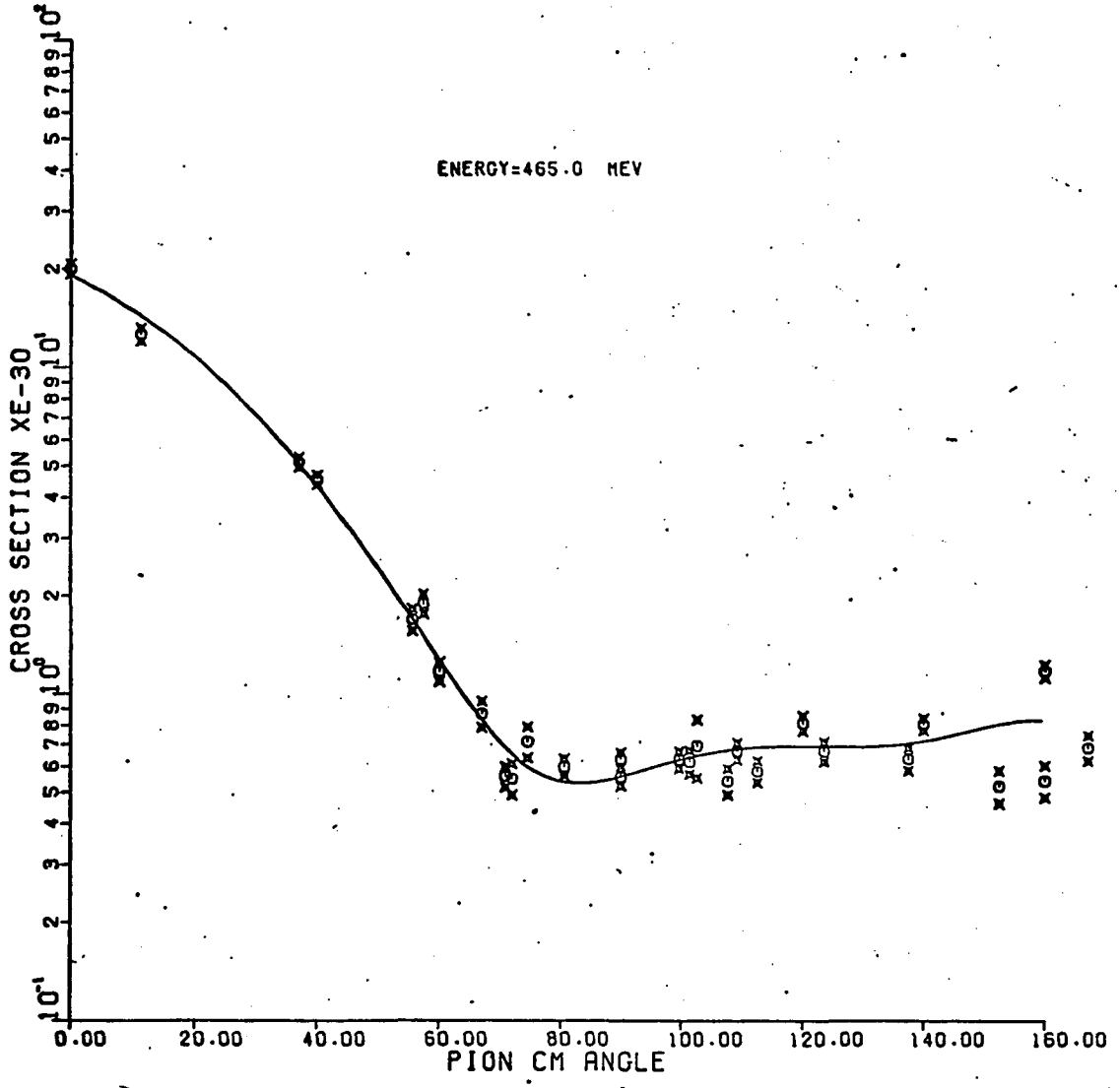
ENERGY=465.0 MEV
CROSS SECTION XE-30
PION CM ANGLE
0.00
20.00
40.00
60.00
80.00
100.00
120.00
140.00
160.00

Figure 18.

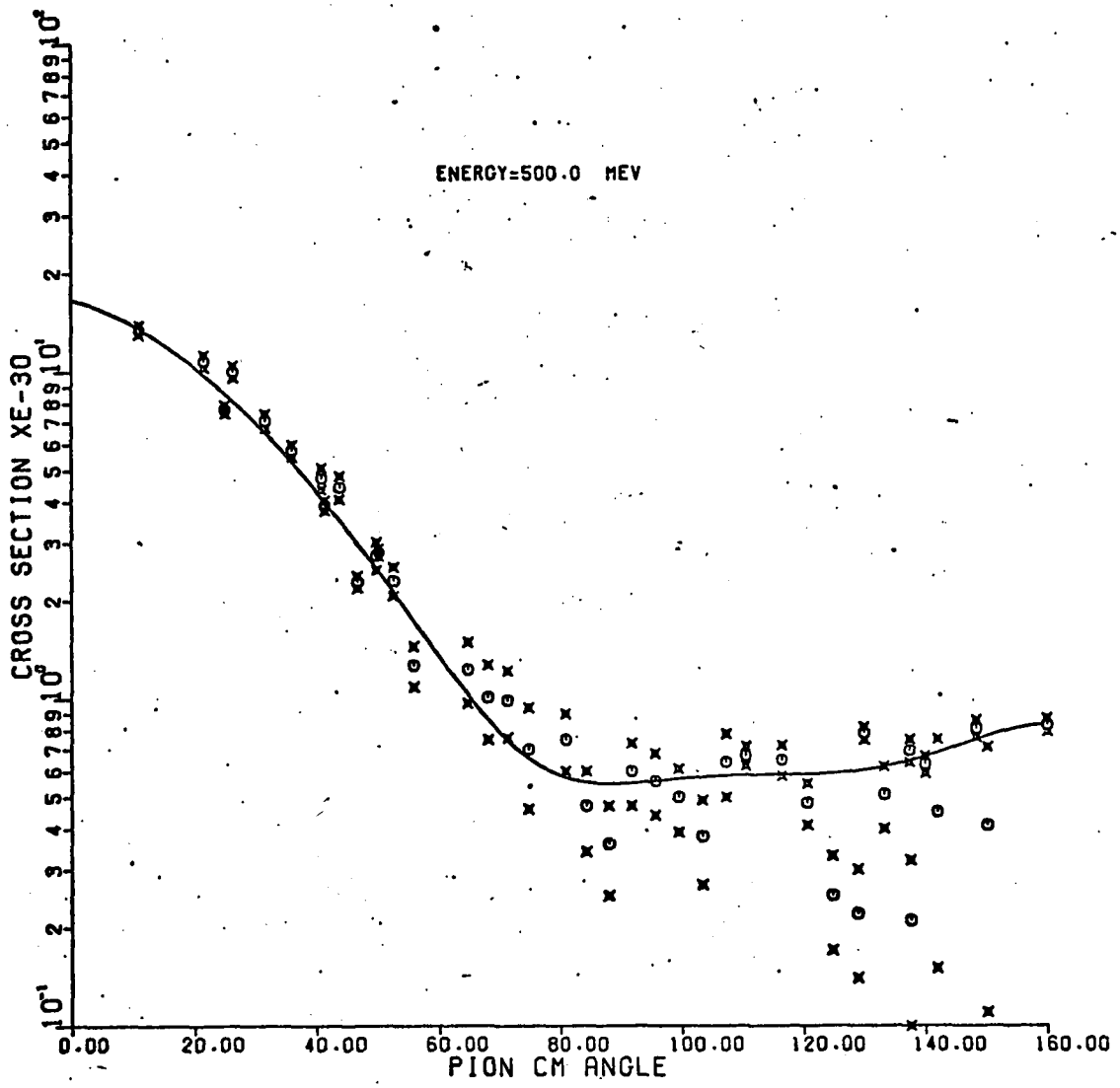
ENERGY=500.0 MEV
CROSS SECTION XE-30
PION CM ANGLE
0.00
20.00
40.00
60.00
80.00
100.00
120.00
140.00
160.00

Figure 19.

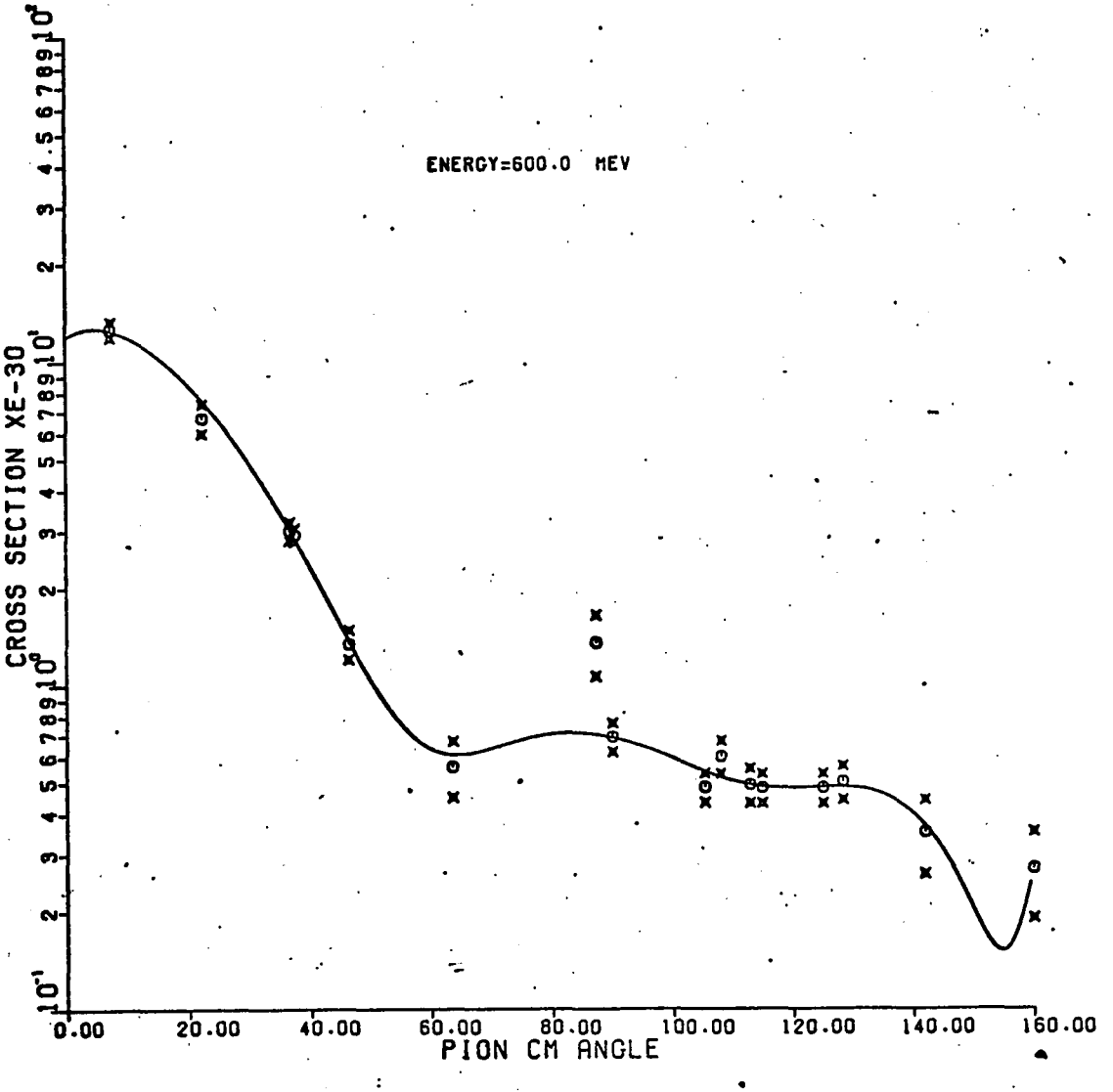
ENERGY=600.0 MEV
CROSS SECTION XE-30
PION CM ANGLE
0.00
20.00
40.00
60.00
80.00
100.00
120.00
140.00
160.00

Figure 20.

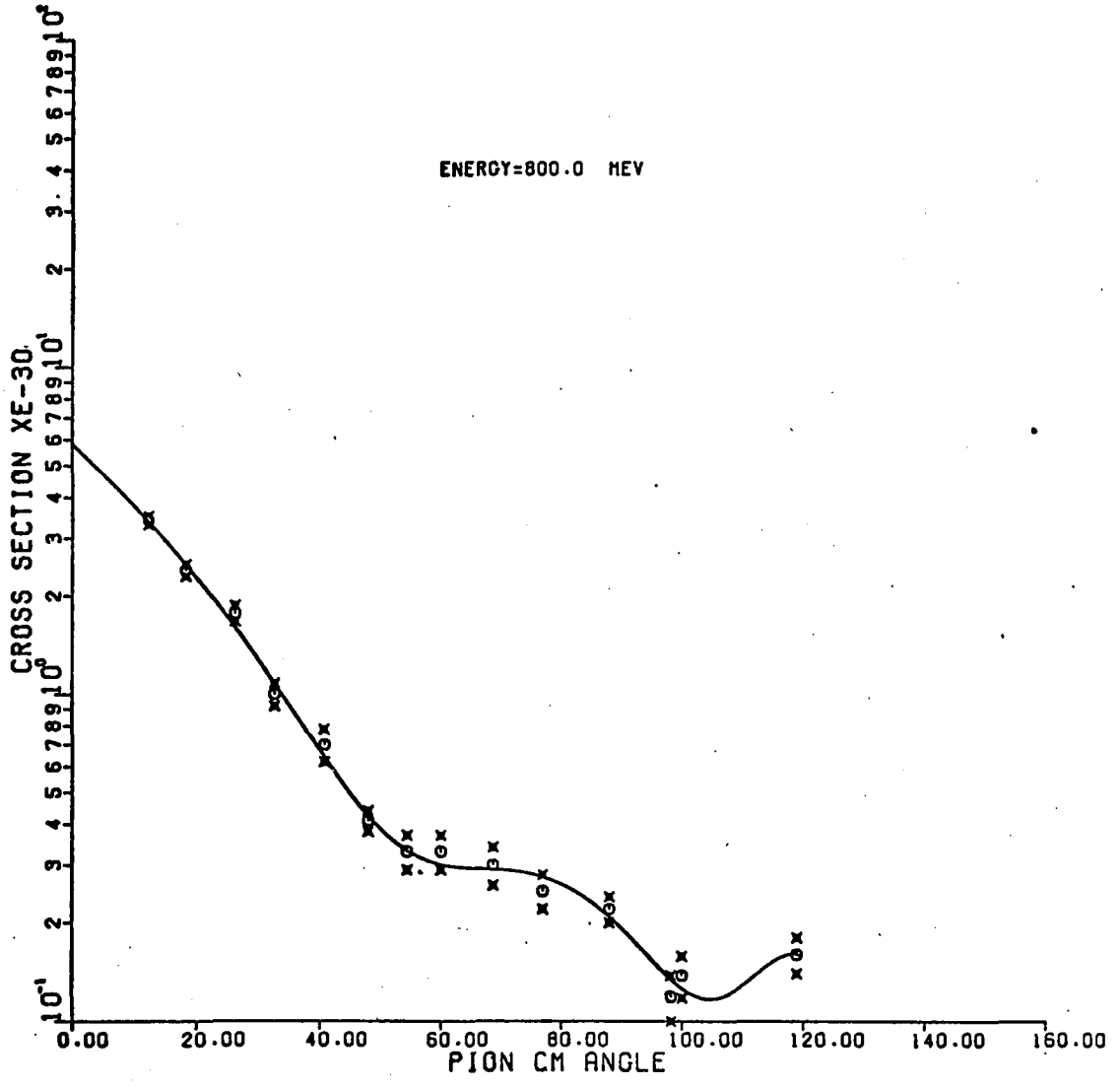
ENERGY=800.0 MEV
CROSS SECTION XE-30
PION CM ANGLE
0.00
20.00
40.00
60.00
80.00
100.00
120.00
140.00
160.00

Figure 21.

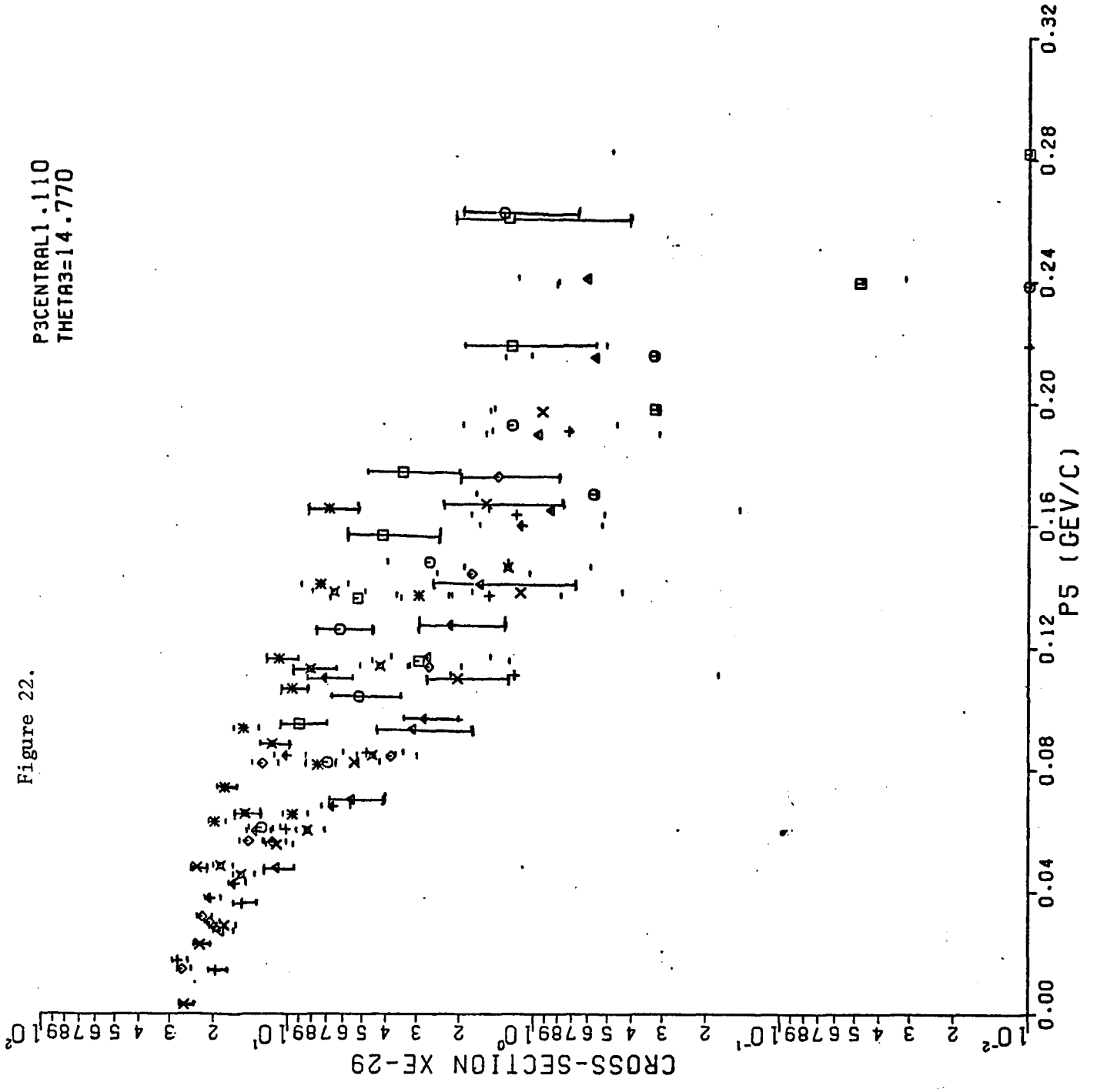
P3CENTRAL1.110
THETA3=14.770
CROSS-SECTION XE-29
P5 (GEV/C)
0.00
0.04
0.08
0.12
0.16
0.20
0.24
0.28
0.32

Figure 22.

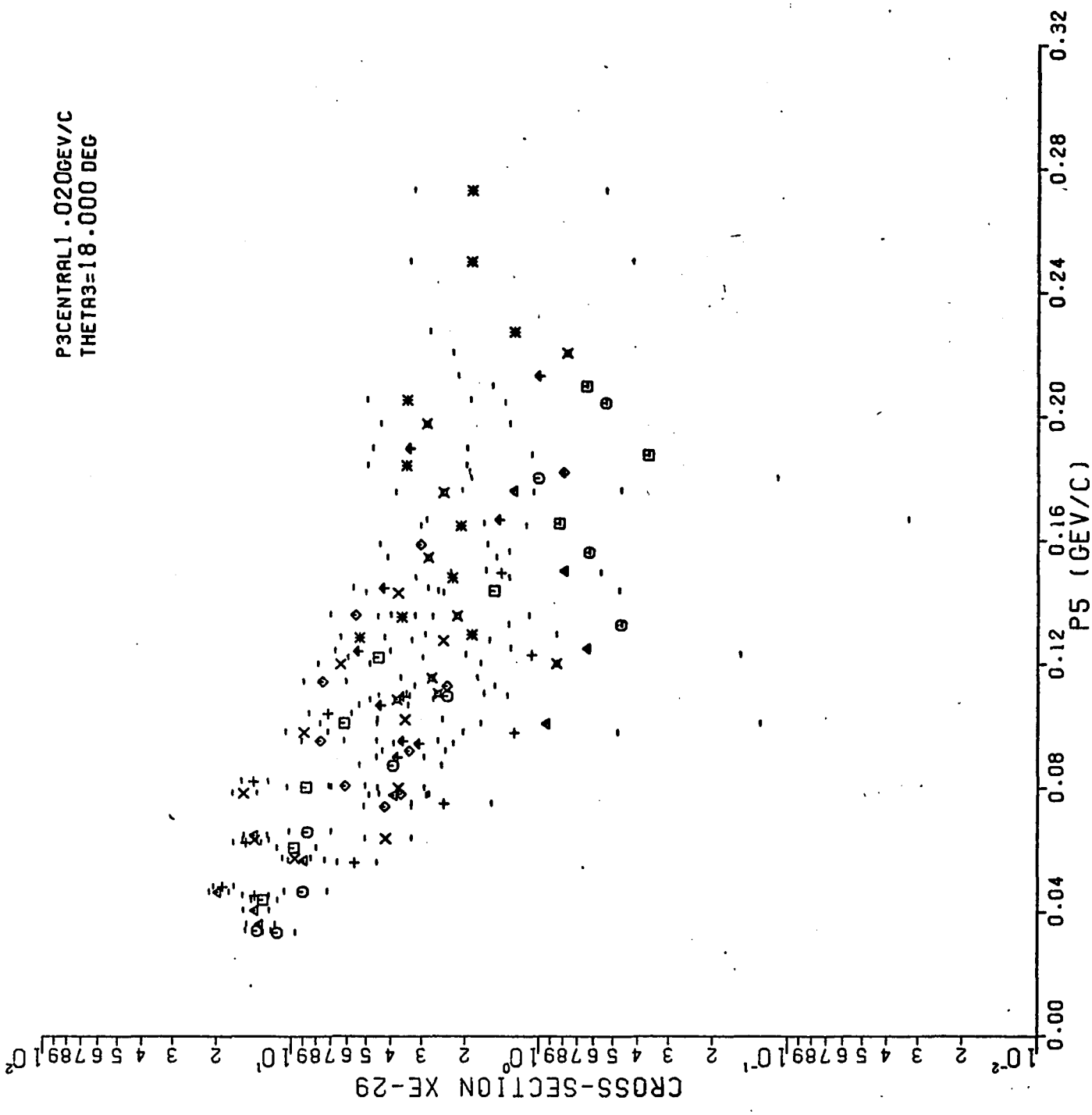
P3CENTRAL1 .020GEV/C
THETA3=18.000 DEG
CROSS-SECTION XE-29
P5 (GEV/C)
0.00
0.04
0.08
0.12
0.16
0.20
0.24
0.28
0.32

Figure 23.

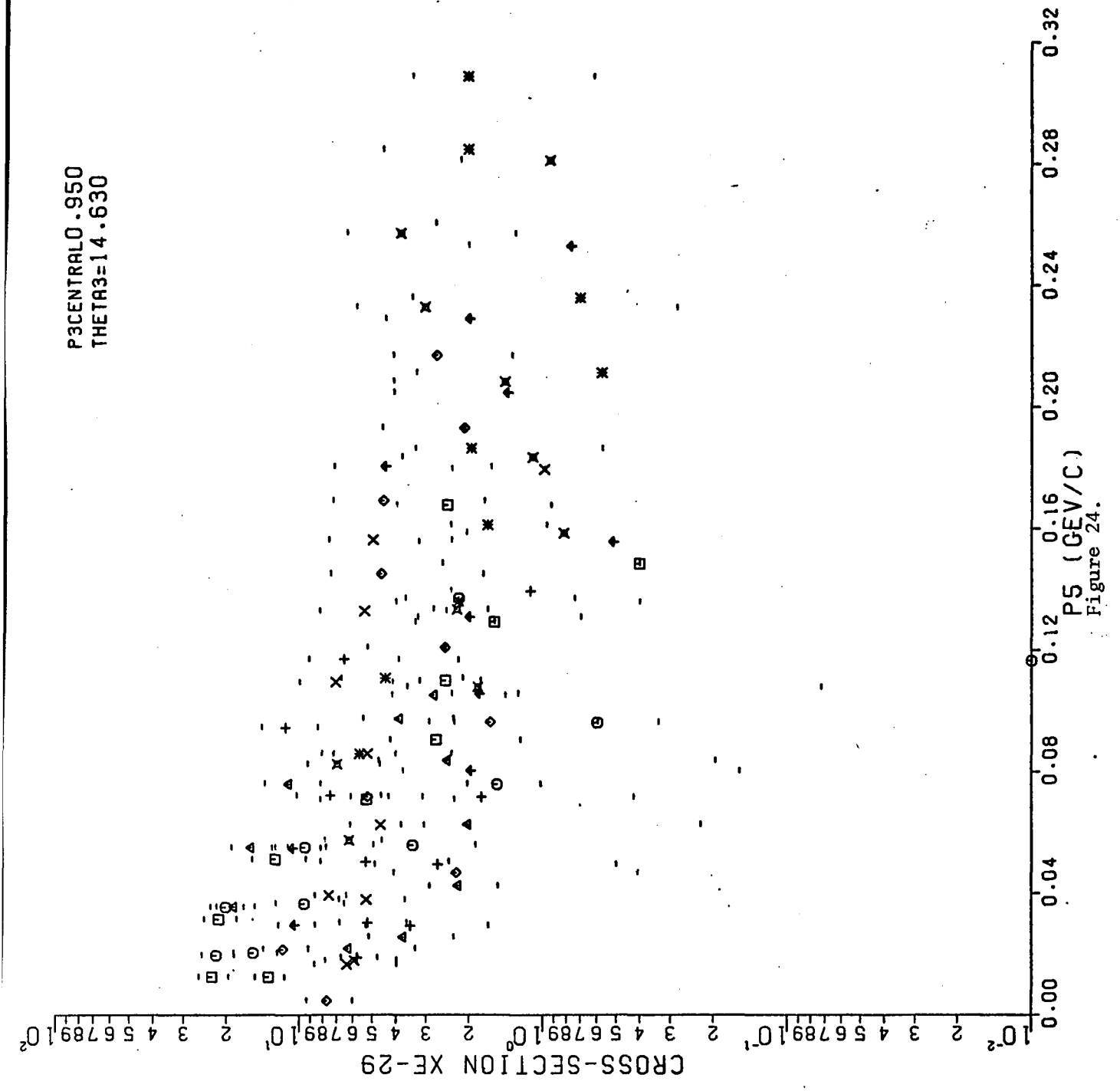
P3CENTRAL0.950
THETA3=14.630
CROSS-SECTION XE-29
P5 (GEV/C)
0.00
0.04
0.08
0.12
0.16
0.20
0.24
0.28
0.32

Figure 24.

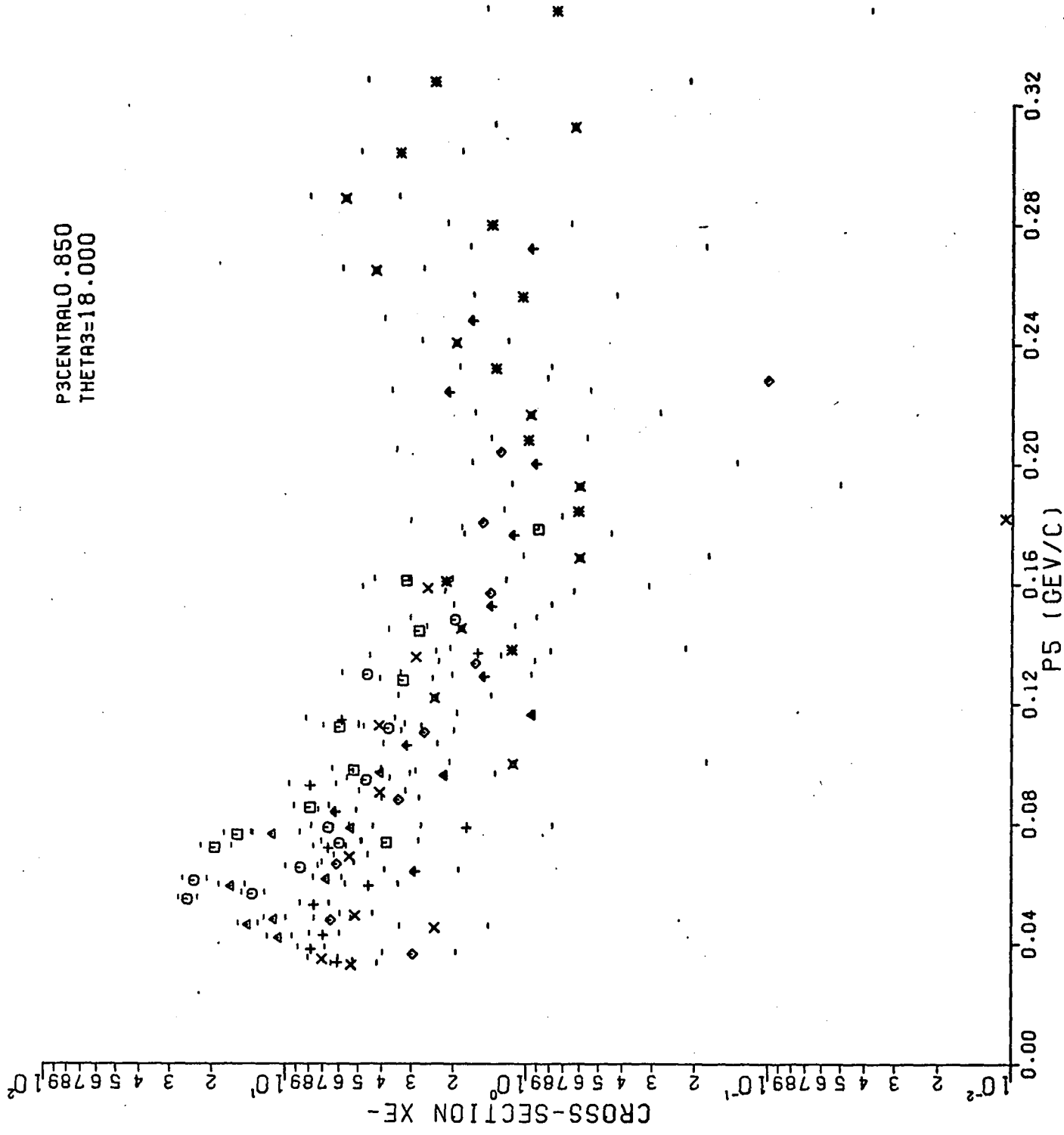
P3CENTRALO.850
THETA3=18.000
CROSS-SECTION XE-
P5 (GEV/C)
0.00
0.04
0.08
0.12
0.16
0.20
0.24
0.28
0.32

Figure 25.

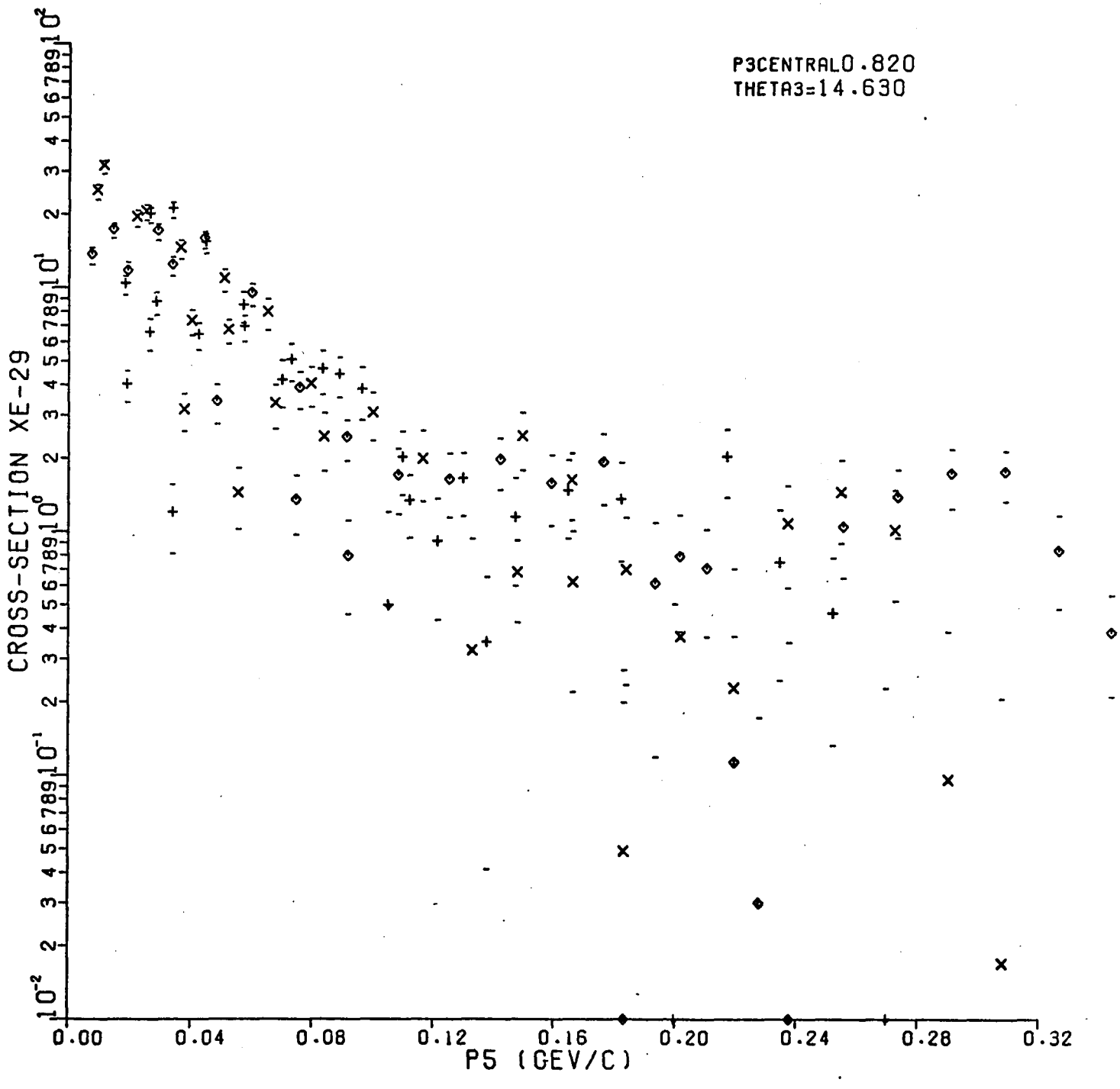
P3CENTRAL0.820
THETA3=14.630
CROSS-SECTION XE-29
P5 (GEV/C)
0.00
0.04
0.08
0.12
0.16
0.20
0.24
0.28
0.32

Figure 26.

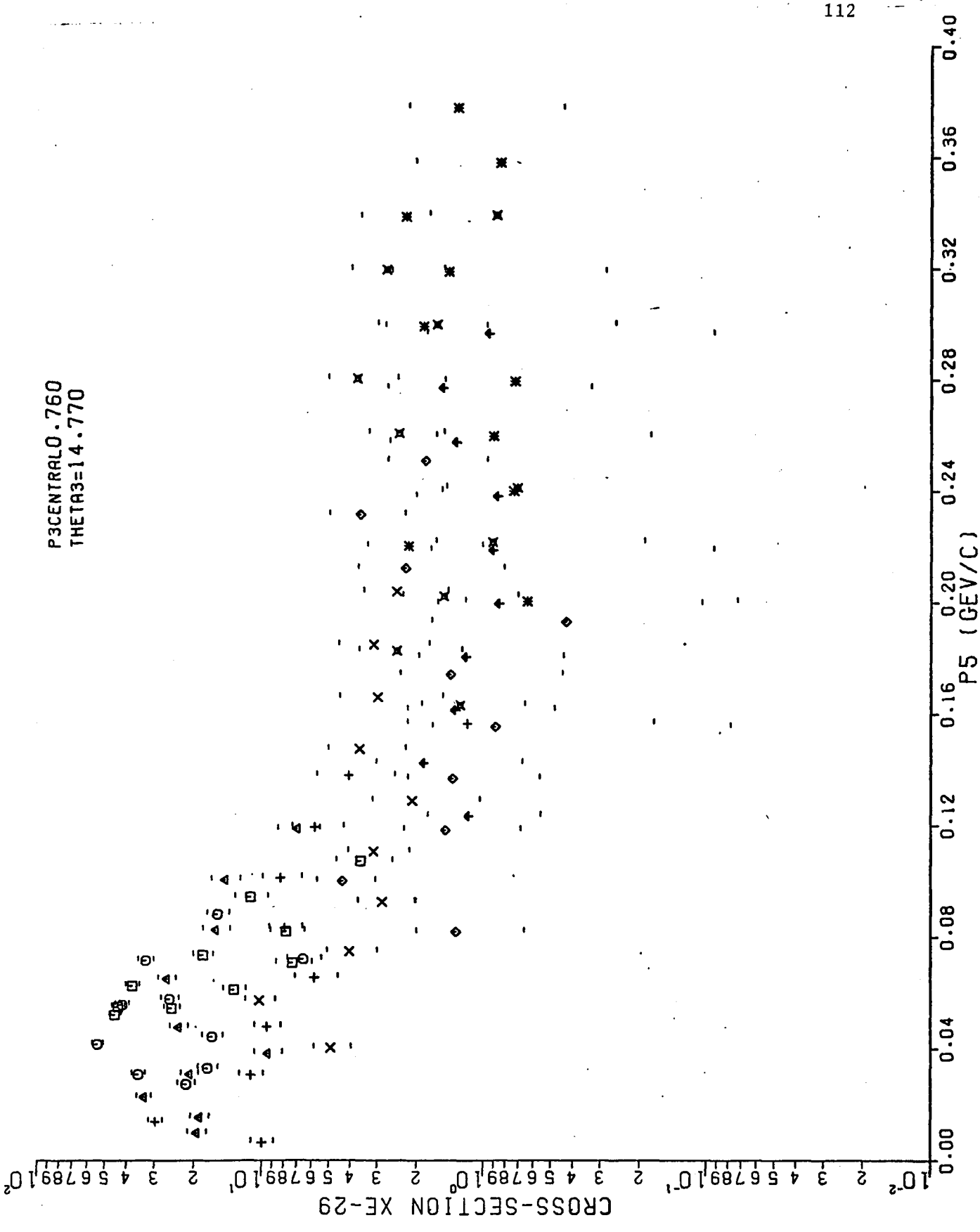

Figure 27.

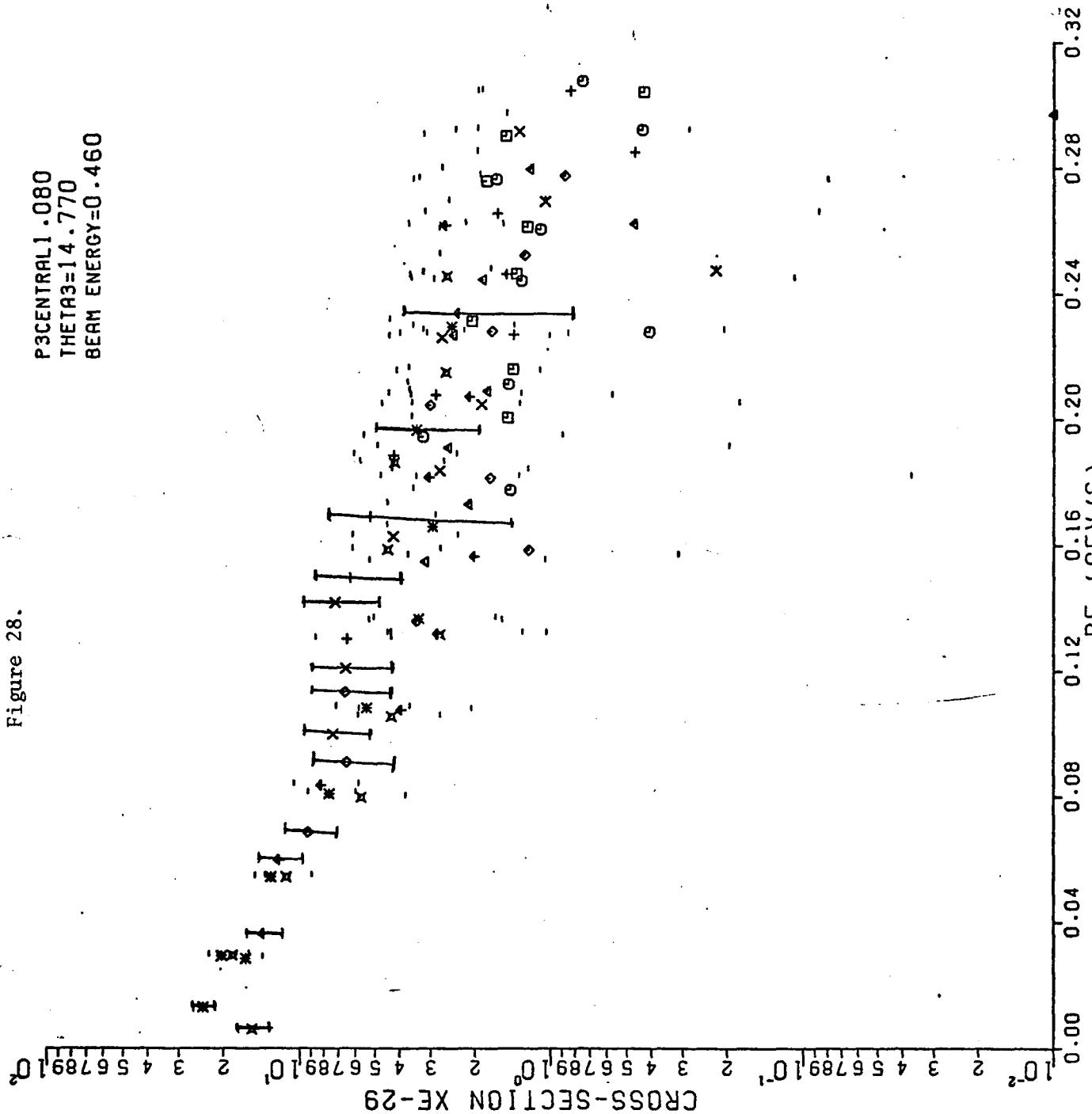
P3CENTRAL1.080
THETA3=14.770
BEAM ENERGY=0.460
CROSS-SECTION XE-29
P5 (GEV/C)
0.00
0.04
0.08
0.12
0.16
0.20
0.24
0.28
0.32

Figure 28.

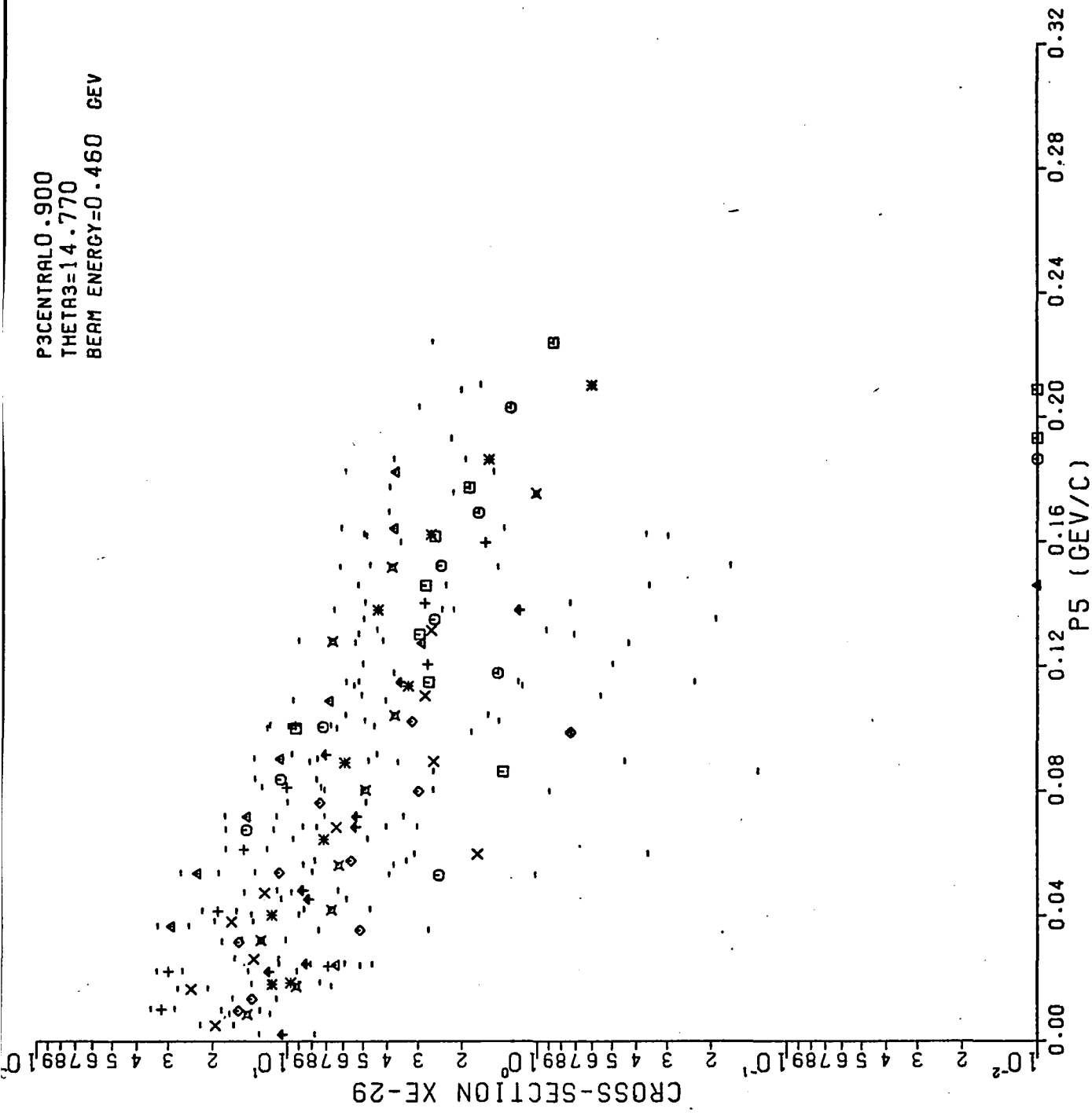
P3CENTRAL0.900
THETA3=14.770
BEAM ENERGY=0.460 GEV
CROSS-SECTION XE-29
P5 (GEV/C)
0.00
0.04
0.08
0.12
0.16
0.20
0.24
0.28
0.32

Figure 29.

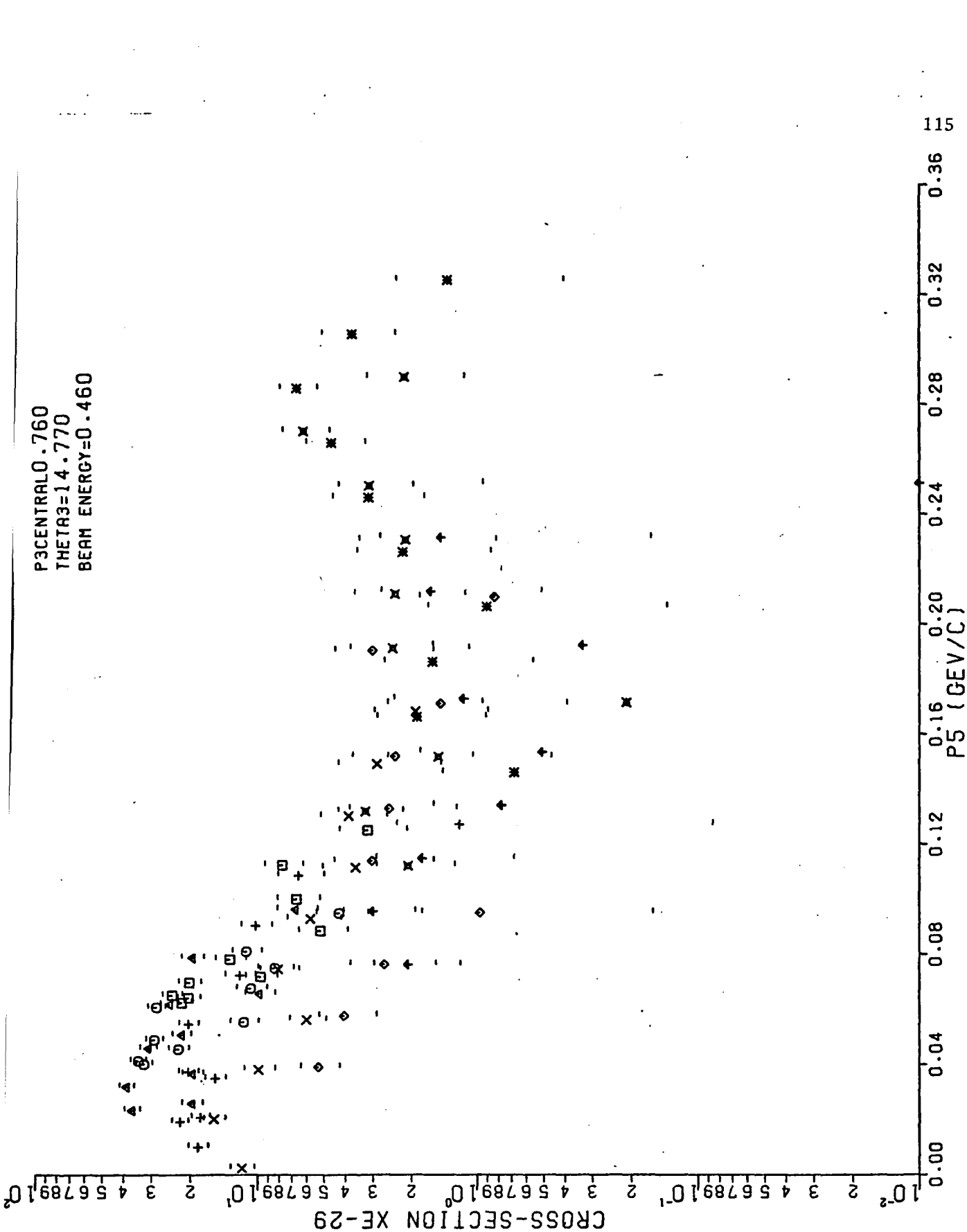
P3CENTRAL0.760
THETA3=14.770
BEAM ENERGY=0.460
CROSS-SECTION XE-29
P5 (GEV/C)
0.00
0.04
0.08
0.12
0.16
0.20
0.24
0.28
0.32
0.36

Figure 30.

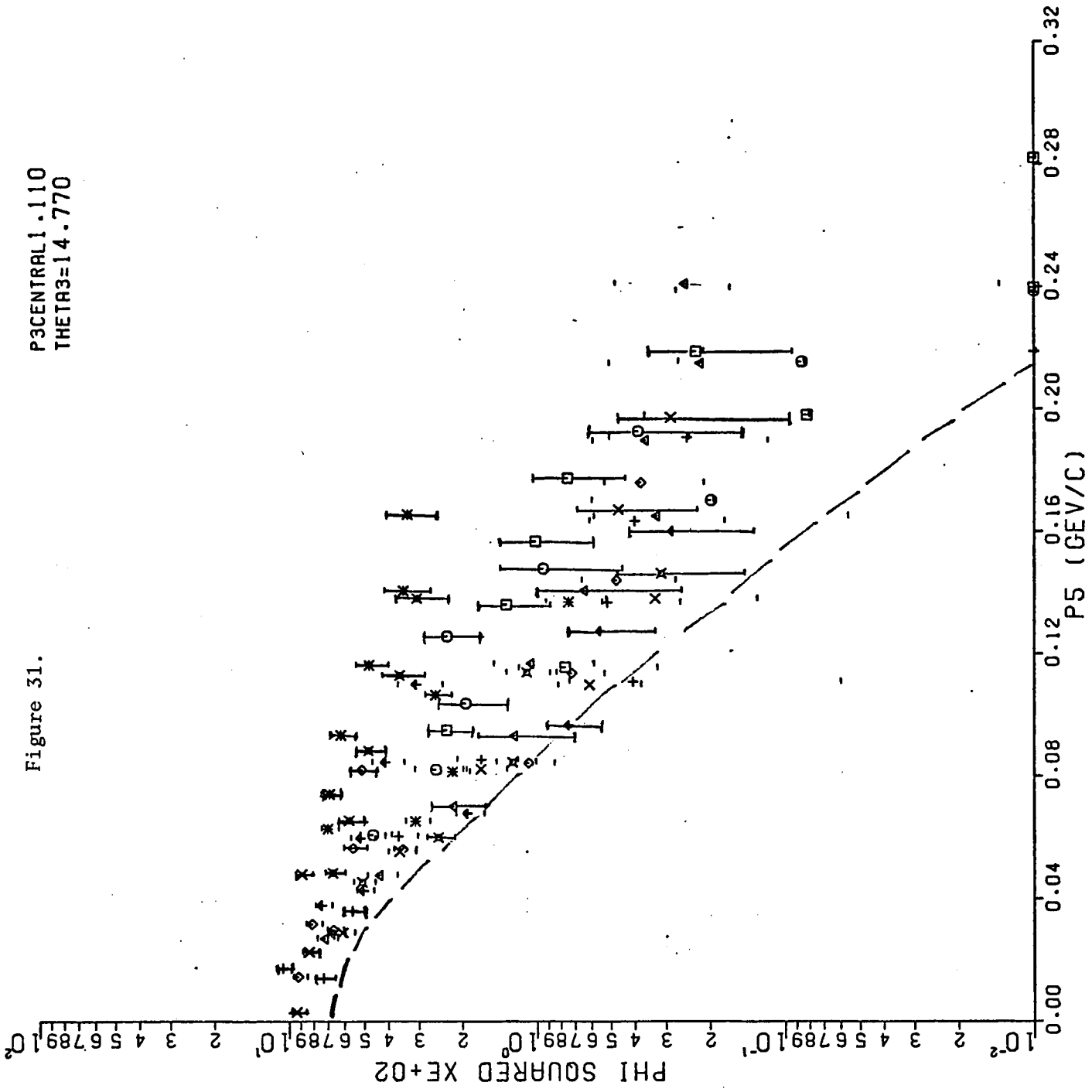
P3CENTRAL1.110
THETA3=14.770
PHI SQUARED XE+02
P5 (GEV/C)
0.00
0.04
0.08
0.12
0.16
0.20
0.24
0.28
0.32

Figure 31.

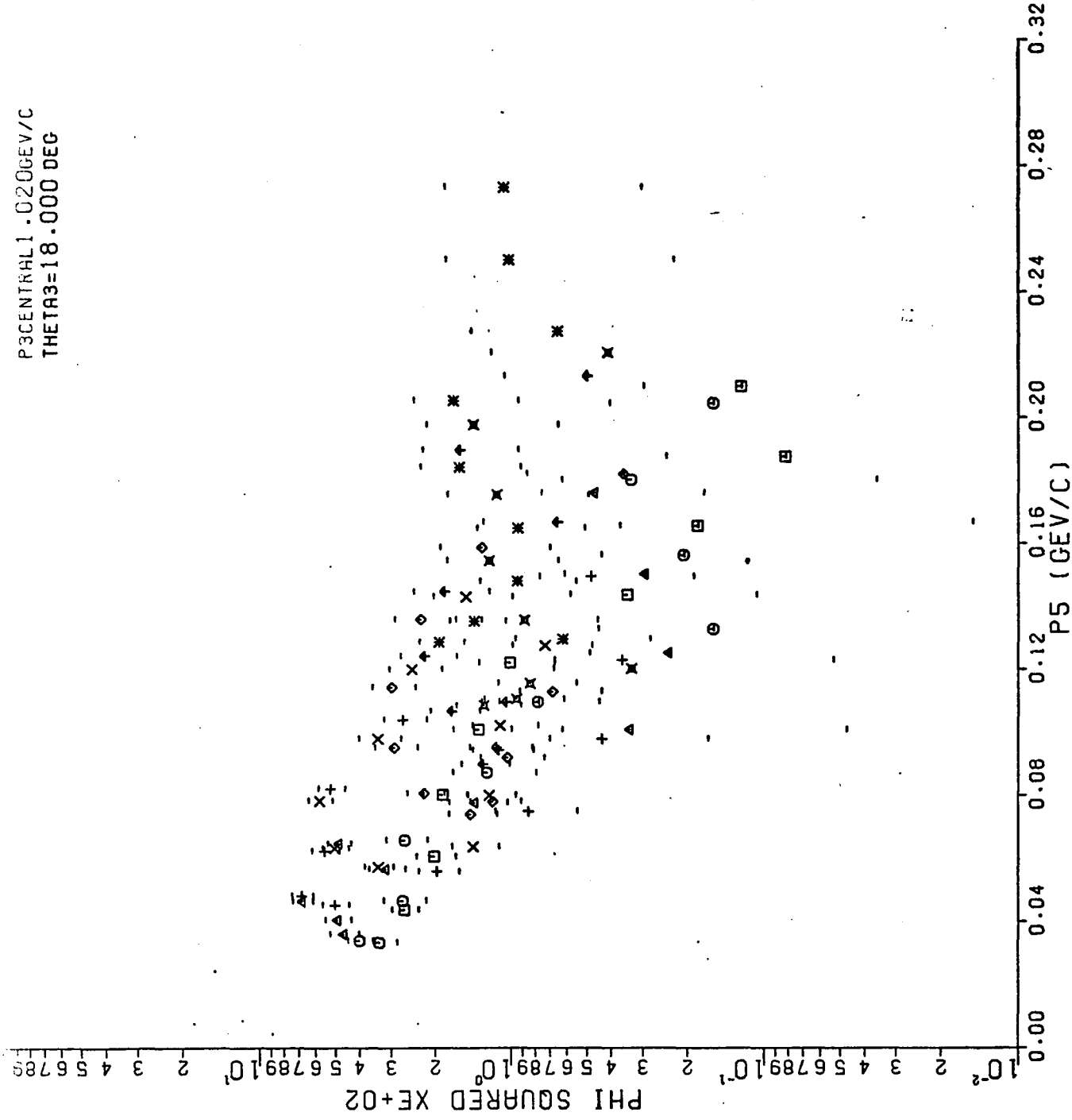
P3CENTRAL1 .020GEV/C
THETA3=18.000 DEG
PHI SQUARED XE+02
P5 (GEV/C)
0.00
0.04
0.08
0.12
0.16
0.20
0.24
0.28
0.32

Figure 32.

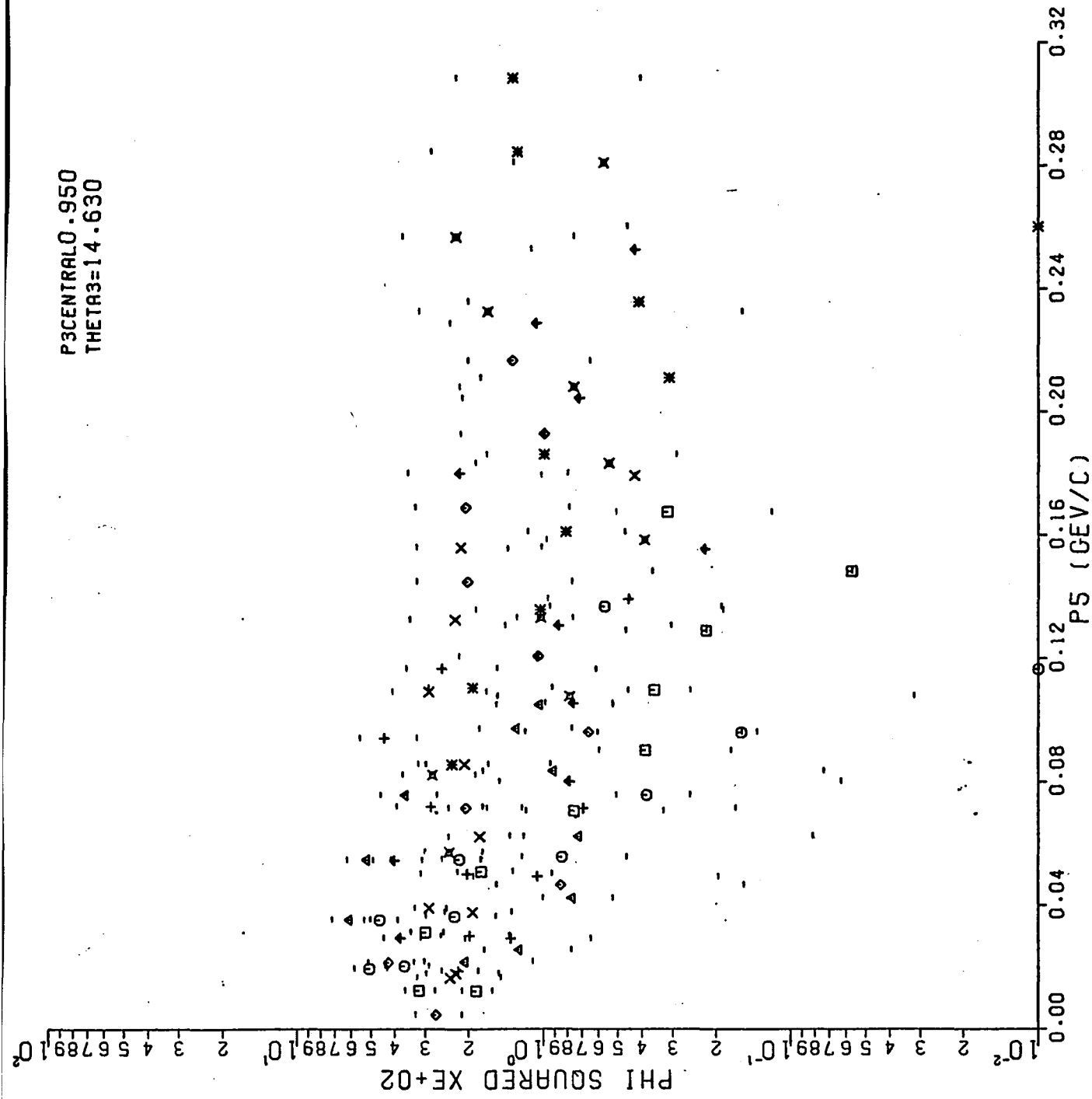
P3CENTRAL0.950
THETA3=14.630
PHI SQUARED XE+02
PS (GEV/C)
0.00
0.04
0.08
0.12
0.16
0.20
0.24
0.28
0.32

Figure 33.

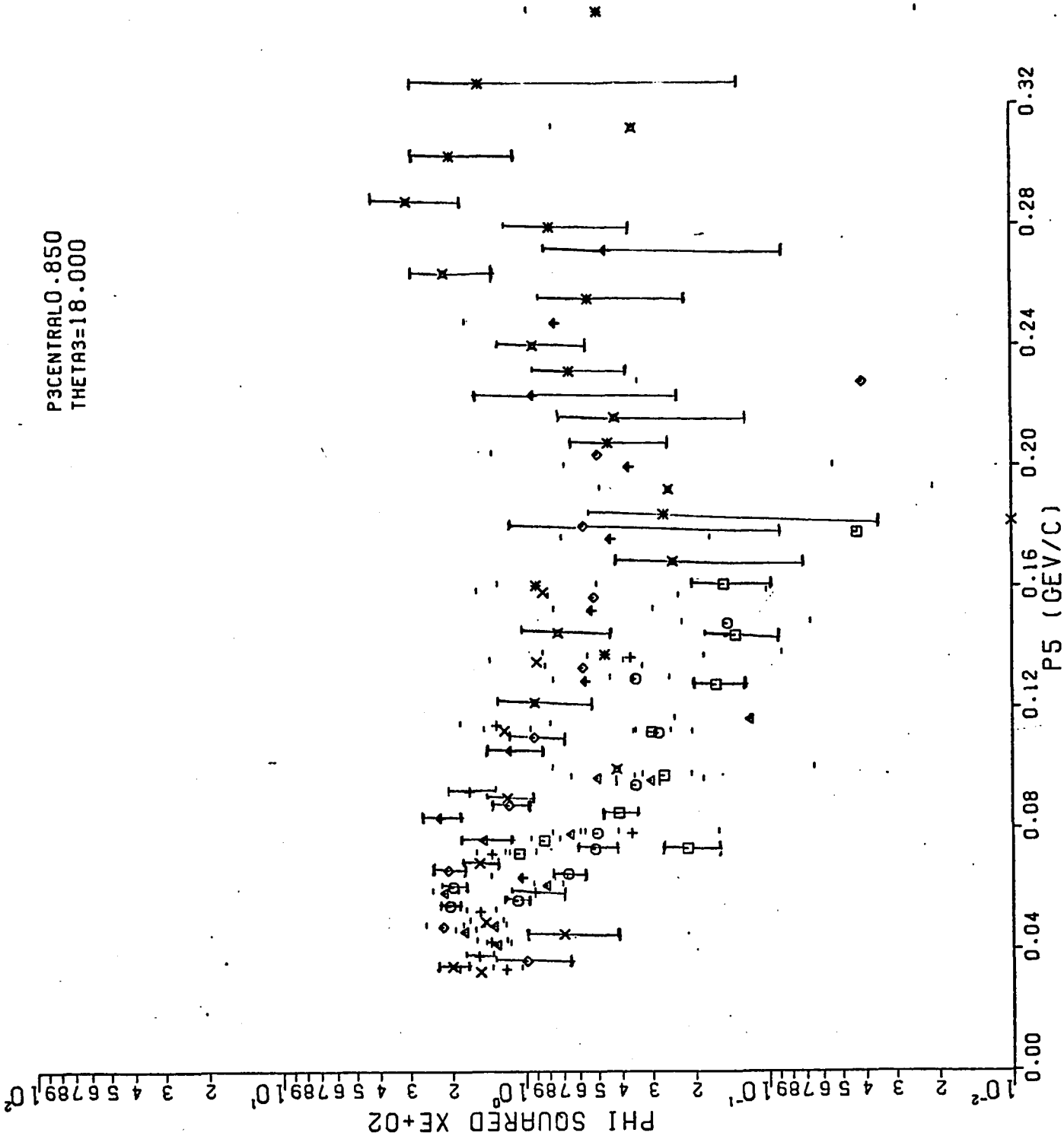
P3CENTRALO.850
THETA3=18.000
PHI SQUARED XE+02
P5 (GEV/C)
0.00
0.04
0.08
0.12
0.16
0.20
0.24
0.28
0.32

Figure 34.

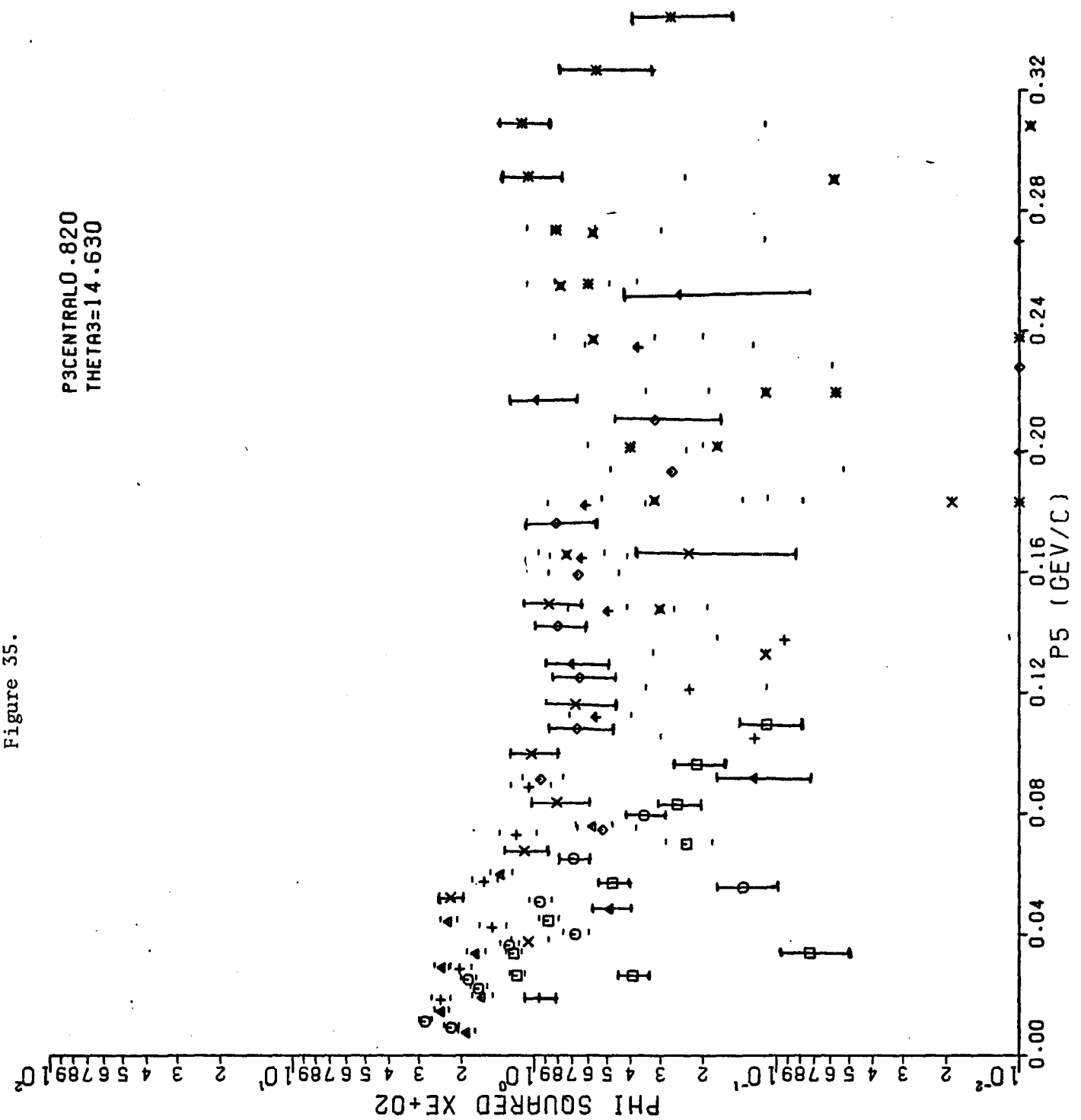
P3CENTRAL0.820
THETA3=14.630
PHI SQUARED XE+02
P5 (GEV/C)
0.00
0.04
0.08
0.12
0.16
0.20
0.24
0.28
0.32

Figure 35.

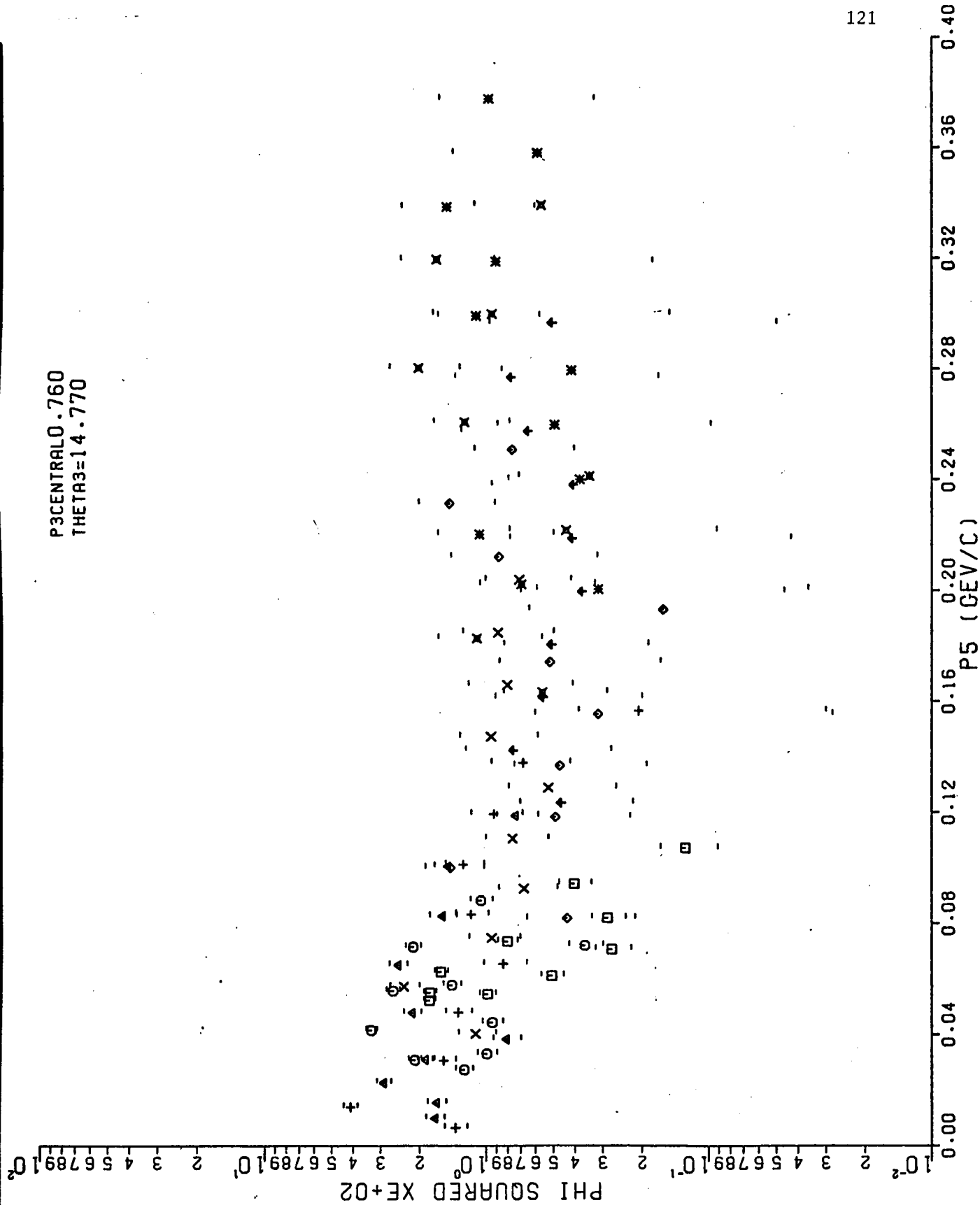
P3CENTRALO.760
THETA3=14.770
PHI SQUARED XE+02
P5 (GEV/C)
0.00
0.04
0.08
0.12
0.16
0.20
0.24
0.28
0.32
0.36
0.40

Figure 36.

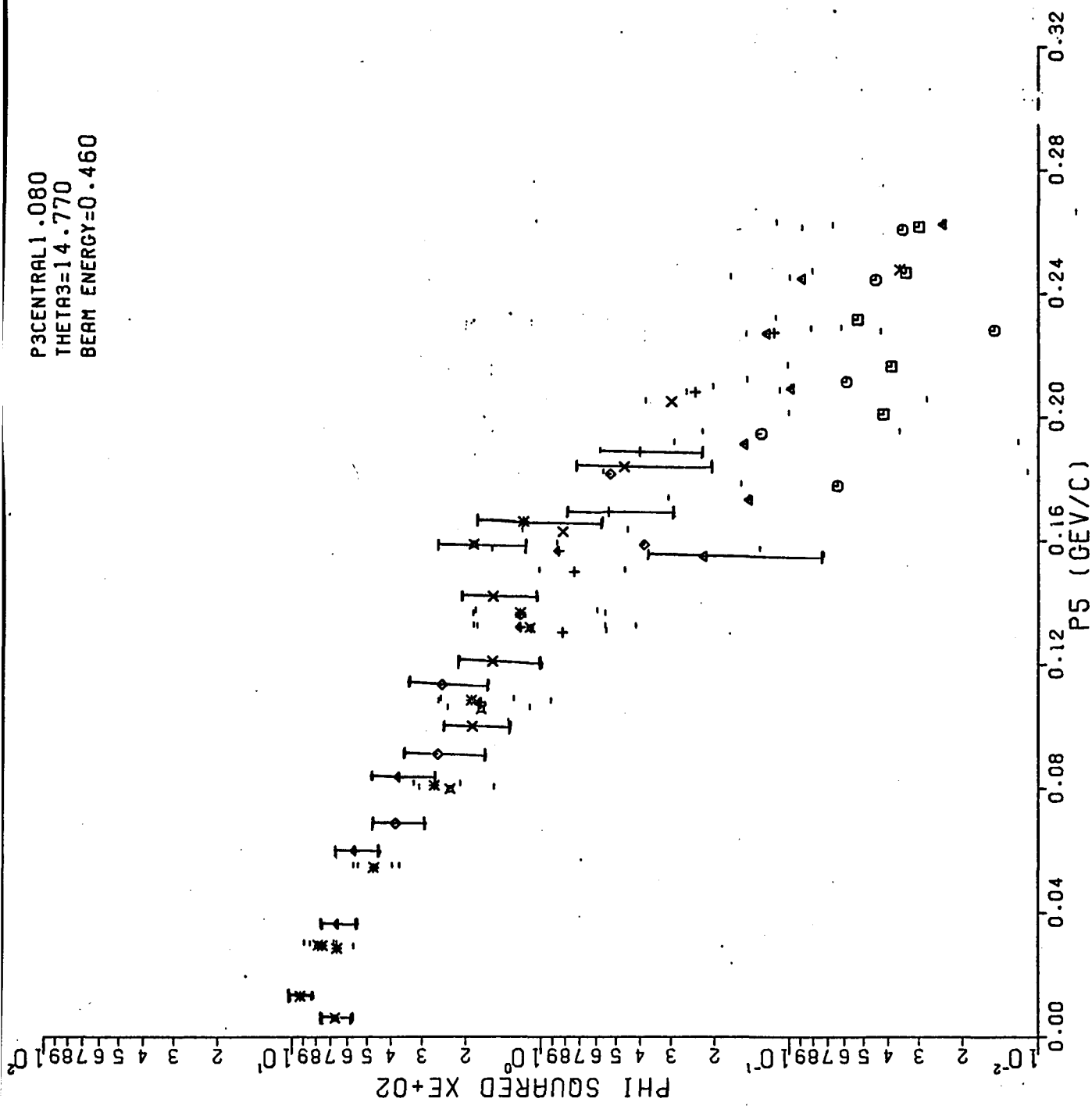
P3CENTRAL1.080
THETA3=14.770
BEAM ENERGY=0.460
PHI SQUARED XE+02
P5 (GEV/C)
0.00
0.04
0.08
0.12
0.16
0.20
0.24
0.28
0.32

Figure 37.

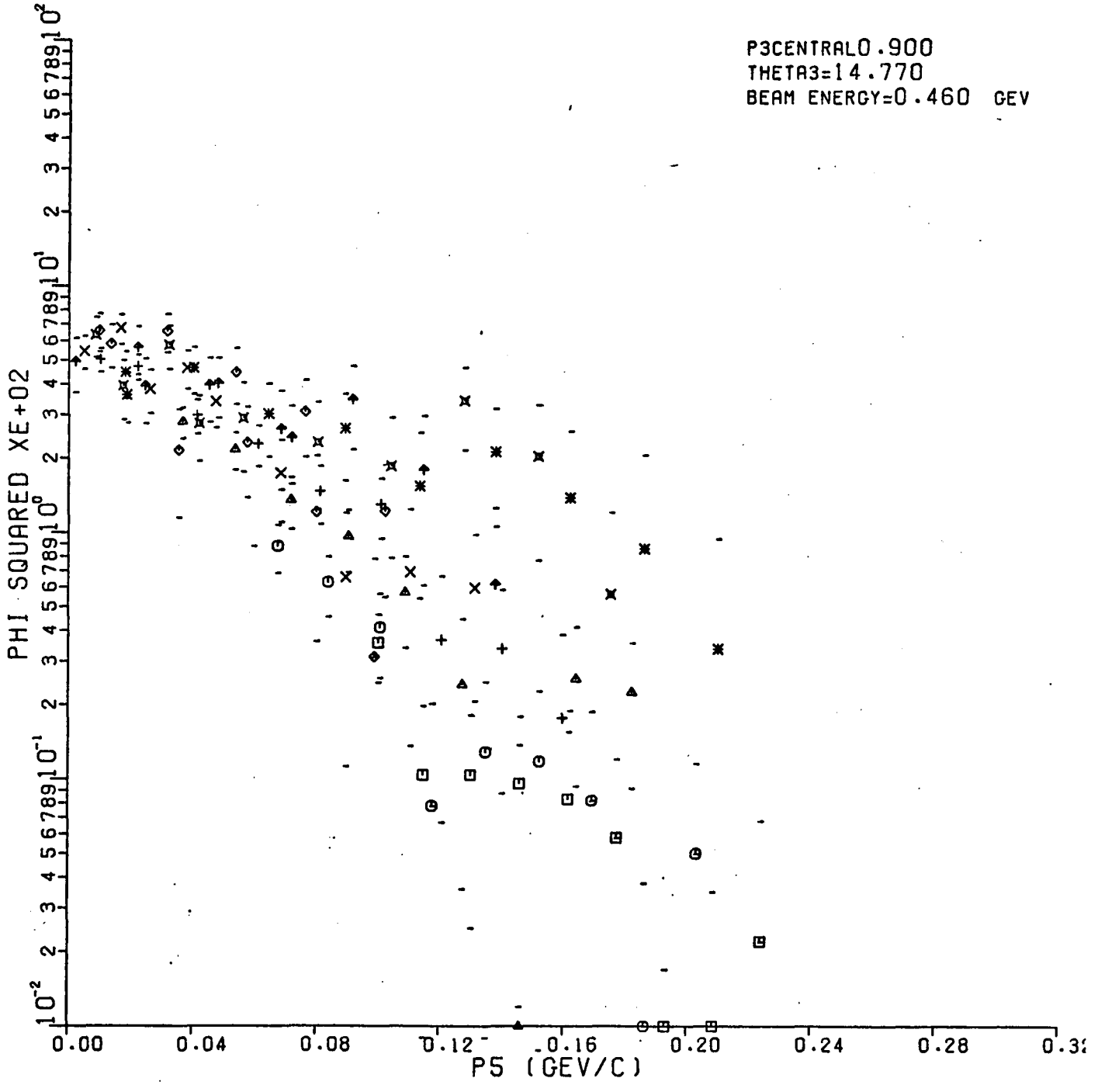
P3CENTRAL0.900
THETA3=14.770
BEAM ENERGY=0.460 GEV
PHI SQUARED XE+02
P5 (GEV/C)
0.00
0.04
0.08
0.12
0.16
0.20
0.24
0.28

Figure 38.

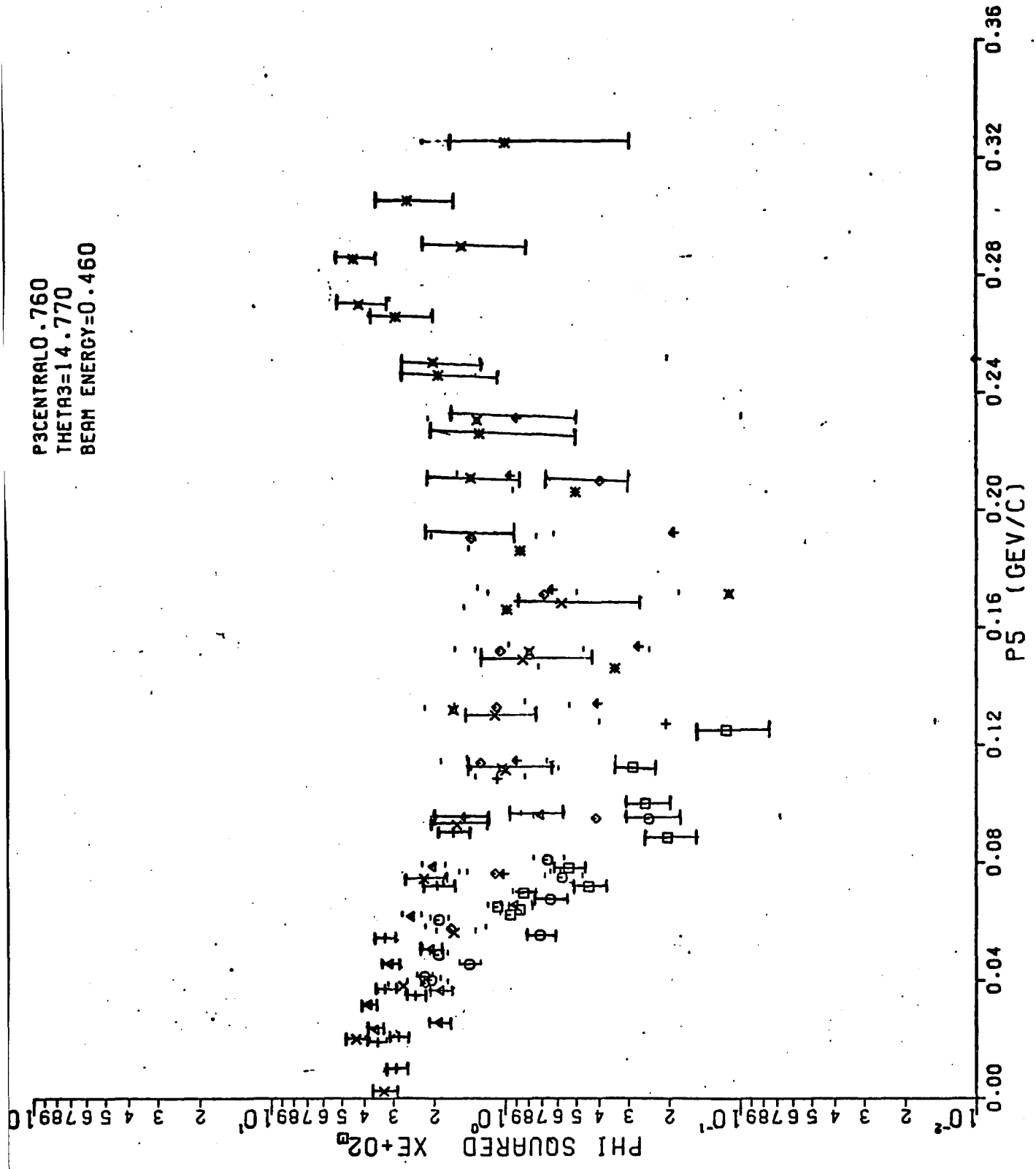
P3CENTRAL0.760
THETA3=14.770
BEAM ENERGY=0.460
PHI SQUARED XE+02
P5 (GEV/C)
0.00
0.04
0.08
0.12
0.16
0.20
0.24
0.28
0.32
0.36

Figure 39.

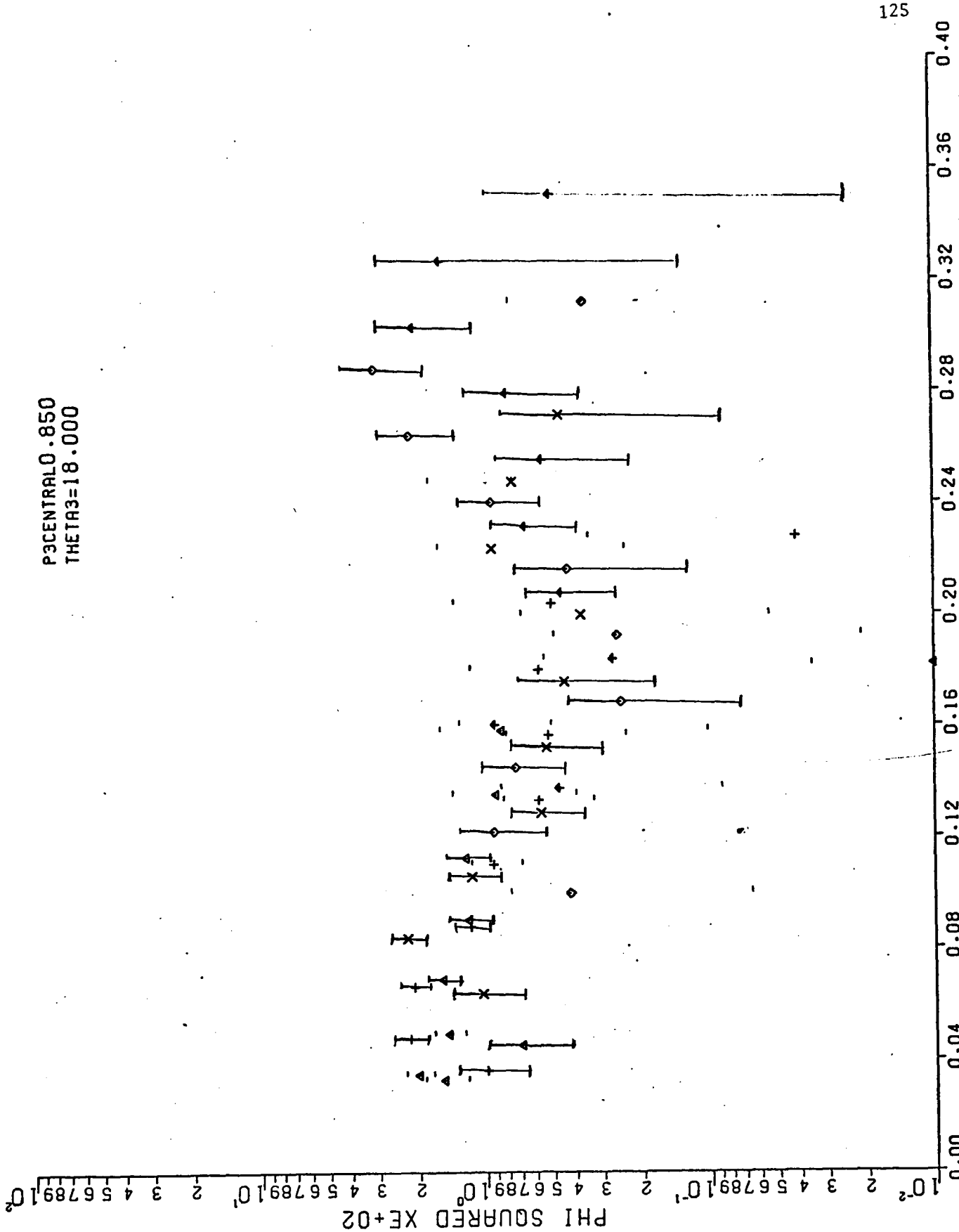
P3CENTRAL0.850
THETA3=18.000
PHI SQUARED XE+02
P5 (GEV/C)
0.00
0.04
0.08
0.12
0.16
0.20
0.24
0.28
0.32
0.36
0.40

Figure 40.

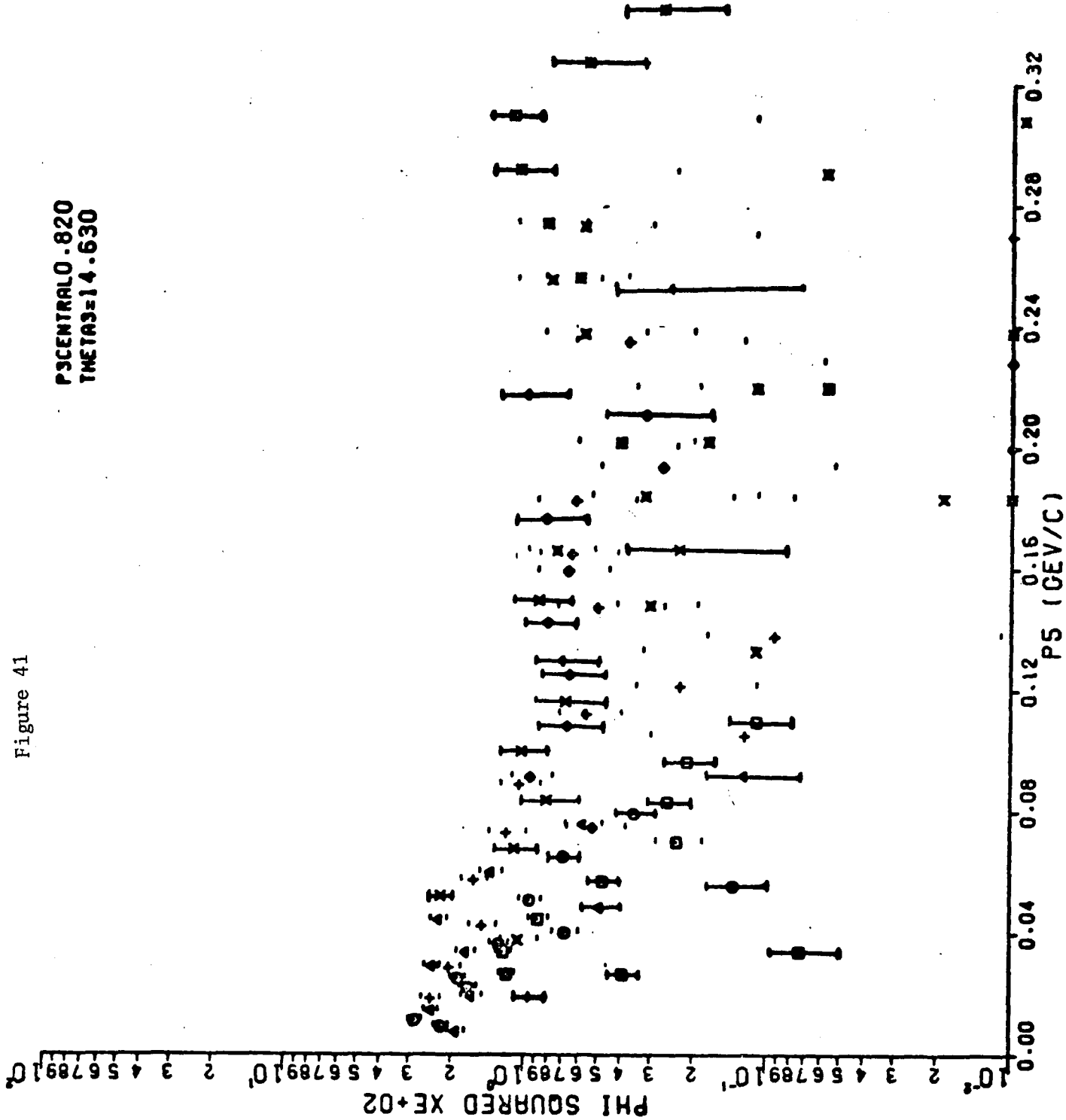
PSCENTRAL0.820
THETA3=14.630
PHI SQUARED XE+02
PS (GEV/C)
0.00
0.04
0.08
0.12
0.16
0.20
0.24
0.28
0.32

Figure 41

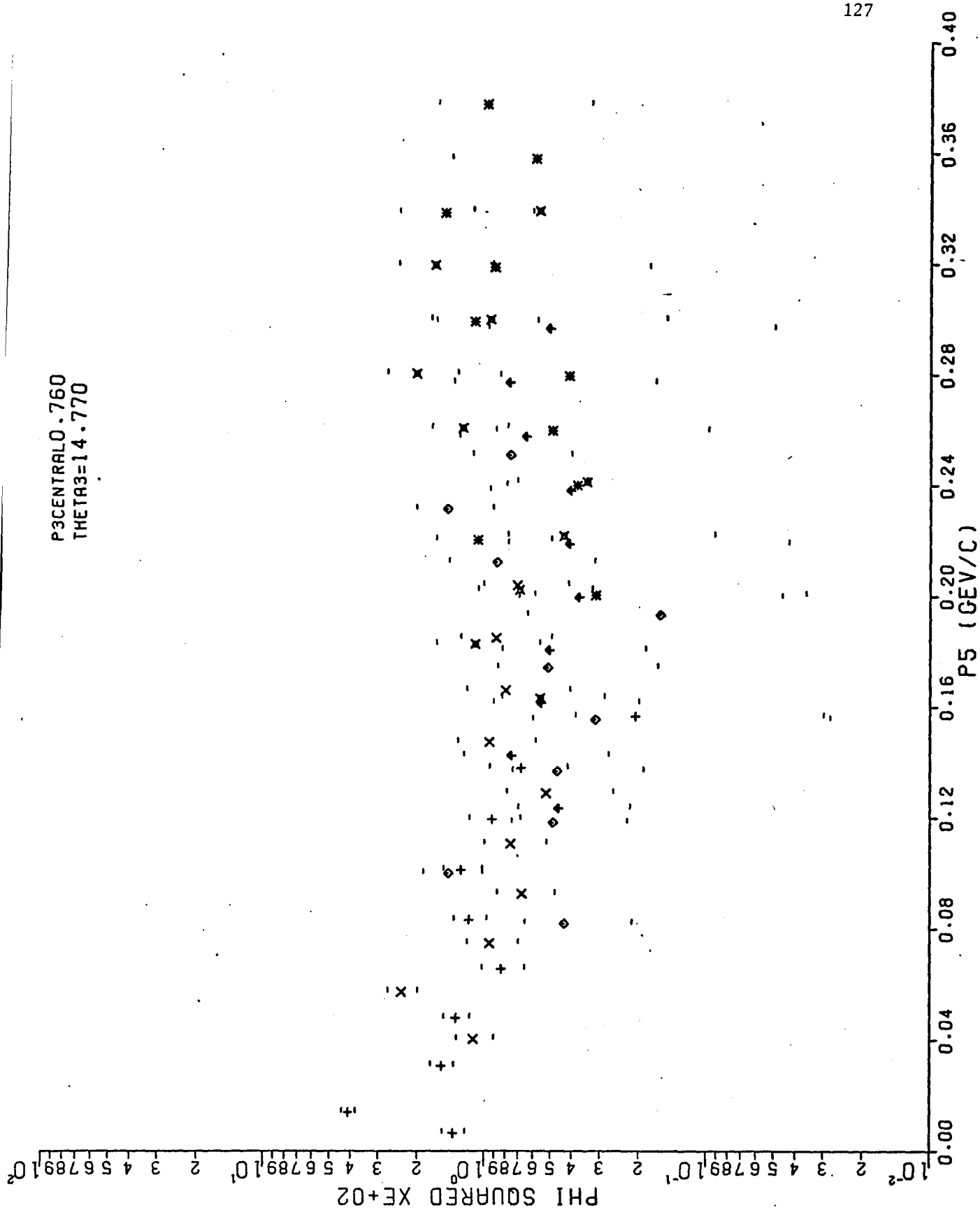
P3CENTRAL0.760
THETA3=14.770
PHI SQUARED XE+02
P5 (GEV/C)
0.00
0.04
0.08
0.12
0.16
0.20
0.24
0.28
0.32
0.36
0.40

Figure 42.

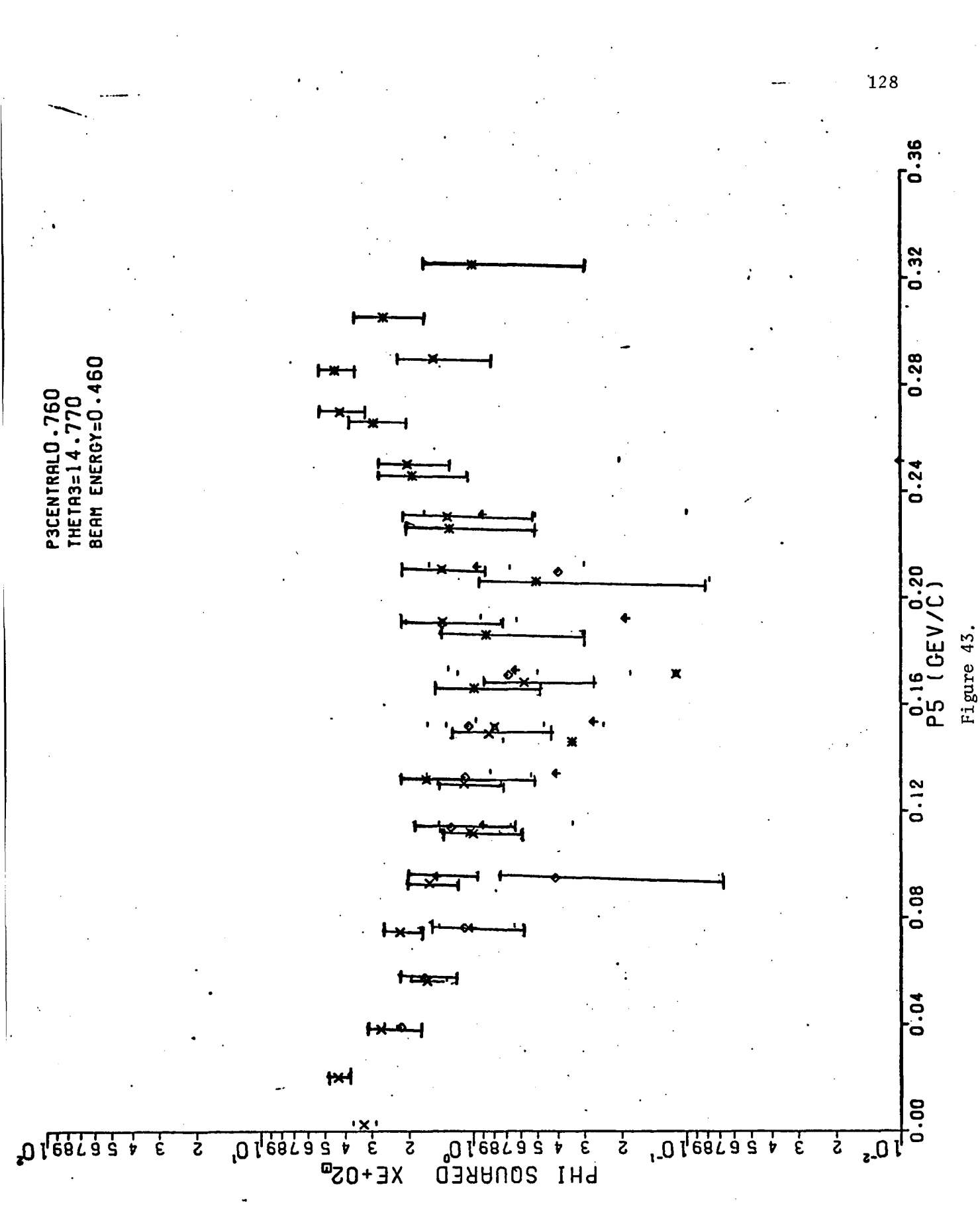
P3CENTRAL0.760
THETA3=14.770
BEAM ENERGY=0.460
PHI SQUARED XE+02
P5 (GEV/C)
0.00
0.04
0.08
0.12
0.16
0.20
0.24
0.28
0.32
0.36

Figure 43.

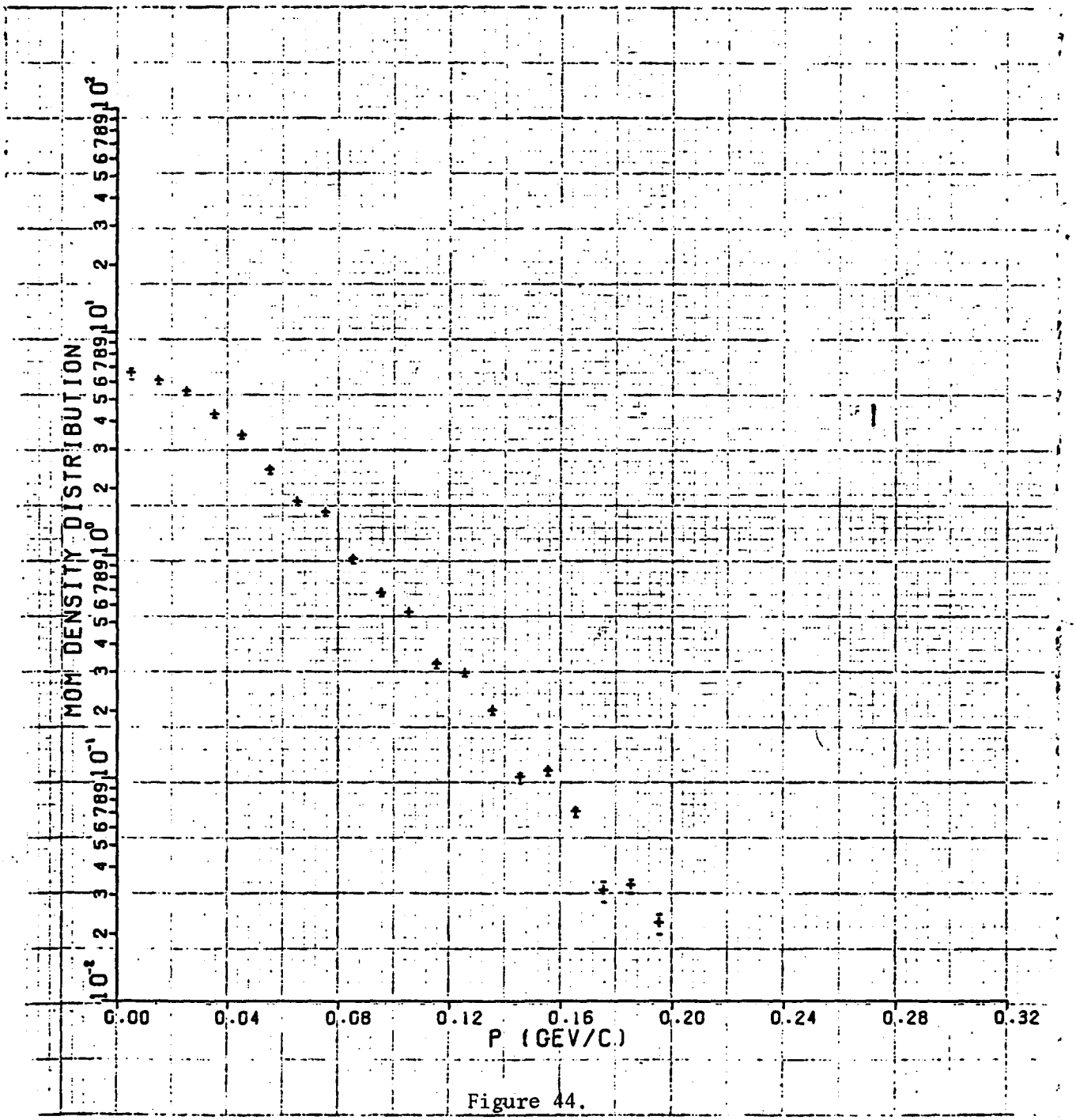
MOM DENSITY DISTRIBUTION
P (GEV/C)
0.00
0.04
0.08
0.12
0.16
0.20
0.24
0.28
0.32

Figure 44.

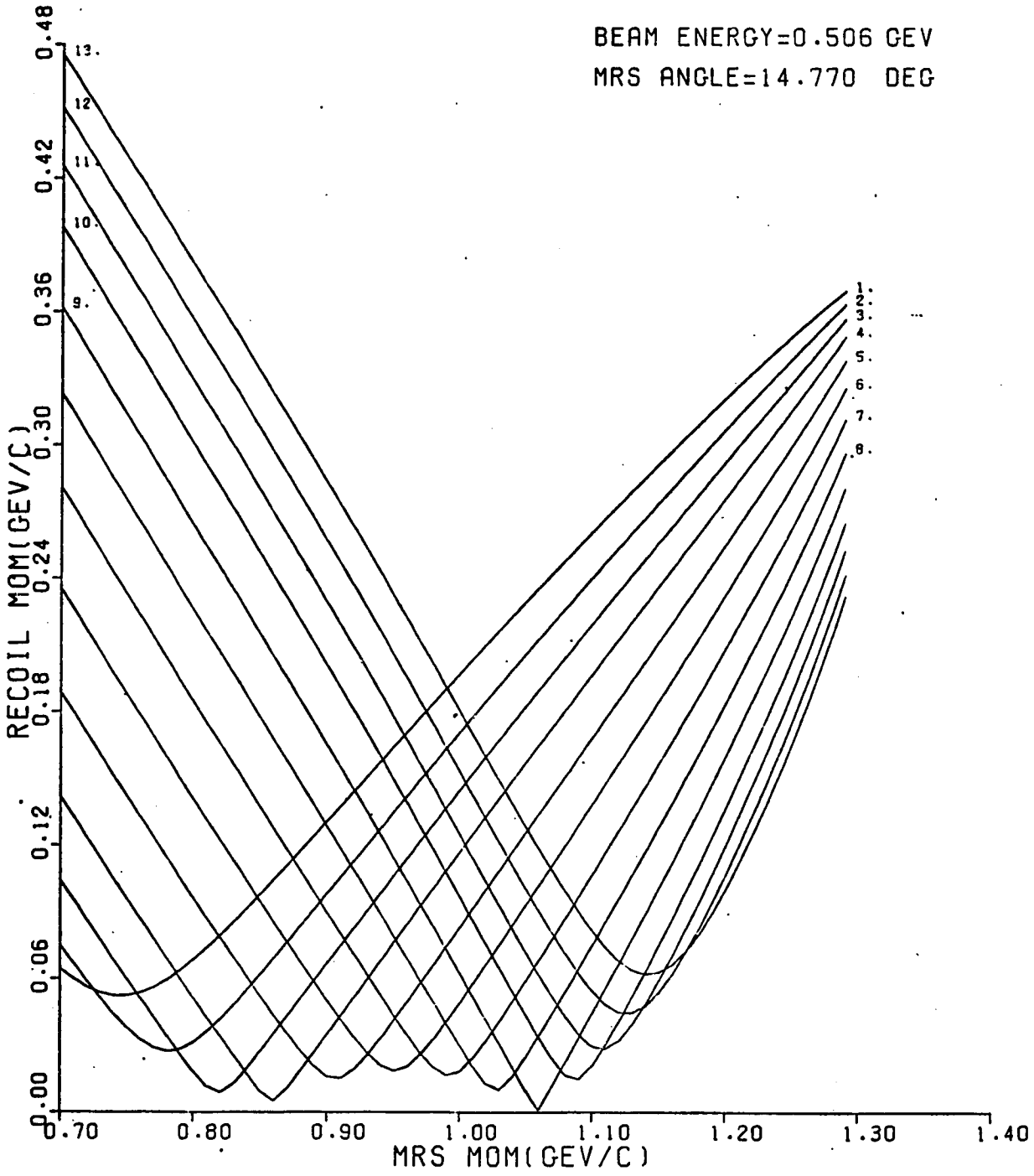
BEAM ENERGY=0.506 GEV
MRS ANGLE=14.770 DEG
RECOIL MOM(GEV/C)
MRS MOM(GEV/C)
0.00
0.06
0.12
0.18
0.24
0.30
0.36
0.42
0.48
0.70
0.80
0.90
1.00
1.10
1.20
1.30
1.40
1.
2.
3.
4.
5.
6.
7.
8.
9.
10.
11.
12.
13.

Figure 45

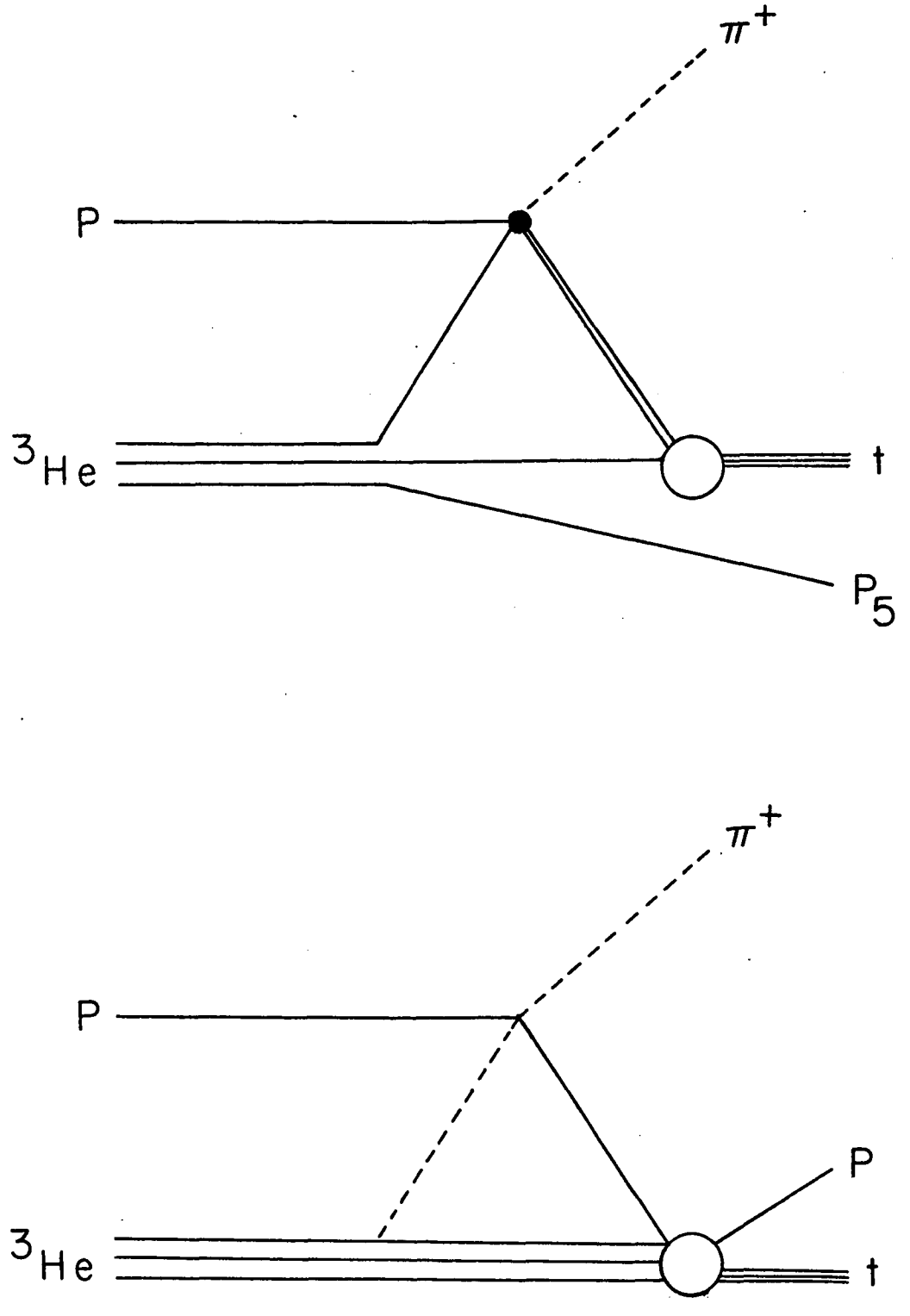

Figure 46

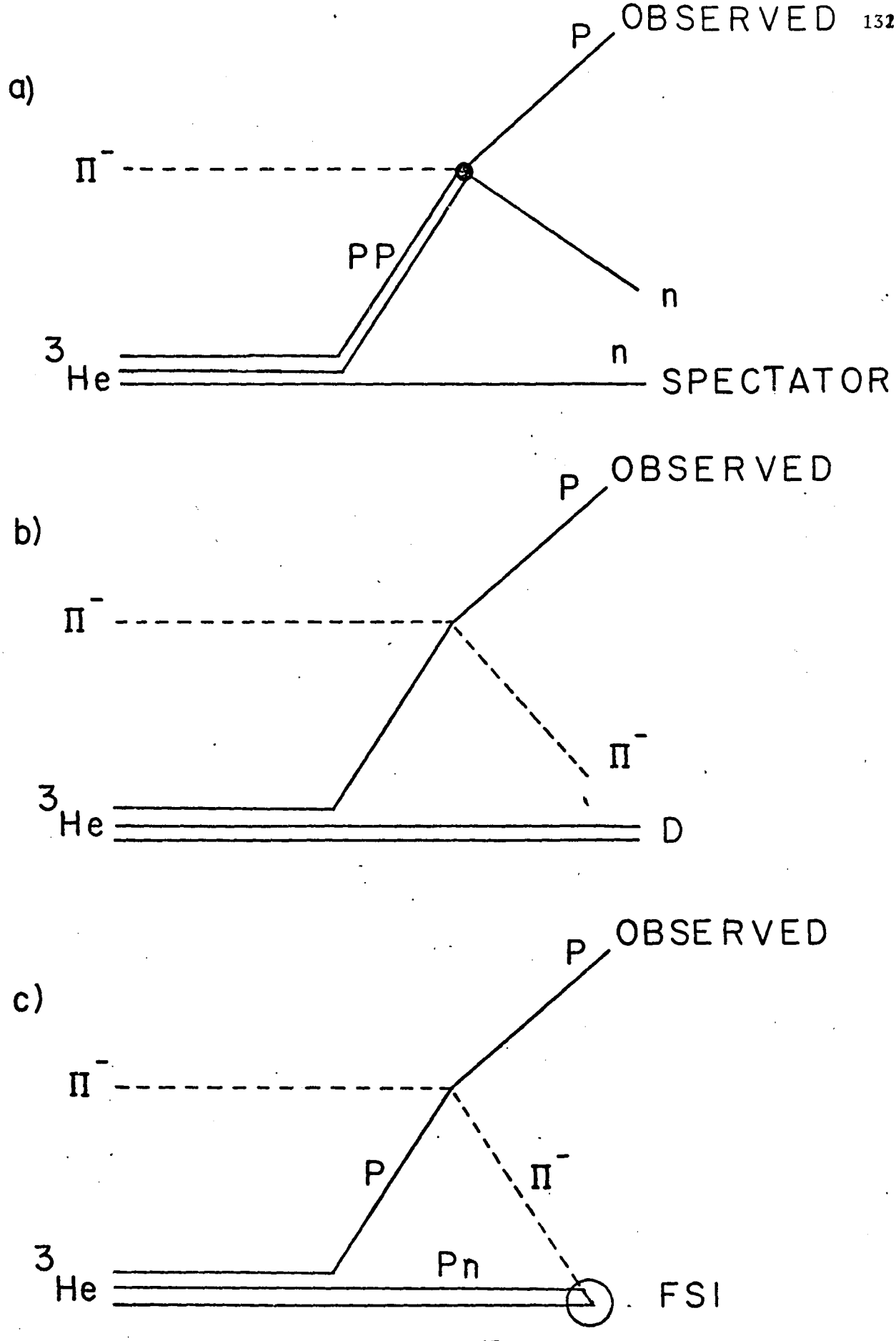
a)
P
OBSERVED
Π⁻
PP
n
³He
n
SPECTATOR
b)
P
OBSERVED
Π⁻
Π⁻
³He
D
c)
P
OBSERVED
Π⁻
P
Π⁻
³He
Pn
FSI

Figure 47.

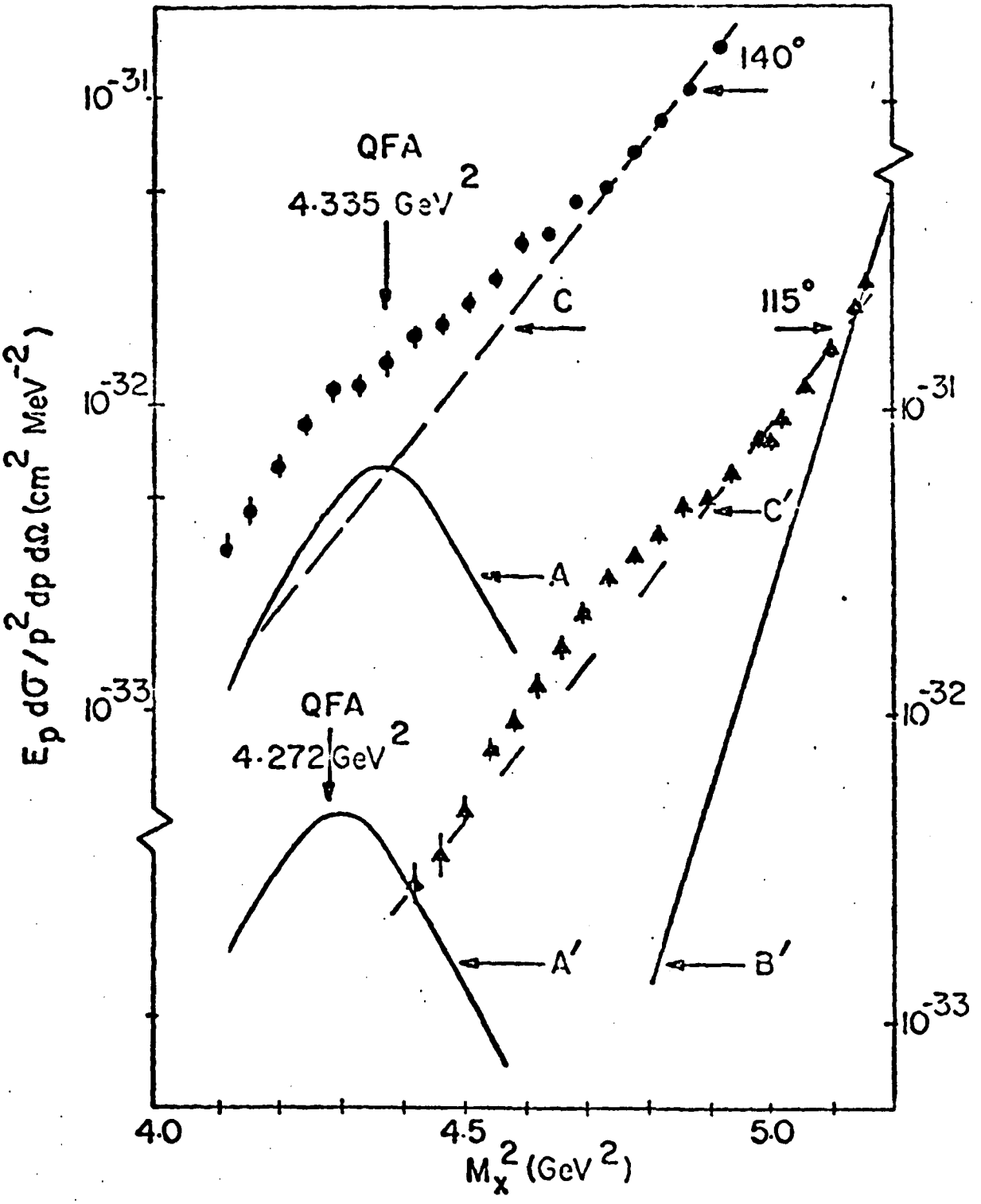
140°
115°
QFA
4.335 GeV 2
QFA
4.272 GeV 2
C
C′
A
A′
B′
10-31
10-32
10-33
4.0
4.5
5.0
Mx2 (GeV 2)
Ep dσ/p2dp dΩ (cm2 MeV-2)

Figure 48.

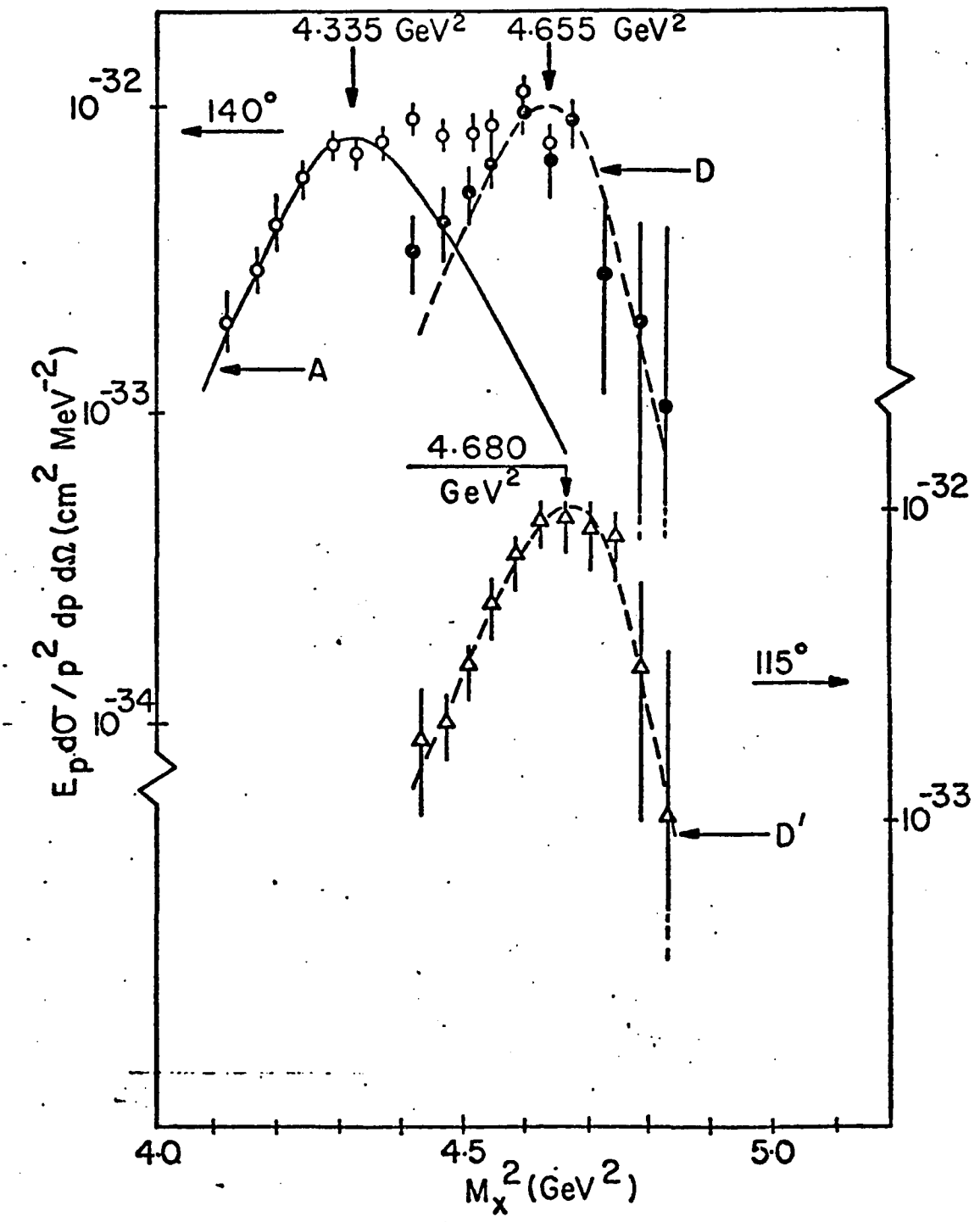
4·335 GeV²
4·655 GeV²
10⁻³²
140°
D
A
10⁻³³
4·680
GeV²
10⁻³²
115°
10⁻³⁴
D'
10⁻³³
E_p dσ/p² dp dΩ (cm² MeV⁻²)
4·0
4·5
5·0
M_x² (GeV²)

Figure 49.

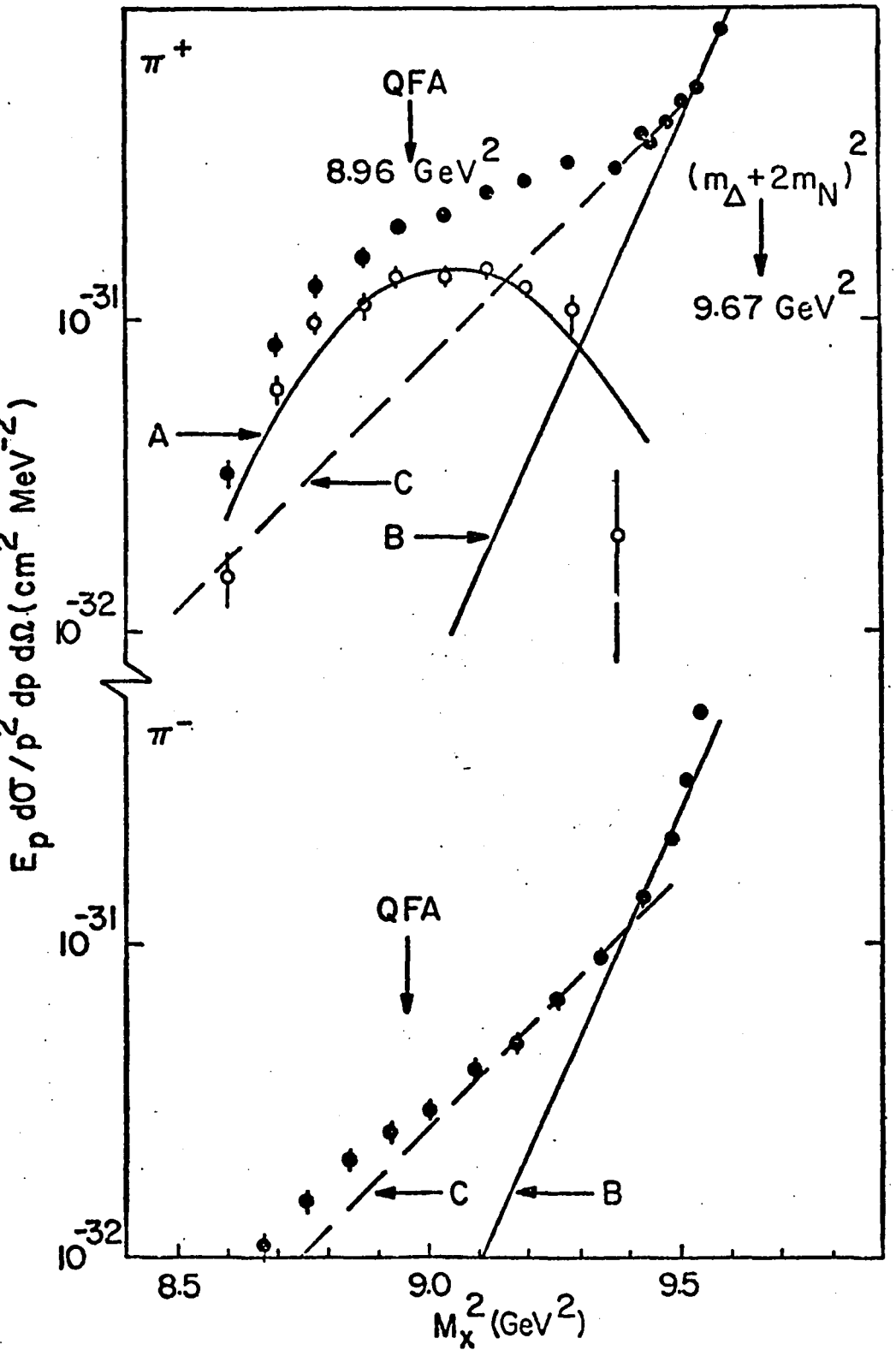

Figure a

Figure b

Figure 50.

pd -> tπ data at 350 MeV

cm angle(degrees)	cross section(μb/sr)
10.0	20.0 ± 1.0
20.0	11.0 ± 1.0
23.3	13.3 ± 0.72
28.8	10.6 ± 0.54
30.0	4.0 ± 1.5
34.5	7.9 ± 0.47
39.6	6.6 ± 0.25
44.1	4.8 ± 0.40
47.1	3.9 ± 0.36
50.2	4.3 ± 0.36
53.3	3.2 ± 0.32
54.0	2.5 ± 0.20
56.2	3.5 ± 0.25
60.1	2.6 ± 0.18
65.4	2.4 ± 0.43
68.7	1.74 ± 0.32
70.0	0.8 ± 0.10
72.1	1.84 ± 0.25
75.5	1.5 ± 0.25
78.8	1.13 ± 0.22
84.9	0.73 ± 0.18
85.4	0.612± 0.04
88.4	0.5 ± 0.13
91.0	0.45 ± 0.05
92.0	0.49 ± 0.15
95.7	0.60 ± 0.14
96.4	0.752± 0.052
99.5	0.46 ± 0.13
103.3	0.59 ± 0.12
107.0	0.836± 0.056
107.1	0.43 ± 0.11
110.8	0.26 ± 0.11
115.0	0.828± 0.086
117.8	0.936± 0.072
118.7	0.24 ± 0.068
122.6	0.25 ± 0.072
124.5	1.038± 0.13
126.6	0.20 ± 0.061
130.0	0.48 ± 0.05
130.6	0.41 ± 0.079
134.7	0.26 ± 0.068
138.9	0.16 ± 0.065
143.0	0.15 ± 0.054
147.0	0.058± 0.049

Appendix B

pd -> tπ data at 465 MeV

cm angle(degrees)	cross-section(μb/sr)
00.0	20.0
11.4	12.62 ± 0.70
37.0	5.14 ± 0.18
40.0	4.536± 0.149
55.50	1.69 ± 0.13
57.4	1.888± 0.13
60.0	1.17 ± 0.08
66.9	0.868± 0.08
70.9	0.558± 0.04
72.0	0.550± 0.06
74.6	0.714± 0.078
80.5	0.596± 0.036
90.0	0.63 ± 0.03
90.0	0.556± 0.034
99.6	0.628± 0.038
101.3	0.618± 0.052
102.5	0.692± 0.140
107.5	0.54 ± 0.05
109.1	0.666± 0.04
112.4	0.578± 0.044
120.0	0.810± 0.0430
123.5	0.664± 0.046
137.5	0.63 ± 0.05
140.0	0.803±0.034
152.5	0.52 ±0.06
160.0	1.167±0.052
160.0	0.54 ±0.06
167.0	0.68 ±0.06

Appendix C

pd -> tπ data for 500 MeV

cm angle(degrees)	cross-section(μb/sr)
11.00	13.45 $\pm$ 0.426
21.6	10.81 $\pm$ 0.48
25.0	7.707$\pm$ 0.227
26.3	10.04 $\pm$ 0.42
31.5	7.10 $\pm$ 0.36
35.9	5.75 $\pm$ 0.24
40.8	4.74 $\pm$ 0.36
41.4	3.916$\pm$ 0.137
43.7	4.44 $\pm$ 0.36
46.6	2.29 $\pm$ 0.095
49.6	2.75 $\pm$ 0.27
50.0	2.809$\pm$ 0.075
52.4	2.30 $\pm$ 0.23
55.8	1.27 $\pm$ 0.18
64.6	1.23 $\pm$ 0.26
68.0	1.01 $\pm$ 0.26
71.3	0.99 $\pm$ 0.23
74.7	0.70 $\pm$ 0.24
80.8	0.75 $\pm$ 0.15
84.3	0.47 $\pm$ 0.13
88.0	0.36 $\pm$ 0.11
91.7	0.60 $\pm$ 0.13
95.6	0.56 $\pm$ 0.12
99.4	0.50 $\pm$ 0.11
103.3	0.38 $\pm$ 0.11
107.2	0.64 $\pm$ 0.14
110.5	0.669$\pm$ 0.046
116.5	0.65 $\pm$ 0.07
120.6	0.48 $\pm$ 0.07
124.7	0.25 $\pm$ 0.08
129.0	0.22 $\pm$ 0.08
130.0	0.782$\pm$ 0.035
133.3	0.51 $\pm$ 0.11
137.4	0.693$\pm$ 0.056
137.6	0.21 $\pm$ 0.11
140.0	0.628$\pm$ 0.038
142.0	0.45 $\pm$ 0.30
148.6	0.809$\pm$ 0.049

Appendix D

pd -> tπ data for 600 MeV

cm angle(degrees)	cross-section(μb/sr)
7.40	12.60 $\pm$ 0.70
22.2	6.7 $\pm$ 0.70
36.5	3.0 $\pm$ 0.20
37.3	2.92 $\pm$ 0.14
46.3	1.34 $\pm$ 0.14
63.5	0.56 $\pm$ 0.11
87.3	1.35 $\pm$ 0.29
90.0	0.69 $\pm$ 0.07
105.3	0.482 $\pm$ 0.05
108.0	0.60 $\pm$ 0.07
112.8	0.49 $\pm$ 0.06
114.8	0.48 $\pm$ 0.05
125.0	0.48 $\pm$ 0.05
128.3	0.50 $\pm$ 0.06
142.0	0.35 $\pm$ 0.09
160.0	0.27 $\pm$ 0.08

Appendix E

pd -> tπ data for 800 MeV

cm angle(degrees)	cross-section(μb/sr)
12.2	3.41 ± 0.10
18.3	2.4 ± 0.10
26.2	1.77 ± 0.10
32.7	1.0 ± 0.08
40.7	0.70 ± 0.08
48.0	0.41 ± 0.03
54.4	0.33 ± 0.04
60.0	0.33 ± 0.04
68.7	0.30 ± 0.04
76.9	0.25 ± 0.03
88.0	0.22 ± 0.02
98.2	0.119± 0.019
100.0	0.138± 0.02
119.0	0.16 ± 0.02

LIST OF TABLES